

POLITECNICO DI TORINO

Corso di Laurea Magistrale in Ingegneria Civile



Tesi di Laurea Magistrale

Parametric Analysis for the Robustness Assessment of RC Systems

Supervisor:

Prof. Ing. Paolo Castaldo

Candidate:

Francesca Rossato

Co-supervisors:

Prof. Dr. Ir. Robby Caspeele

Dr. Ir. Wouter Botte

Ing. Diego Gino

Anno Accademico 2018/2019

Abstract

Structural robustness, intended as the ability of a structure to not suffer disproportionate collapse to the cause, has played an important role in the Guide Lines and Codes for Structural Design in the recent decades. Interest in this phenomenon has increased due to of the disproportionate collapse in several buildings, most notably the collapse of the Ronan Point Building in UK in 1968, where the collapse of some load-bearing walls of an 18th floor apartment led to the disproportionate failure of the entire corner of the building. Many researches on robustness of reinforced concrete and steel structures have defined the importance of the structural capacity to develop alternative load paths as directly linked to the definition of a building to be robust. From this point of view, the definition and evaluation of membrane actions, both compression and tensile, becomes significant as a mechanism that leads to a reserve of structural resistance.

The method of representation and study of the phenomenon of disproportionate collapse consists in the notional removal of a load-bearing column of the building. This assumption is consistent with the occurrence of exceptional events in the structure, such as fires, explosions or vehicle impacts. In this thesis, the capacity of a reinforced concrete structure to develop alternative load paths is first analysed, thus as to be able to change the resisting mechanism from the flexural resisting mechanism to the catenary action, connected to the characteristics of the elements adjacent to the beam subject to the removal of a column and to the mechanical properties, such as the ultimate reinforcement strain and the section resisting moment. This is performed by means of a parametric analysis developed using the finite element software DIANA FEA 10.2 (TNO DIANA). The FEM model used in the analysis consists in the geometric and mechanical representation of a part of the 2D frame, as it is a condition of geometric and loading symmetry, with the respect of the boundary supports and symmetry conditions. This first set of analyses is then extended by an analysis on the variation of the resistance of the frame over time, taking into account the degradation and damage of the building due to environmental exposure. Therefore, the phenomenon of corrosion in reinforced concrete structures is introduced, considering its evolution over time in the numerical evaluation of the reduction of material properties. In this thesis work, the numerical models available in the literature are therefore used for the

evaluation of corrosion considering the initial data provided by the structural geometry. The nonlinear analyses carried out on the model have confirmed that the phenomenon of robustness is influenced by the size of the beam itself, as reported in many studies, but also by the size of adjacent elements, for example how the section of the columns regulates the ability to develop the catenary action. Finally, it was possible to study the effect on robustness due to the reduction of material properties over time due to degradation generated by corrosion.

Contents

| | |
|---|-----------|
| List of Figures | 3 |
| 1 Robustness | 13 |
| 1.1 General definition of Robustness | 13 |
| 1.2 Membrane Actions | 17 |
| 1.2.1 Structural behaviour after the removal of a column | 18 |
| 1.2.2 Structural design after the removal of a column | 20 |
| 1.3 Other Robustness Design Methods | 22 |
| 1.4 Existing structures: Deterioration and Robustness | 23 |
| 1.4.1 Corrosion | 24 |
| 2 Finite Element Analysis with DIANA FEA | 27 |
| 2.1 Finite Element Analysis to Assess Robustness | 27 |
| 2.2 Model with DIANA FEA | 30 |
| 2.2.1 Material Properties | 31 |
| 2.2.2 Mesh and Elements Properties | 35 |
| 2.2.3 Numerical Analysis | 37 |
| 3 Definition of the parameters used to perform the parametric analysis | 41 |
| 3.1 Introduction | 41 |
| 3.2 Model Geometry | 42 |
| 3.3 Parametric Analysis: Geometrical Properties | 45 |
| 3.3.1 Beam Cross-Section | 46 |
| 3.3.2 Beam Length | 48 |
| 3.3.3 Column Length | 48 |

| | | |
|----------|--|------------|
| 3.3.4 | Column Cross-Section | 49 |
| 3.4 | Parametric Analysis: Mechanical Properties | 50 |
| 3.4.1 | Ultimate Reinforcement Strain, ϵ_{su} | 50 |
| 3.4.2 | Resisting Moment, M_{rd} | 51 |
| 3.5 | Parametric Analysis: Elements Stiffnesses | 52 |
| 4 | Analysis of the Results | 55 |
| 4.1 | Variable Beams Geometry | 56 |
| 4.2 | Variable Columns Geometry | 60 |
| 4.3 | Influence of ϵ_{su} | 65 |
| 4.4 | Influence of constant M_{rd} | 73 |
| 4.5 | Influence of the Stiffnesses | 80 |
| 5 | Corrosion | 83 |
| 5.1 | Degradation Mechanism of Corrosion | 84 |
| 5.2 | Corrosion effects on material properties | 88 |
| 5.2.1 | Corrosion rate and initiation time | 89 |
| 5.2.2 | Loss of cross-section in the reinforcing bar | 92 |
| 5.2.3 | Loss of steel ductility | 95 |
| 5.2.4 | Concrete cover reduction | 96 |
| 6 | Analysis in simulated chloride corrosion | 99 |
| 6.1 | Modelling of Corrosion | 99 |
| 6.2 | Analysis of the Results | 103 |
| 7 | Conclusions | 107 |
| | Bibliography | 111 |
| | Ringraziamenti | 115 |

List of Figures

| | | |
|-----|--|----|
| 1.1 | Disproportionate collapse examples | 14 |
| 1.2 | Membrane Actions in structural elements (CNR, 2018): (a) Membrane Actions under load higher than the design load; (b) Membrane Actions under column removal; (c) Load-displacement diagram with and without membrane actions | 18 |
| 1.3 | Frame subjected to the experiment (CNR, 2018) | 19 |
| 1.4 | Experimental behaviour (CNR, 2018) | 19 |
| 1.5 | System Geometry | 21 |
| 1.6 | Building with a transfer floor (CNR, 2018) | 22 |
| 1.7 | Corrosion in reinforced concrete structures | 24 |
| 2.1 | Tensile stress–strain relationship with Hordijk softening | 32 |
| 2.2 | Parabolic compression diagram | 33 |
| 2.3 | Concrete constitutive law input | 34 |
| 2.4 | Constitutive model for Reinforcement | 35 |
| 2.5 | Steel constitutive law input | 36 |
| 2.6 | CQ16M | 37 |
| 2.7 | Arc–length control | 38 |
| 2.8 | Load steps input for the applied load | 39 |
| 2.9 | Equilibrium iteration input for the applied load | 40 |
| 3.1 | Investigate Building Geometry with the removal of a column | 43 |
| 3.2 | Starting geometry of the finite element model in DIANA FEA (from Droognè et al.[5]) | 46 |

| | | |
|------|---|----|
| 3.3 | Simplified Finite Element Model geometry considering springs as the adjacent elements | 53 |
| 4.1 | Load-bearing capacity curve for both variable beam cross-section | 56 |
| 4.2 | Load-bearing capacity curve for variable cross-section of the adjacent beam | 57 |
| 4.3 | Load-bearing capacity curve for variable length of the adjacent beam | 58 |
| 4.4 | Evolution of the concrete strain in the members | 59 |
| 4.5 | Reinforcement Stresses at the bending peak | 59 |
| 4.6 | Load-bearing capacity diagrams for variable columns length | 61 |
| 4.7 | Load-bearing capacity diagrams for variable columns cross-section | 61 |
| 4.8 | Comparison between the maximum load in CMA with variable cross-section | 62 |
| 4.9 | Comparison between the maximum load in TMA with variable cross-section | 62 |
| 4.10 | Comparison between the failure displacement with variable cross-section | 63 |
| 4.11 | Comparison between the maximum load in CMA with variable length | 63 |
| 4.12 | Comparison between the maximum load in TMA with variable length | 64 |
| 4.13 | Comparison between the failure displacement with variable length | 64 |
| 4.14 | Load-displacement diagram with variable ϵ_{su} | 65 |
| 4.15 | Load-bearing capacity diagrams for beam cross-section and $\epsilon_{su} = 0.025$. . . | 66 |
| 4.16 | Load-bearing capacity diagrams for beam cross-section and $\epsilon_{su} = 0.05$. . . | 66 |
| 4.17 | Load-bearing capacity diagrams for beam cross-section and $\epsilon_{su} = 0.125$. . . | 67 |
| 4.18 | Load-bearing capacity diagrams for beam cross-section and $\epsilon_{su} = 0.025$. . . | 67 |
| 4.19 | Load-bearing capacity diagrams for beam cross-section and $\epsilon_{su} = 0.05$. . . | 67 |
| 4.20 | Load-bearing capacity diagrams for beam cross-section and $\epsilon_{su} = 0.125$. . . | 68 |
| 4.21 | Load-bearing capacity diagrams for beam length and $\epsilon_{su} = 0.025$ | 68 |
| 4.22 | Load-bearing capacity diagrams for beam length and $\epsilon_{su} = 0.05$ | 68 |
| 4.23 | Load-bearing capacity diagrams for beam length and $\epsilon_{su} = 0.125$ | 69 |
| 4.24 | Load-bearing capacity diagrams for columns cross-section and $\epsilon_{su} = 0.025$ | 69 |
| 4.25 | Load-bearing capacity diagrams for columns cross-section and $\epsilon_{su} = 0.05$ | 69 |
| 4.26 | Load-bearing capacity diagrams for columns cross-section and $\epsilon_{su} = 0.125$ | 70 |
| 4.27 | Load-bearing capacity diagrams for columns length and $\epsilon_{su} = 0.025$ | 70 |
| 4.28 | Load-bearing capacity diagrams for columns length and $\epsilon_{su} = 0.05$ | 70 |
| 4.29 | Load-bearing capacity diagrams for columns length and $\epsilon_{su} = 0.125$ | 71 |

| | | |
|------|--|----|
| 4.30 | Superposition of load–displacement diagrams of with variable ϵ_{su} and variable Hb_1 | 71 |
| 4.31 | Superposition of load–displacement diagrams of with variable ϵ_{su} and variable Hb_2 | 72 |
| 4.32 | Superposition of load–displacement diagrams of with variable ϵ_{su} and variable Hc | 72 |
| 4.33 | Superposition of load–displacement diagrams of with variable ϵ_{su} and variable Lb | 73 |
| 4.34 | Load–displacement diagram with constant M_{rd} and variable H_b | 74 |
| 4.35 | Membrane Action–displacement diagram with constant M_{rd} and variable H_b | 75 |
| 4.36 | Load–displacement diagram with constant M_{rd} and variable H_c | 76 |
| 4.37 | Membrane Action–displacement diagram with constant M_{rd} and variable H_c | 76 |
| 4.38 | Comparison between the maximum load in CMA with constant M_{rd} and variable H_b | 77 |
| 4.39 | Comparison between the maximum load in TMA with constant M_{rd} and variable H_b | 77 |
| 4.40 | Comparison between the failure displacement with constant M_{rd} and variable H_b | 78 |
| 4.41 | Comparison between the maximum load in CMA with constant M_{rd} and variable H_c | 78 |
| 4.42 | Comparison between the maximum load in TMA with constant M_{rd} and variable H_c | 79 |
| 4.43 | Comparison between the failure displacement with constant M_{rd} and variable H_c | 79 |
| 4.44 | Load–displacement diagram for the two different FEM model | 80 |
| 5.1 | Cover detachment after corrosion of steel reinforcement | 84 |
| 5.2 | Carbonation evolution process | 86 |
| 5.3 | Pitting evolution process | 86 |
| 5.4 | Initiation and Propagation periods in a structure subjected to Carbonation | 87 |
| 5.5 | Indicative design working life from EN 1990:2002 | 89 |
| 5.6 | Qualitative connection between C_{crit} , environmental condition and concrete quality (Gjorv, 2009) | 90 |

| | | |
|------|---|-----|
| 5.7 | Different stages of pitting corrosion in a reinforcing bar (Apostolopoulos et al.,2008) | 93 |
| 5.8 | Loss of cross-sectional area due to pitting corrosion | 93 |
| 5.9 | Pitting area shape model by Val-Melchers | 94 |
| 5.10 | Ductility reduction as function of the cross-sectional bar loss | 97 |
| 6.1 | Reinforcement cross-sectional area reduction during 50 years | 101 |
| 6.2 | Loss of steel ductility during 50 years | 102 |
| 6.3 | FEM model to assess robustness under the corrosion effects | 102 |
| 6.4 | Load-bearing capacity diagram in simulated chloride corrosion | 104 |
| 6.5 | Comparison between the maximum load in CMA under corrosion evolution in time | 105 |
| 6.6 | Comparison between the maximum load in TMA under corrosion evolution in time | 105 |
| 6.7 | Comparison between the failure displacement under corrosion evolution in time | 106 |

Sommario

Il termine *Robustezza* è usato in diversi campi di ricerca e di applicazione tecnologica. Nell'ambito dell'ingegneria strutturale si definisce il concetto di ***Robustezza Strutturale*** come la capacità di una struttura di non subire un collasso sproporzionato alla causa. Questo concetto ha trovato un posto rilevante nelle Linee Guida e nei Codici per la progettazione strutturale, infatti la definizione che è stata adottata di carattere generale è quella della EN 1991-1-7: 2006:

Robustezza è la capacità di una struttura di resistere ad eventi come incendi, esplosioni, impatti o le conseguenze dell'errore umano, senza essere danneggiata in misura tale da smentire la causa originaria.

Uno dei modi più studiati e utilizzati per valutare la robustezza è la capacità di una struttura di sviluppare azioni membranali e quindi di aumentare la sua resistenza. Questa viene poi tradotta nella capacità di cambiare il meccanismo di resistenza da quello di resistenza flessionale al meccanismo a catenaria, cioè di sviluppare oltre che le azioni membranali di compressione anche quelle di tensione. Questo comportamento è stato individuato grazie a modelli sperimentali realizzati mediante l'analisi di un telaio in cemento armato sottoposto alla rimozione della colonna portante intermedia, condizione rappresentativa di eventi eccezionali.

Lo scopo di questa tesi è quindi quello di analizzare la capacità di strutture in cemento armato di sviluppare il meccanismo a catenaria. Questo viene eseguito analizzando l'influenza delle proprietà geometriche e meccaniche sulla capacità rotazionale del nodo trave-pilastro integro del telaio oggetto di studio. A questo scopo viene eseguita un'analisi parametrica statica non lineare su un modello a elementi finiti che tenga conto delle non linearità geometriche e meccaniche. Viene poi affiancata a completamento, un'ulteriore analisi sull'effetto

della corrosione da cloruri sul telaio in cemento armato considerando l'evoluzione del fenomeno nel tempo. Poiché la struttura da analizzare è un edificio adibito ad uffici, la vita utile adottata è di 50 anni, come prescritto dal Model Code 2010.

Nel Capitolo 1 sono introdotte le definizioni di *Robustezza* e *Corrosione*, illustrando inoltre le varie metodologie per valutare la robustezza e l'evoluzione delle azioni membranali. Si riporta l'esperimento condotto da Lew et al. con cui viene studiato il comportamento del telaio sottoposto alla rimozione di una colonna portante, nel quale si evidenzia la capacità di una trave in cemento armato di sviluppare l'azione a catenaria. Nell'ultima sezione viene brevemente introdotto il fenomeno della corrosione su strutture esistenti e i suoi effetti sui materiali.

Il Capitolo 2 ha lo scopo di illustrare i diversi modelli e analisi disponibili per valutare la robustezza come prescritto dalle Normative vigenti. Si descrivono quindi in modo approfondito le caratteristiche del modello FEM adottate e dell'analisi non lineare eseguita con il software ad elementi finiti DIANA FEA 10.2 (TNO DIANA) relative al caso studio di questa tesi. Per poter andare a valutare il comportamento a catenaria diviene importante tenere conto delle non linearità geometriche e dei materiali, quindi l'utilizzo di una analisi non lineare, in particolare è stata utilizzata una analisi statica.

Il Capitolo 3 raccoglie le caratteristiche geometriche del telaio in cemento armato analizzato e la definizione di tutti i parametri utilizzati per effettuare l'analisi parametrica necessaria per studiare come sia influenzato il comportamento ultimo del telaio. Vengono eseguite più analisi per studiare sia l'influenza delle caratteristiche geometriche, come area della sezione e lunghezza di travi e colonne, sia di quelle meccaniche, ad esempio la deformazione ultima dell'acciaio.

I risultati ottenuti da questa analisi vengono illustrati approfonditamente nel seguente Capitolo 4.

Il Capitolo 5 fornisce una descrizione dettagliata del fenomeno di corrosione con i suoi effetti sulle proprietà dei materiali. Il fenomeno viene analizzato durante la vita utile della struttura, di conseguenza il modello matematico tempo-dipendente per definire tutti gli effetti della corrosione sulle proprietà dell'armatura e del calcestruzzo, i modelli adottati

sono descritti nella seconda sezione di questo capitolo.

Viene utilizzato lo stesso modello FEM definito nel Capitolo 3 implementando l'effetto della corrosione in zone localizzate del telaio, in quanto viene analizzata la corrosione da pitting. Tutte le caratteristiche del modello e i valori applicati nell'analisi insieme ai risultati sono illustrati nel Capitolo 6.

Nell'ultimo capitolo vengono descritti i risultati più importanti ottenuti dalle analisi al fine di individuare il parametro che maggiormente influenza il comportamento della struttura in cemento armato e la variazione di quest'ultimo considerando una simulazione di corrosione indotta nel tempo.

Chapter 1

Robustness

1.1 General definition of Robustness

In literature the term *Robustness* is used for several definitions. Depending on the research and technology fields of application, such as Software Engineering, Ecosystems, Statistics etc..., *Robustness* describes a consistent variety of parameters. For example in the field of Software Engineering it is used to define *"The ability [...] to react appropriately to abnormal circumstances (i.e. circumstances "outside of specifications")*. *A system may be correct without being robust* " (Meyer 1997); as this definition, lots of other descriptions refer to the capacity of a system or technique to perform with an acceptable behaviour to an exceptional event.

In the research field of construction the term of robustness has become significant in the past decade following the collapse of many buildings in exceptional circumstances. It was clear than, that the concept of ***Structural Robustness***, intended as the ability of a structure to not suffer disproportionate collapse to the cause, should have taken a relevant place into the Guide Lines and Codes for structural design.

The most famous example of disproportionate collapse is the failure of the Ronan Point Building in UK, 1968, as showed in Figure 1.1(a). In this case the entire south-east corner of the building collapsed after a gas explosion blew out some load-bearing walls of a flat on the 18th floor [8]. Another important example is the collapse of the World Trade Center in New York, 2001, Figure 1.1(b), where the failure of the floors above the airplane impacted

led to the collapse of the entire building.

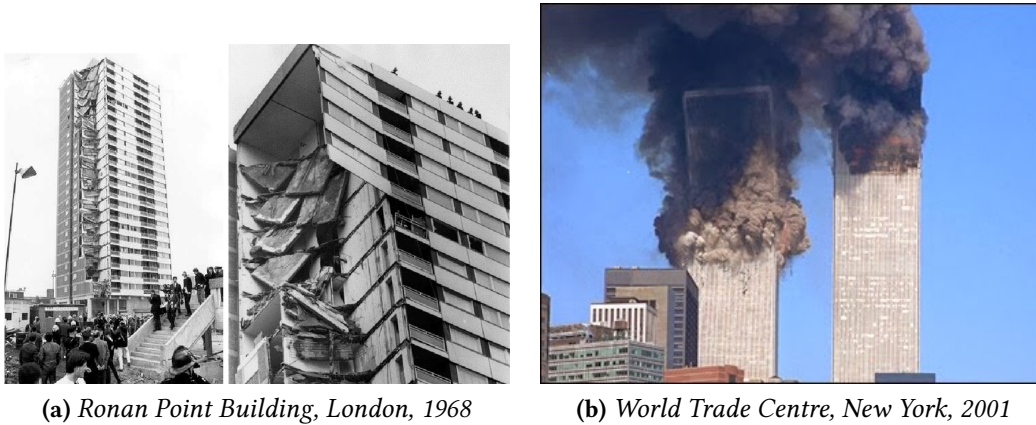


Figure 1.1: Disproportionate collapse examples

In the following years, this new awareness about disproportionate and progressive collapse spread throughout the field of research, leading to the publication of numerous articles, both in reinforced concrete and steel structures, together with the introduction of design criteria about accidental actions, such as explosions, natural disasters or vehicle impacts.

To understand the reason for referring to the two terms of disproportionate and progressive collapse it is necessary to initially explain the difference between them: “a **disproportionate collapse** need not be progressive, but suffers damage that is disproportionate to the original cause of failure. An example is the collapse of a statically determinate structure from the failure of a single member. In the case of a **progressive collapse**, different members of a statically indeterminate structure fail one after the other as they get overloaded with an accompanying redistribution of load” [4]; this distinction shows that a disproportionate collapse cannot be necessarily progressive, while a progressive collapse may lead to a disproportionate collapse. By consequence it is defined a new class of failure as ‘disproportionate collapse’ where the progressive collapse is a particular example. Following this distinction, it was introduced the concept of **Structural Robustness**. As for the general term of robustness, lots of different definitions, together with disproportionate and progressive collapse, can be found in literature.

The general definition, which is accepted, is the one adopted from (EN 1991-1-7: 2006):

***Robustness** is the ability of a structure to withstand events like fire, explosions, impacts or the consequences of human error, without being damaged to an extent disproportionate to the original cause*

Furthermore, according to this code, "a localised failure due to accidental actions may be acceptable, provided it will not endanger the stability of the whole structure, and that the overall load-bearing capacity of the structure is maintained and allows necessary emergency measures to be taken". The ability of a structure to withstand such exceptional events can be translated into its ability to develop alternative load paths by redistributing the loads to the other load-bearing elements. By means of this ability, it can be define the design criterion of a structure to be robust and to avoid disproportional damage, Therefore, it is of significant importance the definition of alternative load paths in the assessment of structural robustness.

This ability to develop alternative load paths is closely related to the *redundancy* of a structure, which in fact refer to the availability of multiple load-carrying paths in such structure. In addition, it has been observed that Structural Robustness depend also on the *ductility* of the members in the structure under consideration.

In order to design a structure to be robust and thus to respect the conditions of redundancy and ductility, different design methods are defined in the CNR, 2018 and in COST, 2011, as briefly describe below and thoroughly in the paragraphs 1.2 and 1.3:

- **Specific Load Resistance (SLR):** This method is based on the definition of the so-called key elements. If these structural members are damaged by an accident the structure can suffer of disproportionate collapse. The design is therefore aimed at providing sufficient strength to resist failure from accident or misuse to these key elements;
- **Alternative Load Paths:** In this method the resistance of a structure to disproportionate collapse is performed by the redistribution of the loads carried originally by the failed elements to the integer structural members. It is a direct method and needs to provide that the integer part of the structure is capable to resist and redistribute the loads after the elements fail;

- **Consequence Reducing Measures:** There are a variety of measures that can be adopted in order to reduce the direct and indirect consequences of failure and thus the total risk. Some important structural and architectural measures are the possible segmentation, or compartmentation of the structure.

These methods are used to design structures or to improve the robustness of existing structure, in this second case it should be taken into account the deterioration level of the buildings, for example the level and the type of corrosion that might be present, in order to lead to an optimal distribution of the funds provided for the recovery of the structure.

In general the design of structures is based on the fact that they should not suffer large displacement under normal load during their service life. Codes and Guide lines have always referred to a design procedure with the respect of small displacements. However, the occurrence of all of these disproportionate collapse due to natural causes, human errors or terrorism attacks, show the importance to extend the Codes considering also the ability of a structure to develop alternative load paths after large displacement occurs. Nowadays the Eurocodes take into account different methods to ensure robustness in a structure, as anticipated above. According to this codes the accidental design load has to be applied as a concentrated load or uniformly distributed load, this action act on the main element and for the design verifications are considered also the adjacent components and their joints, so the entire structure needs to be modelled and not the single elements in isolation.

Lots of recent researches showed that reinforced concrete (RC) structures are able to avoid disproportionate collapse by changing the load resisting mechanism from flexural to the catenary action that occurs when large structural displacements take place in the beams. This collapse is usually represented in all the researches by the notional removal of a load bearing column. After that, the adjacent elements start to deform and large displacement occurs in the RC beam. Together with these larger deformations, membrane actions develops, as it was shown in numerous experiments with both reinforced concrete slabs [10] and beams [9]. Performing all those experiments showed the significant contribution to robustness by the developing of membrane actions. Following this concept, the present thesis is first of all finalized to the parametric study of a reinforced concrete structure to the variation of geometrical and mechanical parameters.

1.2 Membrane Actions

It is commonly accepted that the arising of *Membrane Actions* in reinforced concrete elements lead to a reserve of resistance. This higher resistance in the element is of crucial importance when assessing structural robustness because, taking into account membrane actions, make possible to avoid the application of design criteria (in new structures) or reinforcing strategies (in existing structures) that would be too much restrictive for the designer [3]. Accordingly, alternative load paths, together with the membrane effects, is one of the most used method in the evaluation of structural robustness.

First of all, to define the beneficial effect on the resistance of the element, it has to be identified the different behaviour between horizontally restrained and unrestrained slabs and beams; this is showed by the load-displacement diagram in Figure 1.2(c). The diagram shows that, due to the *Compressive Membrane Actions* (CMA), the load can reach a peak which is consistently higher than the maximum reachable load in the elements without considering the development of membrane actions, i.e. without considering the horizontal restraint. This peak represent the maximum resisting load in the bending resisting mechanism. Moreover, after the peak a phase of softening arise and then, when the load start to increasing again with the displacement in an hardening phase, *Tensile Membrane Actions* (TMA) take place into the element until the failure load is reached which can be higher than the first peak, while for unrestrained elements the failure load is lower than the maximum load, which define the maximum resistance in the bending resisting mechanism.

Figures 1.2(a) and (b) also highlight the ability of a structure to develop membrane actions not only considering the removal of a column, but also when higher load than the design load arise into the structure. The Compressive Membrane Actions arise in the element when cracking starts, while Tensile Membrane Actions arise when the plastic hinges develop into the transverse sections; for this reason we can find them also in overloaded conditions of the elements and not only when accidental events happen. In fact, the membrane effect consist in the establishment of an axial force system into the beam element which improves the resistance of inflected elements.

In order to understand the correct behaviour of an element under the notional removal of a load bearing column the experiment conducted by *Lew et al., 2011* is described in § 1.2.1.

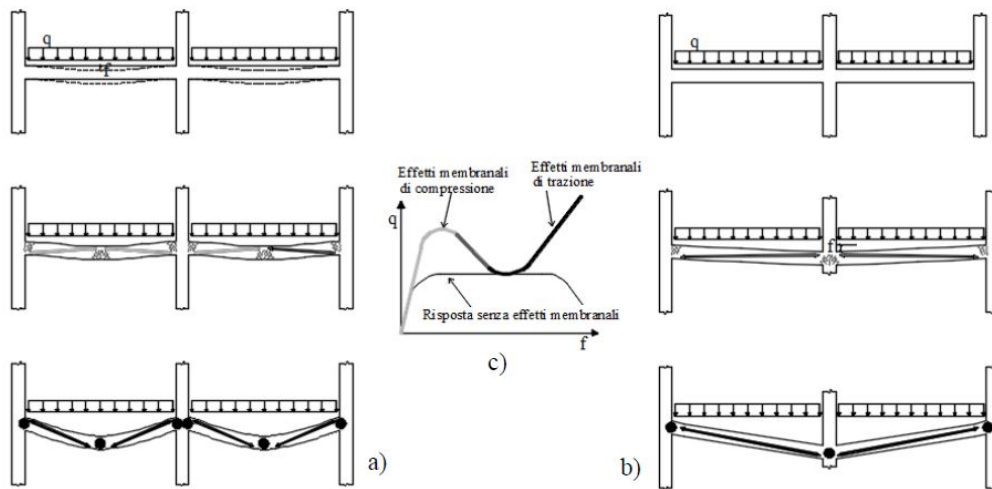


Figure 1.2: Membrane Actions in structural elements (CNR, 2018): (a) Membrane Actions under load higher than the design load; (b) Membrane Actions under column removal; (c) Load-displacement diagram with and without membrane actions

Moreover, it is important to note that membrane actions depend on numerous parameters, such as **geometrical** and **mechanical nonlinearities**. So, when modelling elements, taking into account this nonlinearities is significant to define the development of Compressive and Tensile membrane actions. Some of these fundamental parameters are the length of the element, the height of the transverse section and the geometric percentage of reinforcement.

1.2.1 Structural behaviour after the removal of a column

This section, together with the following one, are aimed to explain the evolution of the load bearing mechanisms under the progressive loading of a beam subjected to the removal of a column and the equation to evaluate the maxima loads that arise in the members. During the removal of a load-bearing column, different phases arise into the structural elements due to the vertical displacement that occurs in the point where the column was removed. The experiment settings able to described this phases is showed in Figure 1.3; a 2D reinforced concrete frame was built considering the removal of the centre column and, with an imposed displacement in this point P1, it is simulated the loss of the load-bearing element. The analysis of the experimental behaviour showed the development of three different stages in the load-displacement diagram (see Figure 1.4).

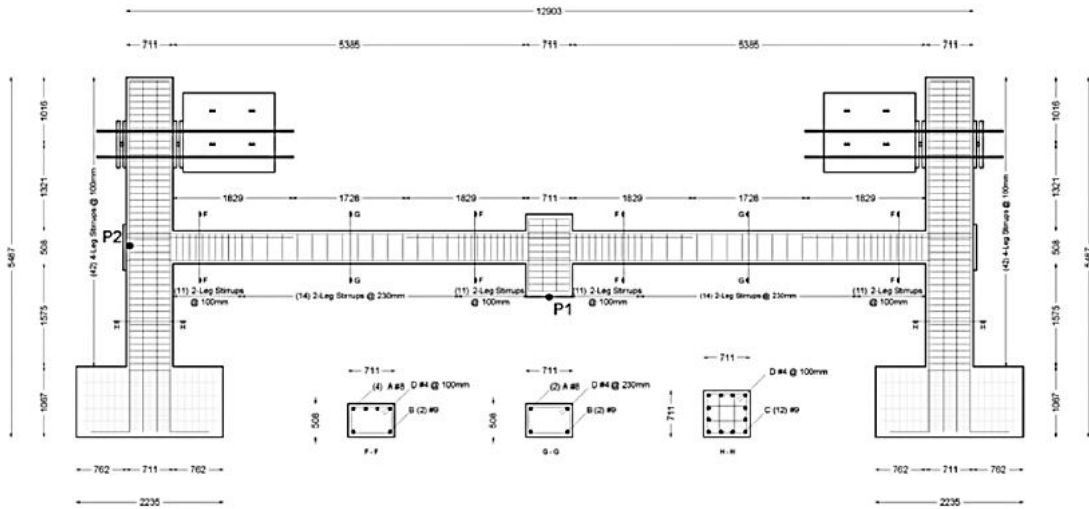
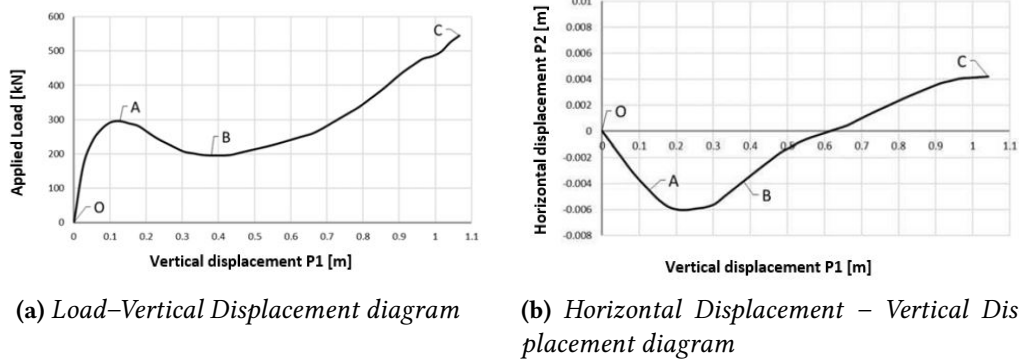


Figure 1.3: Frame subjected to the experiment (CNR, 2018)



(a) Load-Vertical Displacement diagram

(b) Horizontal Displacement – Vertical Displacement diagram

Figure 1.4: Experimental behaviour (CNR, 2018)

- **First phase - OA:** In this first phase the behaviour of the element is dominated by the elastic bending resistance of the beam and it end when plastic hinges develop in the beam – column joint. The point P2, which is used to measure the horizontal displacement, is subjected to an outward horizontal displacement due the lengthening of the beam in cracking condition. The beam is than compressed because the horizontal displacement is not allowed by the columns stiffness, consequently the plastic moment increases;

- **Second phase - AB:** During this phase, softening arise and a reduction of the load with an increasing vertical displacement of point P1 is shown. The horizontal displacement in P2 decreases until being null in point B, accordingly also the compressive membrane action decreases to zero;
- **Third phase - BC:** This is the stage where Tensile Membrane Action arises and the load starts to increase again with an increasing vertical displacement. The horizontal displacement starts to be inward and as a consequence the beam is tensed. In this phase the *Catenary Action* resisting mechanism occurs and increases following the vertical displacement in point P1.

1.2.2 Structural design after the removal of a column

Considering the above mentioned structural behaviour it is possible to defined a criterion to design structures subjected to the removal of a column.

First of all, one can defined two different maxima loads: $P_{MAX,FL}$ in point A and $P_{MAX,CAT}$ in point C as shown in Figure 1.4(a), those are respectively the maximum load in bending resisting mechanism and the maximum load under catenary action.

The first one can be estimated by:

$$P_{MAX,FL} = \frac{2(M_{PL}^+ + M_{PL}^-)}{L} \quad (1.1)$$

where M_{PL}^+ and M_{PL}^- are the positive and negative plastic moment of the beam–column joint. They can be evaluated on the safety side hypothesis of not considering the compressed beam reinforcement, via the following equations:

$$M_{PL}^+ = 0.9A_s^+ f_y d \quad M_{PL}^- = 0.9A_s^- f_y d \quad (1.2)$$

where A_s^+ and A_s^- are tensed reinforcements for positive and negative moment in the beam–column connection, d is the beam effective depth and f_y is the yielding strength of the reinforcement considering the safety coefficients defined in the accidental combination.

The maximum load in catenary action can be computed instead with equation 1.3:

$$P_{MAX,CAT} = 2 \frac{\delta}{L} A_{s,cont} f_t = 2\theta_u A_{s,cont} f_t \quad (1.3)$$

where δ and θ_u are the displacement capacity under the removed column and the rotational capacity of the beam respectively, $A_{s,cont}$ is the continuous reinforcement along the beam length of $2L$ and f_t is the ultimate reinforcement strength considering the safety coefficients defined in the accidental combination. The geometrical definition of δ and θ_u can be found in Figure 1.5.

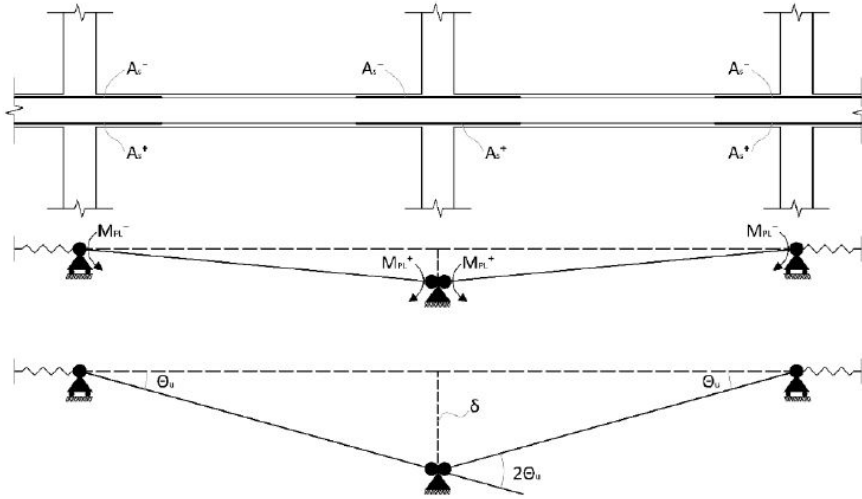


Figure 1.5: System Geometry

The evaluation of θ_u is based on experimental values that refer to element subjected to combined compressive and bending stress or only to bending moment. Is not yet verified that the combined condition of tensile and bending stress takes to different equations of θ_u . Consequently, the same formulas used in combined compressive and bending stresses is adopted also for combination of tensile and bending stresses:

$$\theta_u = \frac{1}{\gamma_{el}} \Phi_u L_{pl} \left(1 - \frac{0.5 L_{pl}}{L_v} \right) \quad (1.4)$$

where $\gamma_{el} = 1.0$ is a safety coefficient, Φ_u is the ultimate curvature evaluate from the ultimate strain of concrete and reinforcement, considering the confinement and the acting tensile stress in the beam, L_v is the shear length and L_{pl} is the length of the plastic hinge.

In conclusion, the catenary action lead to an improvement of resistance, to the respect of the flexural resistance, only when $P_{MAX,CAT} \geq P_{MAX,FL}$

1.3 Other Robustness Design Methods

The ability of a structure to develop the catenary resisting mechanism is the main condition to define it as robust and therefore able to withstand a disproportionate collapse. For this reason, in recent years, studies have focused on the definition of the best methods and conditions to achieve the development of alternative load paths following the accidental removal of a load-bearing element. However, there are structural types in which the ability to develop alternative load paths is very low. As a result, alternative measures have been introduced to ensure structural robustness, in which it can be also identified as the ability of the structure to guarantee safety with regard to human lives, in the case an exceptional event occurs. The following sections illustrate these alternative measures.

Specific Load Resistance (SLR)

The SLR method has the aim to prevent disproportionate collapse, avoiding the local damage of some structural members, the so-called *Key elements*, which could lead to an uncontrolled spreading of the damage [3].

As the robustness depend on the redundancy of a structure and on its ability to develop alternative load paths, this method is used for those structures that have a lack of redundancy, for example tensile structures, reticular structures, cable-stayed and suspended structures where the development of alternative load paths has a low probability of arising. Another example is the one in Figure 1.6, where is present a transfer floor.

In this case, the removal of a transfer column surely lead to a disproportionate collapse be-

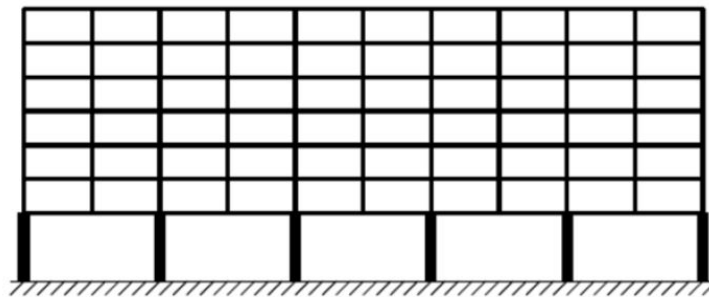


Figure 1.6: Building with a transfer floor (CNR, 2018)

cause the structure is not capable to develop alternative load paths and different measures to ensure the structure to be robust need to be applied.

This method is the most used when improving robustness of existing structures because the designer can define the key elements in the structure and improve their resistance to accidental actions. To design such key elements is considered a uniformly distributed load of 34 kN/m^2 [1]. As SLR is used for existing structures, the initial damage can also be caused by occurrences such as corrosion or fire-events that are more effectively counteracted by 'Event Control' measures [4]. The final purpose of this method is to design structural details in order to guarantee ductile mechanisms during failure and avoiding fragile failure, this is done considering confinement and continuous reinforcement in the beam-column joints for reinforced concrete structure and stiffeners in steel frames.

Consequence Reducing Measures

These kind of measures are indirect methods of providing robustness to a structure. They deal with both the consequences of the failure and the risks during the failure. Their main purpose is to reduce the risk of spreading failure and especially the risk on human safety. For example, in this approach are also consider the use of escape routes or appropriate alarm systems in order to make easier the evacuation of the building. Speaking about structural and architectural measures, the approach used is to identify the so-called segment borders that isolate the failing part. This method is called compartmentation and its border are defined by 'strong' elements that disconnect the 'weak' collapsed elements of the compartment, or, vice versa, by 'weak' elements that collapsed dividing the damage part from the integer structure.

1.4 Existing structures: Deterioration and Robustness

The design of RC structures usually does not take into account the deterioration processes due to aging of the materials and environmental factors, such as the percentage of chlorides in aggressive environments, which can involve the development of corrosion of steel reinforcement and deterioration of concrete. All this degradation mechanisms increase the risk of structural failure and the structural performances may not satisfy the correct safety level due to decrease of the mechanical properties, by consequence the structure is not able to withstand the applied load. This last deterioration condition is also an issue when assessing the structural robustness of a building.

It is defined in the previous sections that Structural Robustness became significant in the past decade due to the observed disproportionate collapse of many buildings in exceptional events. The main design method used when assessing robustness is the definition of alternative load paths that arise inside the reinforced concrete structure. When the reinforced concrete structure is affected by degradation phenomena, a lack of structural performance arise and, as a consequence, the capacity of developing alternative load paths decrease. In this thesis is investigated the contribution of the main degradation mechanism, i.e. corrosion, on the activation of membrane action in reinforced concrete frame. In the following section a brief introduction to the process of corrosion is given.

1.4.1 Corrosion

Most of the existing structures suffer of deterioration and corrosion is usually the main deterioration phenomenon present which lead to a loss of safety in the structures. Maintaining the safety and the serviceability of existing buildings is a significant challenge for the countries and to distribute the resources in a better way, in order to guarantee the establishment of the correct safety level, plays a crucial role.

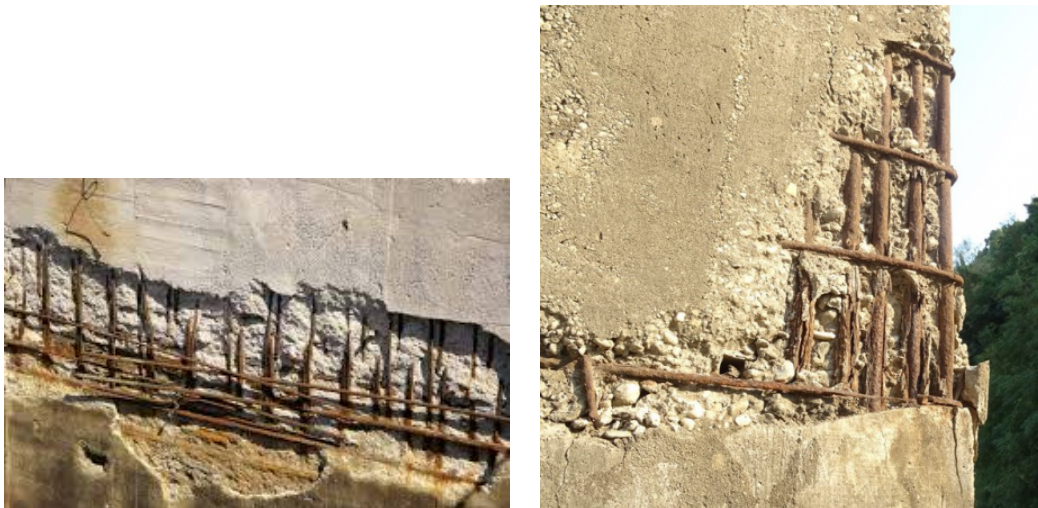


Figure 1.7: Corrosion in reinforced concrete structures

Corrosion has many effects on the reinforcement and the concrete properties, some of them are listed below:

- *Cross-section* of reinforcing bars is reduced;
- Reduction of reinforcement *ductility*;
- *Concrete strength* is affected by splitting cracks, delamination and spalling of the concrete cover.

Corrosion also affects the bond strength between steel and concrete, but this aspect is not investigated in this study.

The development of corrosion may occur in two different ways, **uniform corrosion** which is associated to carbonation and **pitting** corrosion due to chloride diffusion in the concrete cover, this second process is the most dangerous because it creates localized pits, i.e. holes along the bars diameter, and depending on the percentage of chloride which is present they can develop through all reinforcing bars causing a strong reduction of their mechanical properties.

As described in all the models about corrosion, this process can be divided into two phases:

- **Initiation period:** this phase occurs when the carbonation reaches the reinforcement or the chlorides concentration exceed the critical value, the reinforcement is depassivated;
- **Propagation period:** during this second phase the reinforcement is directly affected and its cross-section is reduced. In addition, corrosion products are accumulated around the reinforcing bars and this may eventually lead to cracking and spalling of the concrete cover.

If the corrosion process continues, structural failure may happen and considering its interaction with the structural robustness, alternative load paths may not arise in the reinforced concrete element.

In conclusion, this degradation mechanism is of crucial importance when studying existing structures and their robustness.

Chapter 2

Finite Element Analysis with DIANA FEA

2.1 Finite Element Analysis to Assess Robustness

In order to model structures to assess their robustness there are different ways recommended by the Codes of Construction [3] [4].

The phenomenon of disproportionate collapse is difficult to depict due to all the uncertainties that are involved. These uncertainties regard the geometrical and mechanical properties; they cover a large amount of parameters, starting from the material properties, the way the action is applied and the time of application of the load. From this point of view, modelling of structures becomes an important issue when assessing robustness.

The accuracy of the result depends on many factors, such as the type of analysis and modelling and the material constitutive laws. In particular the adopted constitutive laws can be very simple, for example *Linear-elastic* laws, otherwise they can be very complicated, such as the *Nonlinear hysteretic* laws.

Depending on the type of constitutive law, model and analysis adopted, therefore depending on the complexity of the carried-out analysis, the computational load increases and also the processing times. The compromise between the accuracy of the result and the computational time is decided by the sensitivity and experience of the designer. The task

of the Codes is to make available the choices between the constitutive laws and analysis explaining the different characteristics they have, and the problems one can encounter choosing between them.

Some of the models with their characteristics are listed below:

- **Linear–elastic Constitutive Models:** This is the easiest model, but it is also not adapt to evaluate all the phenomena of the disproportionate collapse because it does not consider the material nonlinearities that are involved as a result of the large displacement of the structural members. However, it is useful during the preliminary study phase to point out the critical aspects of the structure;
- **Nonlinear Constitutive Models dependent / independent on the load application rate:** Nonlinear constitutive models are the most suitable when assessing disproportionate collapse. With these types of models, it is possible to take into account the plasticity of the materials which is crucial in the process of energy dissipation. It is also an important factor the load application rate, because it influences the results due to an increasing resistance or stiffness of the materials;
- **Local and Global Models:** This classification is done in order to improve the computational load and time. Global models are really time consuming from the computational point of view, as a consequence, it is better to realize local model when evaluating particular regions in the structure. Global models are used to evaluate the stress and displacement characteristics of the whole structure.

Following the classification of the available models in the Codes, also different analysis can be performed to assess structural robustness. Disproportionate collapse can be very fast and this lead to dynamic effects that are implemented in the analysis in different ways depending on the Linear or Nonlinear behaviour which is adopted. In the following are listed the available analysis in the Codes of construction, from the simplest to the most complete:

- **Static–linear analysis:** This is a very approximated analysis which cannot evaluate effects such as:
 - Stress redistribution;
 - Geometrical Nonlinearities;

- Material Nonlinearities;
- Membrane Actions.

As it is so approximated, this analysis is used only for really easy structures, however it is also possible to consider dynamic effects by a dynamic amplification coefficient;

- **Static–Nonlinear analysis:** Unlike the described previous analysis, Nonlinear analysis allow the designer to take into account Nonlinear characteristics, as a consequence it is possible to evaluate the catenary effect in the structural members which was proved to increase structural robustness (§ 1.2).

Moreover, it is important the choice of the material constitutive laws and the representation of the nonlinear behaviour of the joints (for example with Nonlinear springs); usually it is better to develop local models in order to evaluate the correct behaviour. To consider the dynamic effect an amplification factors is used;

- **Dynamic–linear analysis:** as this is a linear analysis, geometrical and material nonlinearities cannot be model, but it is possible to evaluate directly dynamic effects;
- **Dynamic–Nonlinear analysis:** This is the most complete analysis with which is possible to consider both dynamic effects and nonlinearities. Three-dimensional nonlinear models are used, due to this the computational cost is very high and only expert designers can perform this kind of analysis.

Considering all the aforementioned features, to perform the analysis in this thesis it is used a **Static–Nonlinear analysis** with the finite element software DIANA FEA 10.2 (TNO DIANA) considering both material and geometrical Nonlinearities. The DIANA FEA 10.2 software also allows to define the model both through a graphical interface and the implementation of an encoding language developed in parallel with the Python programming language.

2.2 Model with DIANA FEA

This section describes the characteristics of the Finite Element Model used for the parametric study developed in this thesis and the following analysis on the effects of corrosion on the material properties. As it was chosen to perform a Nonlinear analysis the finite element software DIANA FEA (TNO DIANA) is used. This software allows to take into account geometrical and material nonlinearities and it has been widely used for this type of analyses.

The operation of the software is based on several steps. The sequence to be followed is the one used in most of the finite element software, which is to define all the geometries and the material properties first, choosing between a 2D or 3D model depending on the complexity of the structure under consideration and the results that one wants to obtain. In this thesis a 2D model is preferred due to the symmetry condition and the fact that only in-plane loads and displacement are studied. Furthermore, the material properties are applied to the element geometry, the mesh is defined in order to be sufficient to evaluate geometrical and material nonlinearities and to be as much regular as possible, in the end the analysis characteristics are defined. The measure used in the FEM model are defined as starting input in N for loads and mm for dimensions.

Following the aforementioned steps, first it is defined the model geometry with all the characteristics of the materials and the mesh elements that are used, after which it is possible to proceed with the assignment of all the characteristics to the individual elements geometry. The mesh and analysis features are the last to be defined.

All these steps can be defined using the software graphical interface or using the command console which allows to define the characteristic of the model through the programming language *Python*. This interaction between DIANA FEA 10.2 (TNO DIANA) and Python facilitates the development of the parametric study through the use of loops; to do so is necessary to parameterize all the geometrical and mechanical properties depending on the starting parameters, such as the geometrical inputs and the material properties, some of them that are fixed and other that are variable depending on the characteristic that want to be studied. For example, to define the concrete constitutive law inputs it is necessary only the starting value of the compressive strength, f_c , from which all the other parameters are derived by the equation listed in the following paragraph 2.2.2.

Furthermore, the FE software has implemented a variety of different elements, material properties and more features that are useful for this kind of analysis.

In the following are thoroughly described all the characteristic used in the model which follow the rules of the *Guidelines for Nonlinear Finite Element Analysis of Concrete Structures (Rijswaterstaat Technical Document)*. The starting characteristics of the model are based on the validated model developed by *Botte et al.* [11] and then is modified and extended to te considered study.

2.2.1 Material Properties

The disproportionate collapse leads to the development of large deformations in the structural members, as a result of which, plasticisation in the materials are generated. In order to be able to represent the correct behaviour of the elements under this conditions, it is necessary to model the materials considering nonlinear constitutive models, both for concrete and steel.

In addition, as crushing of concrete and rupture of the reinforcement is expected, those two conditions are implemented in the material properties considering the full development of the constitutive models with softening branches after the maximum stress is reached.

CONCRETE

The concrete behaviour needs to be represented both in tensile and compressive state in the stress–strain relationship as cracking and crushing are expected during the development of the displacement–controlled analysis. Furthermore, a *total strain–based rotating crack model* is used, which allows the rotations of principal strains with increased load and so the crack plane is always normal to the principal tensile strain direction. In addition, using this crack model allows to not consider a shear stiffness reduction, thus no variable shear retention is modelled. The material properties of concrete are based on the linear–elastic properties of the Young’s modulus E_c , and the Poisson ratio, ν .

In the tension and compression stress–strain relationships are considered the softening branches that depends on different parameters and they can be approximated with different curves.

First of all, to model the tensile behaviour of concrete is assumed the Hordijk relationship

to represent the exponential-type softening diagrams as shown in Figure 2.1. The parameters necessary to represent this behaviour are the tensile strength, f_t , the fracture energy, G_f , and the equivalent length, h_{eq} . As it is shown in Figure 2.1, the area under the curve should be equal to the fracture energy divided by the equivalent length. The equivalent length is an important parameter for this kind of constitutive models where the softening branches are considered in the stress-strain relationships, this is also known as the crack-band width. The method used to define h_{eq} is based on the initial direction of the crack and the element dimensions.

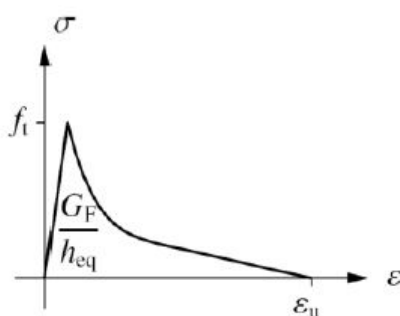


Figure 2.1: Tensile stress-strain relationship with Hordijk softening

The compressive behaviour of concrete is instead defined by the parabolic compression diagram (see Figure 2.2), where the compressive softening is a function of the compressive fracture energy G_c , which is derived from the tensile fracture energy (see equation (2.4)). This diagram is recommended when performing this kind of analysis where plasticisation of the material is expected, while simple elastic-plastic diagram or the parabolic-rectangular diagram are not advisable because they do not model the degradation after the peak strength.

In the software DIANA FEA, this stress-strain relationships can be defined with the Material library once it is chosen the total strain based crack model as first input. It is possible to define separately the tensile and compressive curve typing all the necessary parameters that are derived from the compressive strength, f_c , of concrete.

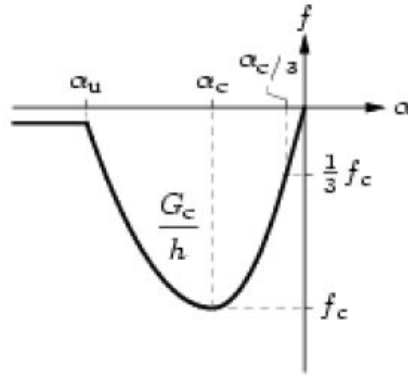


Figure 2.2: Parabolic compression diagram

The equations to derive the input parameters of the diagrams are listed below:

Young's modulus [MPa]:

$$E_c = 22000 \left(\frac{f_c}{10} \right)^{0.3} \quad (2.1)$$

Tensile Strength [MPa]:

$$f_t = 0.3 f_c^{\frac{2}{3}} \quad (2.2)$$

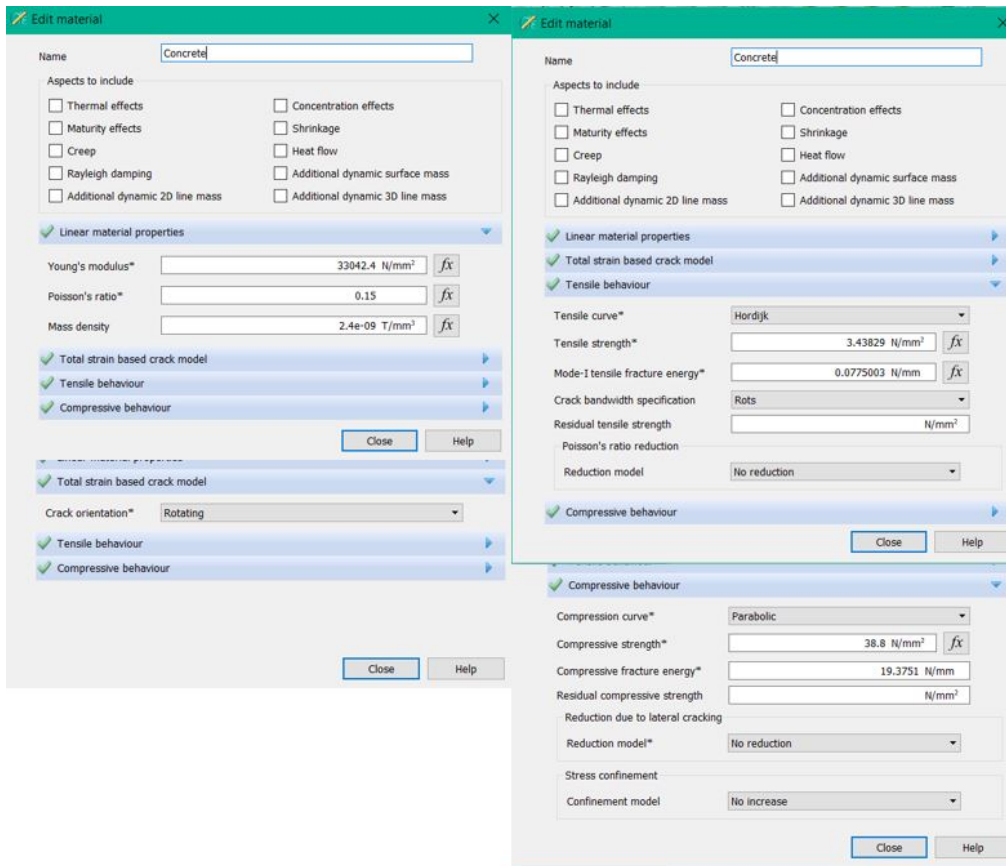
Fracture Energy [N/mm]:

$$G_{f1} = G_{f0} \left(\frac{f_c}{10} \right)^{0.7} \quad G_{f0} = 0.030 (d_{max} = 16\text{mm}) \quad (2.3)$$

Compressive Fracture Energy [N/mm]:

$$G_{f_c} = 250 G_{f1} \quad (2.4)$$

By computing all these equation in the command console and using the programming language connected to DIANA FEA for the material library, both the tensile and compressive laws are obtain as input as shown in Figure 2.3



(a) Graphical interface

```
#PROPERTIES
f = 38.8 #compressive strength
Ec = 22000*(pow((f/10),0.3)) #Young's modulus
fct = 0.3*(pow(f,(2/3))) #tensile strength
Gf0 = 0.03 #dmax 16 mm
Gf1 = Gf0*(pow((f/10),0.7)) #Fracture energy
Gfc = 250*Gf1 #Compressive fracture energy
nu_c = 0.15 #poisson coefficient
gamma_c = 2.4e-09 #peso specifico cls

#1. CONCRETE CONSTITUTIVE LAW
addMaterial( "concrete", "CONCR", "TSCR", [ ] )
setParameter( "MATERIAL", "Concrete", "LINEAR/ELASTI/YOUNG", Ec )
setParameter( "MATERIAL", "Concrete", "LINEAR/ELASTI/POISON", nu_c )
setParameter( "MATERIAL", "Concrete", "LINEAR/MASS/DENSIT", gamma_c )
setParameter( "MATERIAL", "Concrete", "MODTYP/TOTCRK", "ROTATE" )
setParameter( "MATERIAL", "Concrete", "TENSIL/TENCRV", "HORDYK" )
setParameter( "MATERIAL", "Concrete", "TENSIL/TENSTR", fct )
setParameter( "MATERIAL", "Concrete", "TENSIL/GF1", Gf1 )
setParameter( "MATERIAL", "Concrete", "COMPRS/COMCRV", "PARABO" )
setParameter( "MATERIAL", "Concrete", "COMPRS/COMSTR", f )
setParameter( "MATERIAL", "Concrete", "COMPRS/GC", Gfc )
```

(b) Encoding language

Figure 2.3: Concrete constitutive law input

REINFORCEMENT

In modelling the reinforcing steel an elastic–plastic material model with hardening is used. In the stress–strain relationship it is also explicitly represented the rupture of the reinforcement once it is reached the ultimate strain with a descending branch and a consequently horizontal branch after the complete loss of resistance. The constitutive law

adopted is shown in Figure 2.4.

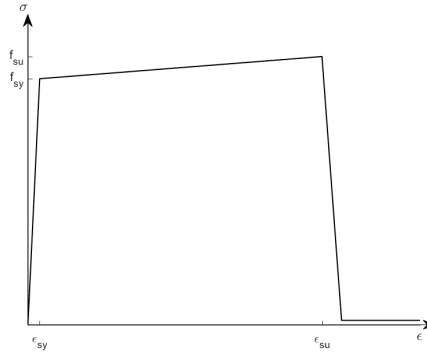


Figure 2.4: Constitutive model for Reinforcement

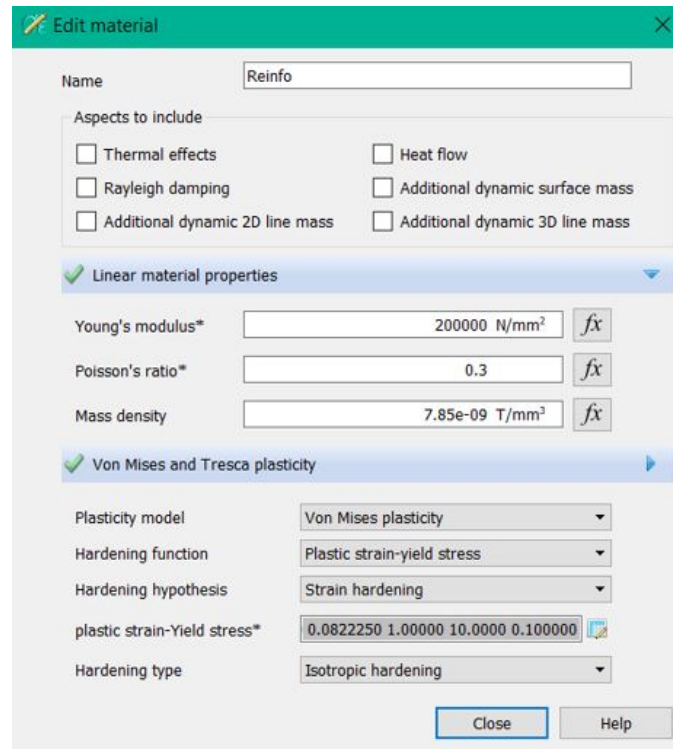
In order to define this diagram in the finite element software, the Tresca/Von Mises Plasticity option is used considering an isotropic hardening. The parameters necessary to describe the diagram are the Young's modulus for reinforcement, E_s , the yielding strength, f_y , the yielding strain, ϵ_y , the ultimate strength, f_u , the ultimate strain, ϵ_u , and the value of σ and ϵ that are necessary to define the last point of the tensile diagram after rupture of the reinforcement.

This diagram is used both for tensile and compressive behaviour of reinforcement as it is sufficient for this analysis and no cycling loads are considered, thus buckling of reinforcement is not modelled in this study.

2.2.2 Mesh and Elements Properties

The finite element software DIANA FEA allows to model the geometry separately in the first step, then during meshing and analysing are considered all the interaction between concrete and reinforcement elements. As the model is composed by 2D reinforced concrete elements, only reinforcement and concrete elements need to be modelled.

For the concrete elements, *Plane stress elements* are used as in this analysis are analysed only in-plane membrane actions, vertical reactions and the applied loads, such the self-weight and the uniform distributed load. The value of the thickness, which is uniform throughout the respective element, is defined with the appropriate command box.



(a) Graphical interface

```
#Reinforcement
Es = 200000 #Young's modulus
fyd = 555 #MPa Yielding strength
fud = 605 #MPa Ultimate strength
epsyd = fyd/Es #Yielding strain
epsud = 0.075 #Ultimate strain
nu_s = 0.3 #poisson coefficient
gamma_s = 7.85e-09 #peso specifico acciaio

#3. STEEL CONSTITUTIVE LAW
addMaterial( "Reinfo", "KSTEL", "TRESCA", [ ] )
setParameter( "MATERIAL", "Reinfo", "LINEAR/ELASTI/YOUNG", Es )
setParameter( "MATERIAL", "Reinfo", "LINEAR/ELASTI/POISSON", nu_s )
setParameter( "MATERIAL", "Reinfo", "LINEAR/MASS/DENSITY", gamma_s )
setParameter( "MATERIAL", "Reinfo", "TREPLA/TRESSH", "KAPSIG" )
setParameter( "MATERIAL", "Reinfo", "TREPLA/KAPSIG", [ ] )
setParameter( "MATERIAL", "Reinfo", "TREPLA/KAPSIG", [ 0, fyd, (epsud-epsyd), fud, (epsud-epsyd)+0.01, 1, 10, 0.1 ] )
```

(b) Encoding language

Figure 2.5: Steel constitutive law input

The numerical integration scheme is defined by default depending on the type of mesh element which is applied. In this study eight–node quadrilateral isoparametric plane stress elements are used to model beams and columns, because geometry nonlinearities are considered and four–node quadrilateral isoparametric plane stress elements showed to not be compatible with this condition in the performed nonlinear analysis.

In particular, the mesh defined to be sufficient for the beam is composed by 12 elements

along the height and along the length is divided considering the elements dimension in order to obtain a regular mesh and to not have distortion. The mesh elements in the columns are defined consequently to maintain a regular mesh correctly connected to the beam elements.

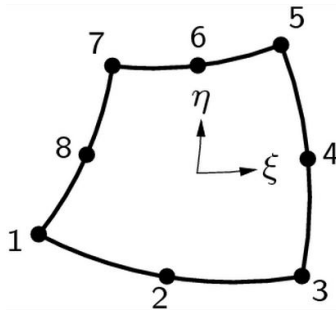


Figure 2.6: CQ16M

The elements are indicated with the name **CQ16M**. They are based on quadratic interpolation and Gauss integration, by default DIANA applies 2×2 integration scheme.

The modelling of reinforcement is realized considering the *Embedded reinforcement* option from the Element Library implemented in DIANA. This type of reinforcement discretisation add its stiffness to the element it is embedded in, but it does not contribute to the weight of the element. The main characteristics that are defined in the manual are:

- Reinforcement are embedded in structural elements, the so-called *mother elements*. In this case the structural elements are beams and columns;
- This type of reinforcement does not have degrees of freedom of its own;
- The strains in the reinforcements are computed from the displacement field of the *mother elements*;

The last feature implies perfect bond between reinforcement and concrete, so slip of the reinforcement is not considered because not investigated in this study. As the reinforcement is defined by a line in the 2D model, the area of the cross-section is the first input during the properties assignment. In the study is applied the processing from section input option to locate the points of the reinforcement that is embedded in the plane stress element.

2.2.3 Numerical Analysis

To perform this study the Static–nonlinear analysis available in DIANA FEA is used. The input of the analysis are the last to be defined in the Analysis command console adding a Structural Nonlinear Static Analysis as dynamic effect are not investigated. As it is defined

in the section 2.1 the analysis takes into account geometrical and material nonlinearities and this is possible with the Static–Nonlinear Analysis which is adopted in the model.

Once it is add the Analysis file and the Command file related to the structural nonlinear analysis it is possible to add the execution steps that define how the analysis is performed. In this model is used a load controlled procedure considering the input *Execute steps Load steps* in the execute command block. As it is applied this kind of procedure and in the load–displacement graphs are expected softening branches, the general arc–length algorithm method is implemented in the calculation scheme, this option allows to analyse such behaviours as *snap-through* and *snap-back* using a load controlled procedure as shown in Figure 2.7. The load controlled procedure is used in order to evaluate the ultimate behaviour of the reinforced concrete elements in the model by applying the loads step–by–step, i.e. the self–weight and the uniform load.

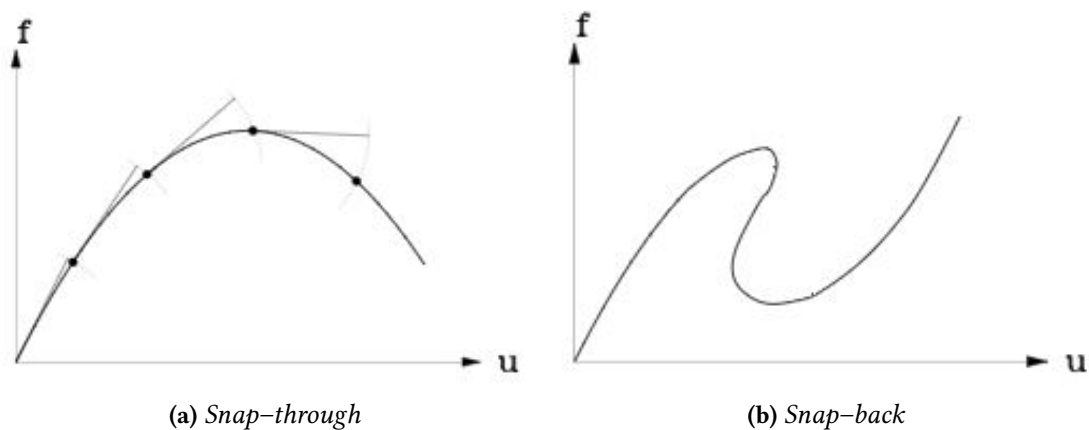


Figure 2.7: Arc–length control

The input to be applied in the analysis are several and they can be defined by the Execute blocks available in DIANA; with these blocks it is possible to define the type and number of steps to consider, the same command file may contain more execute blocks depending on the different parameters that have to be applied. For example, in this model are used two execute blocks, one for the self–weight and the another for the acting uniform load which represent the incremental action used to study the ultimate behaviour of the beam because it is more representative for the failure mode under consideration.

The characteristic of the execute blocks are given below:

- **Load steps:** This command defines the number and size of steps in which the load are applied. For both the execute blocks is used the *User specified sizes* option, the Self-weight is applied in 10 load steps with a size of 0.1, while the uniform load is applied in a number of steps that is sufficient for the performed analysis, in general are performed from 800 to 1400 load steps; the size is 1.0 for all the analysis;

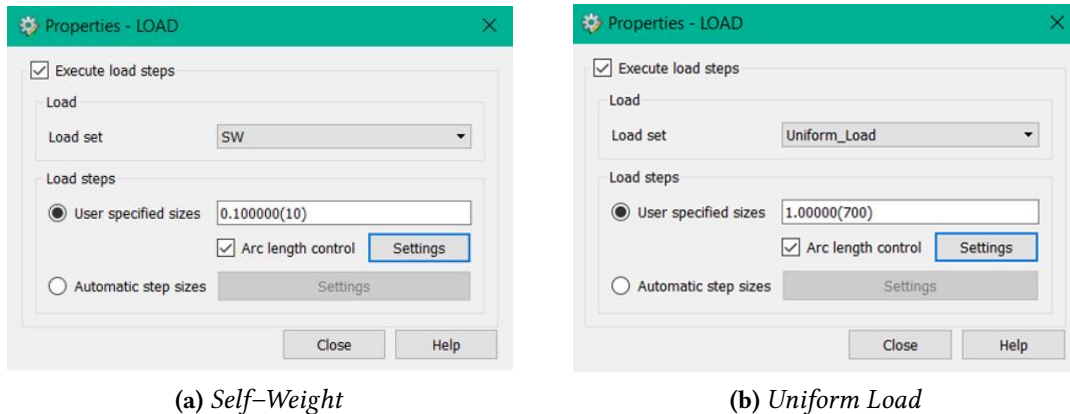


Figure 2.8: Load steps input for the applied load

- **Equilibrium iteration:** The Secant (Quasi-Newton) iteration method is applied with a maximum number of iteration equal to 50 for the applied uniform load, while for the self-weight is sufficient the Newton-Raphson iteration method with 10 iteration as it is totally applied after 10 load steps. The line search algorithm is also implemented to enlarge the radius of convergence of the iterative solution method;
- **Convergence criteria:** in this analysis the combination of both force and displacement convergence criteria are applied simultaneously with a tolerance of 0.01;

The output of the analysis are the global displacement and the reaction forces in the supports as the aim of the parametric analysis is to evaluate the load-displacement diagram in order to define the ultimate behaviour of the RC frame in the situation of loss of a load bearing column. DIANA allows to use the option *Tabulated* in the output command box in order to define an output file, which contain the displacement and the reaction forces, for the specified nodes. In particular it is defined as output for the displacement in midspan, where the column is removed, and the membrane action at the supports. As the obtain Tabulated output file contains many unnecessary information, it is possible, thanks to the

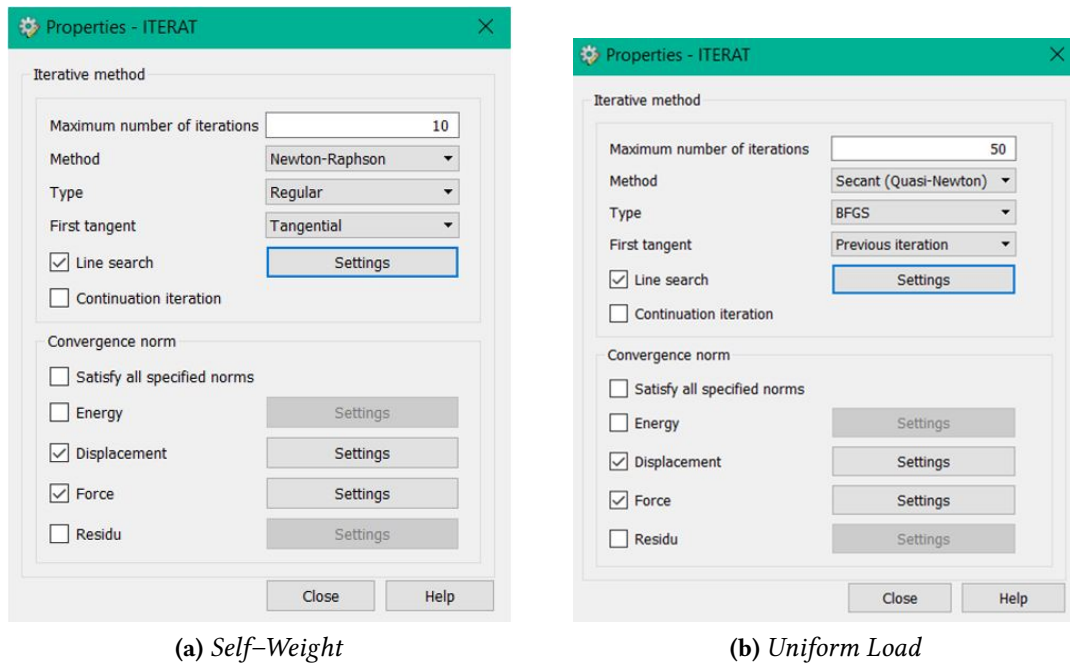


Figure 2.9: Equilibrium iteration input for the applied load

Python encoding language associated to DIANA to extrapolate a .txt file from the Tabulated output collecting only the values of interest with the appropriate set of commands. This facilitates the analysis of the result with the post-processing done with Matlab.

The Nonlinear analysis is thus performed until failure of the elements which is governed by crushing of concrete and then rupture of the top reinforcement in the beam-column joint; after that the analysis can be considered ultimated and it is possible to process all the results obtained from the analyses collecting them considering the common parameter as it is defined in Chapter 3

Chapter 3

Definition of the parameters used to perform the parametric analysis

3.1 Introduction

This thesis has two main objectives, one is to perform a parametric analysis on the robustness assessment in reinforced concrete systems defining a 2D FEM model using the DIANA FEA software, this analyses are aimed on defining the parameter which influence the most the development of membrane actions in the investigated reinforced concrete frame ultimate behaviour; the second purpose is to analysed the interaction between the degradation phenomenon of corrosion and the ability of the RC structure to develop alternative load path during its working life.

In this Chapter are thoroughly described the model geometry realized with the software DIANA FEA 10.2 (TNO DIANA) and the characteristics of the performed parametric analysis. In particular are investigated the influences of geometrical and mechanical parameters, such as the cross-sections and the lengths of beams and columns, the ultimate reinforcement strain, ϵ_{su} , and the resisting moment of the elements, M_{rd} , on the development of membrane actions in the structural members after the notional removal of a load-bearing

column. The results of all the performed analysis are plotted and then commented in the following Chapter 4.

Performing a parametric analysis in DIANA FEA can be done in different ways. The simplest way is to change by hand the model's inputs, one by one, using the geometrical software interface and creating as many models as the analysis require; this procedure is already time consuming without considering the computational time needed to run the nonlinear analysis itself. In addition, each model will occupy a lot of space in the processor as for the analysis output files. For these reasons and considering that the parameters to be changed are several, this way is not suitable and thus not adopted.

The other method which can be used to define the analysis inputs require the use of the Python programming language as it is described in the previous Chapter. In fact, by saving the file `.py` from the specific command in DIANA or taking it from the folder `.DianaIE` where is automatically saved, it is possible to parameterize all the characteristics of the model, geometrical and mechanical. Once the `.py` file which include the starting geometry is complete and all the data are defined as functions of the starting inputs, it is possible to create all the necessary codes to perform the parametric analysis. In this study, as it is performed a parametric analysis, i.e. it is studied the behaviour considering one variable parameter maintaining constant the others, it is sufficient to perform only *for loops* for each variable input that is considered. This method also allows the direct definition of the before mentioned formulas with which calculate the mechanical inputs (see equations in § 2.2.2).

3.2 Model Geometry

The starting geometry of the model is based on the structure designed by *Droogné et al.* [5]. This is then implemented in the FEM model and adapted to the considered situation in order to perform all the analyses.

The structure under consideration is a reinforced concrete frame (a regular office building) designed following the Belgian Code of construction and the Eurocodes EN 1992-1-1 to evaluate the acting loads, such as wind and gravity loads, seismic actions are not considered. The building investigated in this thesis is a 3 floor building, each floor is 3 m high, the beams span is 6 m and the building imprint cover a surface of 2592 m² as shown in Figure 3.1. The reinforced concrete structure has an extension in y-direction of 72 m and

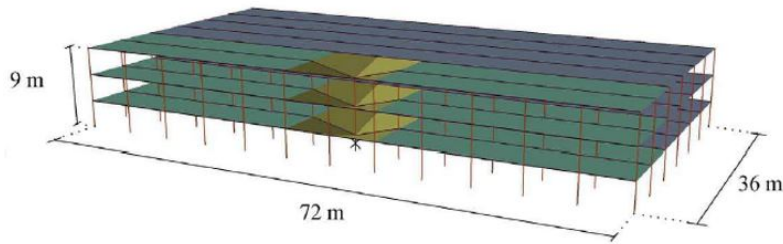


Figure 3.1: Investigate Building Geometry with the removal of a column

in x -direction of 36 m. As it is a RC frame it is sufficient to realize a 2D model (as introduced in section 2.2) of the frame which is subjected to the column removal in order to perform all the necessary analyses instead of a 3D model. As a result, 3D effects are not considered and also the restraint in transverse direction is not investigated in this study. This simplification is also done to reduce the computational time.

Furthermore, with the respect of the symmetry condition it is possible to represent only half of the frame subjected to the column removal placing the correct symmetry support where the column is removed (see Figure 3.2). As the aim of this thesis is to investigate the ultimate behaviour of the frame directly connected to the removed column depending on the rotational capacity of the joint, the 2D model is defined including the direct affected beam and the adjacent elements, such as the two columns and the adjacent beam.

The boundary condition adopted in this first approximation are hinges for all the adjacent elements in order to evaluate the behaviour of the RC frame allowing an higher rotation in the joint, which will mainly depend on the cross-section of the elements. All the geometrical features, the boundary conditions and the loading conditions can be found in Figure 3.2

The design is based on the requirements regarding robustness according to EN 1991-1-7. In order to satisfy these requirements, the reinforcements is designed to be sufficient to act as horizontal and vertical ties. Moreover, the horizontal stiffness is provided in one direction by the RC frames, while in the other direction, i.e. the x -direction, a bracing system is placed to cover this purpose. The floors consist of precast hollow core concrete slabs supported by the transverse beams.

The design of the structural members and reinforcement is defined according to the permanent load applied on the beams which consists of the self-weight g_k of the concrete

Table 3.1: Geometrical properties

| | | Internal frame | Edge frame |
|----------------|----------------------|-----------------------|-------------------|
| Columns | Dimensions b x h | 420x350 | 420x350 |
| | Reinforcement | 12 Φ 14 | 8 Φ 14 |
| Beams | Dimensions b x h | 420x450 | 420x450 |
| | Top Reinforcement | 4 Φ 25 | 4 Φ 18 |
| | Bottom Reinforcement | 3 Φ 20 | 2 Φ 18 |
| | Shear Reinforcement | Φ 10 | Spacing 150 |

Distances, dimensions and diameters in mm

floors, equal to 6.25kN/m^2 and to the applied variable load q_k equal to 3kN/m^2 , as recommended by EN 1991-1-1 for office building. The snow and the wind loads are computed following the Belgian National Annexes of the EN 1991-1-3 (2003) and EN 1991-1-4 (2005). The concrete used in the design is C30/37 and steel is BE500S (ductility class C) from the Belgian sample. As a Latin Hypercube Sampling was performed to evaluate the most important material properties, the values of concrete and steel strengths are taken as: $f_c = 38.8\text{MPa}$ for the concrete compressive strength, while, for the reinforcement yielding and ultimate strengths, are assumed respectively $f_y = 555\text{MPa}$ and $f_u = 605\text{MPa}$

In this study is investigated the ultimate behaviour of the structural members of the edge frame of the building, chosen considering also the following analyses on the corrosion effects, which are worst on elements directly exposed to the environment. The acting loads on the edge frame are half of the loads acting on the inner frames, as a result, is placed less reinforcements in the edge beams than in the inner one, as can be seen in Table 3.1, together with the cross-sectional dimensions of the elements. In order to represent the structure in a more realistic way and to analyse the ultimate behaviour of the RC beam, in the FEM model it is applied a uniform load which is incremented step-by-step during the nonlinear analysis. This method showed to be a more representative way for the failure mode of the RC frame [5].

The parametric analysis consists of the different phases. First of all, it is investigated the influence of the members geometry changing, for example, the cross section or the length of the structural elements. This is done changing one geometrical parameter at the time

and keeping constant the others. Then the investigation is extended considering a variable ultimate strain of the reinforcement for all the geometrical variable properties studied in the first analysis. Finally it is performed a last parametric analysis on the influence, on the ultimate behaviour of the frame, of a constant resisting moment with the variable geometry, this consists in a variable amount of reinforcement with the variable geometrical cross-section.

It is chosen to start from the edge frame because it has less reinforcement, as a result the resistance is lower than the inner frame, plus this choice is connected to the following analysis of the corrosion effects of the frame. As the only difference between the two frames consist in the reinforcement amount, the behaviour of the inner frame can be obtained just performing a nonlinear analysis considering a variable geometric percentage of reinforcement, $\rho = \frac{A_s}{A_c}$ correspondent to the one in the inner frame. Various researches denote that the increment of reinforcement percentage maintaining the same geometry of the element lead to a consistent improvement in the load-bearing capacity, thus it is expected to have a higher resistance both in compressive and in tensile membrane actions, this is also showed by the last set of analyses on the influence of a constant resisting moment.

3.3 Parametric Analysis: Geometrical Properties

The first part of the parametric analysis aim to define the influence of geometrical parameters on the development of membrane actions in the investigated case.

First of all, the geometry of the direct affected beam is changed. Then is investigated the condition of a variable geometry in the adjacent members in order to define their influence on the capacity of developing alternative load paths.

The starting geometry of the reinforced concrete frame is designed with a beam length $L_b = 6\text{m}$ and a column height $L_c = 3\text{m}$, while the cross-sections are 420x450 mm and 420x350 mm respectively, as shown in Table 3.1. Starting from these values the parametric analysis proceeds as explained in the following sections. The mechanical parameters when performing these analyses are assumed constant and equal to the designed office building.

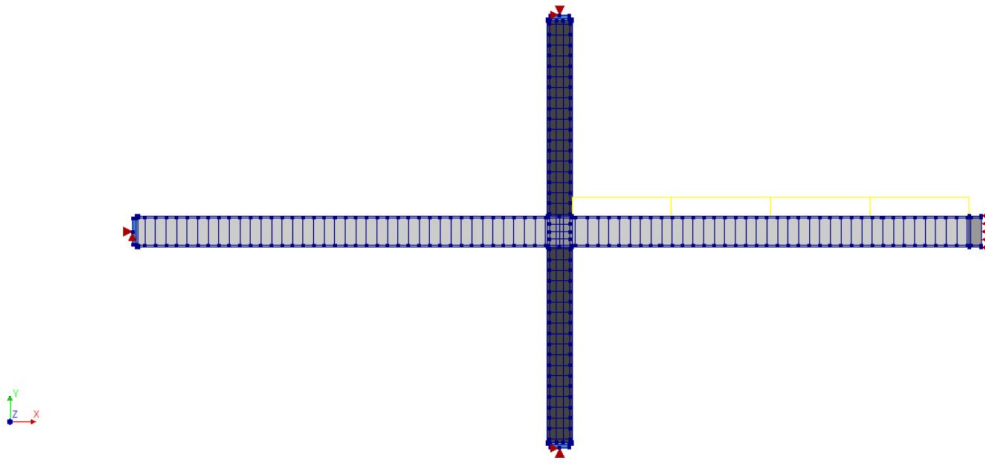


Figure 3.2: Starting geometry of the finite element model in DIANA FEA (from Droognè et al.[5])

3.3.1 Beam Cross-Section

The cross-section shows in numerous researches to have the highest influence on the development of alternative load path, especially on the development of compressive membrane actions (CMA) which is the first branch in the load-displacement diagram, as it is defined in Chapter 1 and showed in Figure 1.4. In fact, the behaviour depending on the Compressive membrane actions can be seen in the load-displacement diagram if the horizontal restraint is considered when defining it, if the element is considered unrestrained horizontally, the load-displacement diagram shows to reach a lower maximum value of resistance and this stays constant until failure of the element as shown in Figure 1.2.

During the loading procedure the joint is subjected to a horizontal displacement, first outward when CMA starts to develop and then inward when the tensile membrane action regime take place in the beam. As it is studied the behaviour considering the load-displacement diagrams, it is possible to define the element behaviour as related to the stiffness following the relationship $F = K\delta$, where the stiffness K represent the slope of the curve.

The horizontal displacement, δ , is governed mainly by the horizontal stiffness of the

beam as it is defined in the force–displacement relationship:

$$F = \frac{E_b A_b}{L_b} \delta \quad \longrightarrow \quad K_\delta = \frac{E_b A_b}{L_b} \quad (3.1)$$

where E_b is the Young's modulus of concrete, L is the beam length and $A_b = A_c + nA_s$ is the homogenised area of the beam cross–section. Further, δ depends in minimum part by the flexural stiffness of the columns, in fact if one analyses the behaviour of the two columns, this corresponds to the one of an element loaded in midspan by a concentrated force. In this condition the relationship between load and displacement can be obtained from the following equation and from that is derived the stiffness to the horizontal translation given by the two columns:

$$F = \frac{48E_c I_c}{L_c^3} \delta \quad \longrightarrow \quad K = \frac{48E_c I_c}{L_c^3} \quad (3.2)$$

where E_c is the Young's modulus of concrete in the columns (if different from the concrete in the beams), I_c is the moment of inertia of the columns evaluated in the direction of the displacement and L_c is the total length of the two columns. In the equation 3.2 is illustrated the simplified condition where the two columns have the same length.

Consequently, the ability to develop membrane actions and, therefore, the way in which the load–displacement diagram develops, are directly proportional to the cross–section of the RC beam subjected to the column removal, and inversely to the length, which is shown in the analyses to have a lower effect on the load–bearing capacity.

The parametric analysis is performed considering a variable base–height ratio between 1.4 and 0.76, the parameter that is changed is the beam height, H_b , while the beam base is kept constant equal to the starting geometry $B_b = 420\text{mm}$. All the others geometry parameters are kept constant equal to the starting geometry, their variation is investigated in the following sections.

The adopted variable beam heights are listed below, with the correspondent base–height ratios:

- $H_b = 300\text{mm} \quad \frac{B_b}{H_b} = 1.4$
- $H_b = 350\text{mm} \quad \frac{B_b}{H_b} = 1.2$
- $H_b = 450\text{mm} \quad \frac{B_b}{H_b} = 0.93$

$$\bullet H_b = 550\text{mm} \quad \frac{B_b}{H_b} = 0.76$$

First of all it is changed the dimensions of both the beam, then it is investigated the ultimate behaviour of the reinforced concrete frame considering only the dimensions of the adjacent unloaded beam as variable.

3.3.2 Beam Length

The starting geometry of the reinforced concrete frame is designed with a beam length of 6 m. Following the removal of a load bearing column, the direct affected beam is subjected to a loss of support on one side. As a results the static scheme changes and the beam duoble its length, in order to represent this in the FEM model a symmetry support is placed in correspondence of the removed column as shown in Figure 3.2.

It is adopted a variable length of the beam in the range of 3 to 6 meters as listed below:

$$\begin{aligned} \bullet L_b = 3\text{m} & \quad \frac{L_b}{H_b} = 6.67 \\ \bullet L_b = 4\text{m} & \quad \frac{L_b}{H_b} = 8.89 \\ \bullet L_b = 5\text{m} & \quad \frac{L_b}{H_b} = 11.11 \\ \bullet L_b = 6\text{m} & \quad \frac{L_b}{H_b} = 13.33 \end{aligned}$$

This sets of analyses is performed considering a variable length in the adjacent beam in order to complete the investigation on the influence of the adjacent beam geometry on the ultimate behaviour of the direct affected beam to the notional removal of the load-bearing column.

3.3.3 Column Length

In the considered model it is investigated also the influence of the adjacent column to the development of compressive and tensile membrane action. These structural components influence the joint behaviour with their stiffnesses, as a consequence they have an effect on the horizontal displacement, δ , and on the rotation, ϕ , that arise in the joint after the removal of the supporting column. They act on the horizontal displacement as explained in

§ 3.3.1 through the stiffness in equation 3.2, while on the rotation with the flexural stiffness related to the acting moment:

$$M = c \frac{EI_c}{L_c} \phi \quad \longrightarrow \quad K_\phi = c \frac{EI_c}{L_c} \quad (3.3)$$

where c is a coefficient which depends on the support conditions.

It is possible to observe that the column length, L_c , in both the equations is located at the denominator. As a result, increasing the length the stiffnesses decrease and then the resistance should decrease with an increasing length.

The different length dimensions investigated in this analysis considered a variable column length as:

- $L_c = 3\text{m}$ $\frac{L_c}{H_c} = 8.57$
- $L_c = 4\text{m}$ $\frac{L_c}{H_c} = 11.42$
- $L_c = 5\text{m}$ $\frac{L_c}{H_c} = 14.28$

3.3.4 Column Cross-Section

The columns cross-section has the same effect as the length, i.e. it acts on the horizontal displacement and the rotation in the beam-column joint. The differentiation of the analysis considering first a variable length and secondly a variable cross-section allows to define the parameters that influence the most the ultimate behaviour of the joint and in which way they act on it. The effect of the cross-section is contained in the moment of inertia equation, in particular it depends on the height of the column cross-section to the power of 3, as a result, this is the parameter which is changed in the parametric analysis while the base is kept constant to the one in the starting geometry, $B_c = 420\text{mm}$. The base-height ratios are the same in § 3.3.1

- $H_c = 300\text{mm}$ $\frac{B_c}{H_c} = 1.4$
- $H_c = 350\text{mm}$ $\frac{B_c}{H_c} = 1.2$
- $H_c = 450\text{mm}$ $\frac{B_c}{H_c} = 0.93$
- $H_c = 550\text{mm}$ $\frac{B_c}{H_c} = 0.76$

3.4 Parametric Analysis: Mechanical Properties

3.4.1 Ultimate Reinforcement Strain, ϵ_{su}

The steel used in the design is the Belgian BE500S with ductility class C and the ultimate strain considered in the starting geometry and mechanical parameter is taken as $\epsilon_{su} = 7.5\%$. The parametric analysis described in the previous paragraphs are performed with this constant ultimate strain. Once all the results are obtained and the influence of the geometrical parameters on the development of compressive and tensile membrane actions is observed, it is possible to evaluate the influence of the mechanical parameters.

As a start of this analysis it is chosen to investigate the ultimate reinforcement strain, ϵ_{su} , therefore the ductility of the reinforcement is changed. In fact, the plastic deformation capacity and so the robustness of a reinforced concrete structure depends mainly on the ductility of the reinforcing steel. Based on this parameter the reinforced concrete frame can show or not the arise of tensile membrane action. It was found that the ultimate reinforcement strain has a big influence on the load bearing capacity in the regime of tensile membrane action [11].

The same analysis performed varying the geometrical properties with an ϵ_{su} of 7.5% are performed with different values of ultimate strain capacity as listed below:

- $\epsilon_{su} = 2.5\%$
- $\epsilon_{su} = 5.0\%$
- $\epsilon_{su} = 12.5\%$

These values are considered in order to define the influence of the ultimate strain on the load-bearing capacity of the investigated reinforced concrete frame. As these analyses are performed with a variable geometry of the investigate frame, it is also possible to evaluate if the ultimate strain varies its influence changing the geometrical properties.

The ultimate reinforced strength used in all the analysis is equal to $f_u = 605\text{MPa}$ and the yielding strength is $f_y = 555\text{MPa}$ according to the steel mechanical properties and as explained in section 3.2.

3.4.2 Resisting Moment, M_{rd}

The last set of parametric analysis is based on the elements resisting moment M_{rd} which is kept constant to the one computed in the starting geometry. The beam resisting moment is evaluated in the support section because the element final failure is the rupture of the top tensed reinforcement in correspondence of the connection between beam and columns while the resisting moment in the columns is computed considering the acting axial force $N_{Ed} = 650\text{kN}$. The respective value of resisting bending moment are $M_{b_{rd}} = -195\text{kNm}$ and $M_{c_{rd}} = 170\text{kNm}$.

This analysis is associated with the variable geometry of the elements, as a consequence, in order to keep constant the resisting moment with the variable concrete resisting area, the area of the reinforcement need to be changed.

In the investigate RC frame, the beam which is analysed is subjected to prevalent bending moment, and the designed reinforcement in the edge frame correspondent to the starting geometry is $A_{s_{tensed}} = 4\Phi 18$ (at the top) and $A_{s_{compressed}} = 2\Phi 18$ (at the bottom), these are continuous along the beam section. As approximation on safety side, the area of compressed reinforcement is not considered. The tensed reinforcement areas associated with a variable beam height are listed below:

- $H_b = 300\text{mm}$ $A_{s_{tensed}} = 7\Phi 18$ ($\rho_s = 0.014$)
- $H_b = 350\text{mm}$ $A_{s_{tensed}} = 6\Phi 18$ ($\rho_s = 0.01$)
- $H_b = 550\text{mm}$ $A_{s_{tensed}} = 3\Phi 18$ ($\rho_s = 0.003$)

The columns are subjected to both bending moment and axial force. In this condition of buckling the reinforcement computed in the starting geometry is equal to $A_s = 8\Phi 14$ distributed homogeneously in the columns. The variable concrete area in the columns lead to the variable reinforcement areas as defined below:

- $H_c = 300\text{mm}$ $A_{s_{tensed}} = 12\Phi 14$ ($\rho_s = 0.014$)
- $H_c = 450\text{mm}$ $A_{s_{tensed}} = 4\Phi 14$ ($\rho_s = 0.003$)

The section $H_c = 550\text{mm}$ is not considered in this study because the constant M_{rd} lead to a reinforcement geometrical percentage ρ_s inferior than the minimum percentage defined in the Eurocode.

In this way it is possible to compare the same concrete cross-section with variable percentage of reinforcement while keeping constant the resisting moment. The results are show in Chapter 4

3.5 Parametric Analysis: Elements Stiffnesses

In the previous Chapters is introduced the important role of the horizontal restrain conditions to the development of alternative load paths in concrete structures.

As it is showed in the load-displacement diagram in Figure 1.4 the compressive membrane actions effect on the load-bearing capacity can be evaluated only if it is considered the horizontal restrained condition of the RC beam, the same consideration is done for the development of the second phase in tensile membrane actions. Therefore, thanks to the horizontal restrain condition, the load-bearing mechanism can change from bending mechanism to catenary action (see Chapter 1).

Membrane actions consist of a significant increase in the load-bearing capacities in the bending resisting mechanism and catenary action, as a result the horizontal restrain conditions become relevant in the assessment of structural robustness. In this thesis it is investigated the influence of the geometrical and mechanical properties on the development of both the load-bearing capacities, which can be translated into the influence of the members stiffnesses to the horizontal translation and to the rotation as shown in Figure 1.5.

In the study case of this thesis the restraining conditions are given from the adjacent elements, horizontally by the beams axial stiffness and the columns stiffnesses to the horizontal translation, that act as mentioned in paragraph 3.3.1, the rotation in the beam-column joint is restrained by the adjacent beam and column bending stiffness. The stiffnesses depends on the supports conditions adopted in the adjacent elements. As first approximation are adopted hinges as external supports for all the elements in order to consider a condition which allow a higher rotation (this support conditions are used for all the parametric analyses). This is a simplified way to define the formulas for all the stiffnesses that give restrain to the horizontal and vertical displacement and to the rotation of the RC beam, the formulas are defined from the linear elastic equation solutions, as given in the literature of Science of Construction. In the following formulas are considered both the contribution to the stiffnesses given by the beam and the columns:

- **Horizontal Stiffness:**

$$K_{\delta} = \frac{E_c A_b}{L_b} + \frac{48 E_c I_c}{L_{c,tot}^3} \quad (3.4)$$

- **Bending Stiffness:**

$$K_{\phi} = \frac{3 E_c I_b}{L_b} + \frac{3 E_c I_c}{L_c} + \frac{3 E_c I_c}{L_c} \quad (3.5)$$

- **Vertical Stiffness:**

$$K_v = \frac{E_c A_c}{L_c} + \frac{6 E_c I_b}{2 L_b^2} \quad (3.6)$$

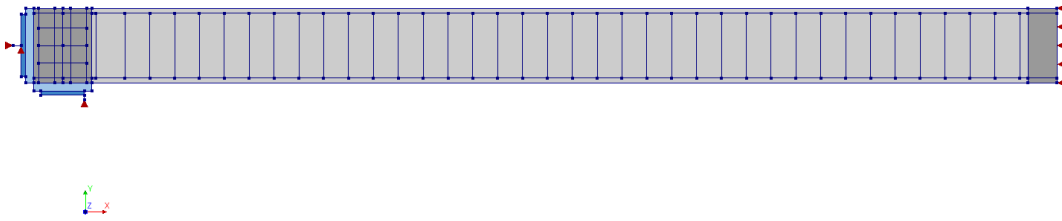


Figure 3.3: Simplified Finite Element Model geometry considering springs as the adjacent elements

Once the stiffnesses are computed it is possible to define a simplified 2D model which contains only the RC beam subjected to the notional removal of the column and the adjacent elements stiffnesses are applied by 2 *Spring elements*, one translational and one rotational. This simplified model is often use in order to evaluate the behaviour of a full frame with a lower computational time and to fastener the analysis.

The aim of this part is to compare the ultimate behaviour of the RC beam between the two models for a part of the before mentioned analysis. One can note that by substituting Plane Stress Elements with Spring element lead to a decrease in the stiffnesses implemented by the FEM model elements equations. This way of approximation is widely used in the definition of FEM model where the analysis is highly time consuming if the full frame it is represented in the model, thus as the restraining effect is done by the members stiffnesses it is possible to use this model to perform the nonlinear analysis even though the two different model lead to a different approximation of the loads.

Chapter 4

Analysis of the Results

The results observed in all the analyses are illustrated in this Chapter. In order to evaluate the load-bearing capacities, both in the bending resisting mechanism and in the catenary mechanism, of the analysed RC frame and how they are influenced by the geometrical and mechanical parameters used in the parametric analysis, the load-displacement and membrane action-displacement diagrams are given and commented in the following sections.

Accordingly to the previous Chapters, the load-bearing capacities of the members, when considering the horizontal restraining conditions, can be distinguished into two phases: the first phase where the behaviour of the beam is governed by compressive membrane actions and the resisting mechanism is based on the bending resisting mechanism and the second phase when plastic hinges arise and tensile membrane actions take place in the members. In this second phase the catenary action is the resisting mechanism which occurs when large displacement arise in the frame. Following this distinction, it is possible to define the two load-bearing capacities, first for compressive membrane actions, corresponding to the peak in the load-displacement diagram, and then for tensile membrane actions, if they have the opportunity to arise, which corresponds to the maximum load reached after the first peak when the rupture of the top reinforcement in the joint occurs. Those two load-bearing capacities are influenced by the geometrical and mechanical parameters that are analysed in the parametric analyses. Different parameters may influence them in different ways and the same parameter may affects more the first peak comparing to the TMA resistance and

vice versa. For example the ultimate reinforcement strain, ϵ_{su} , influence the ductility of the members and thus it influence the ability to develop TMA of the RC frame, while it does not have any influence on compressive membrane actions. In fact, the maximum load resistance is the same for all the different ϵ_{su} investigated values. It is clear from the performed analyses that the main influence on the load-bearing capacities is given by the directly affected beam characteristics, accordingly to other researches [11], while the adjacent elements geometry contribute more to the development of TMA as they have a higher influence on the rotational stiffness of the beam-column joint. All the following diagrams are stopped in correspondence of the rupture of the top reinforcement in the beam-column joint.

4.1 Variable Beams Geometry

CROSS-SECTION

In Chapter 3 is defined the range of variation of the beam cross-section. The analysis of this parameter is performed firstly by changing the geometry of both the beams represented in the FEM model, in this way it is possible to evaluate the influence given by the cross-section of the RC beam directly subjected to the column removal. Then the analysis is extended to a variable cross-section of the adjacent beam, thus it is investigated the effect of the horizontal stiffness $K_\delta = \frac{EA_b}{L_b}$ given by the adjacent beam. In order to distinguish these two cases, the variable heights are indicated respectively with Hb_1 and Hb_2 .

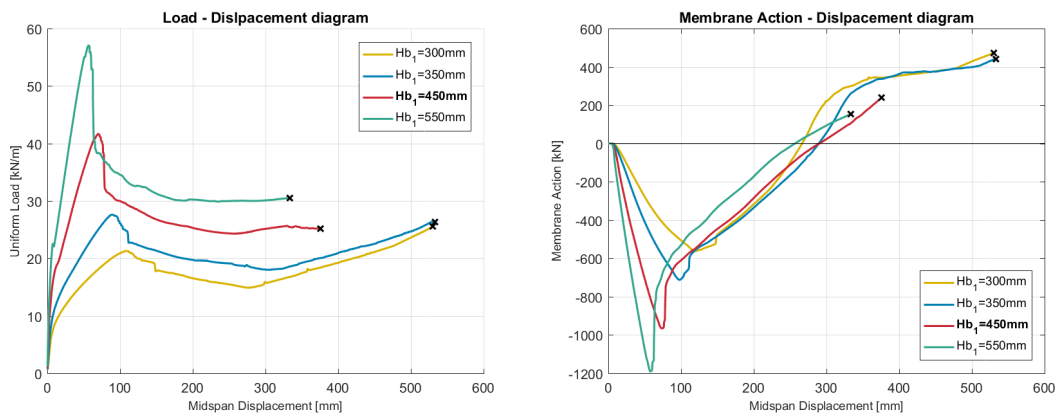


Figure 4.1: Load-bearing capacity curve for both variable beam cross-section

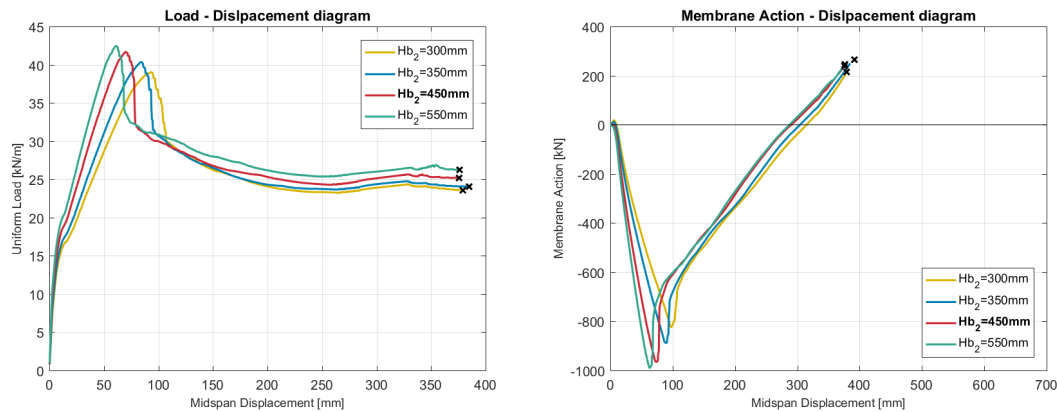


Figure 4.2: Load-bearing capacity curve for variable cross-section of the adjacent beam

Figure 4.1 and in Figure 4.2 clearly show the different effect on the load-bearing capacities.

First of all, the variable cross-section in the directly affected RC beam shows a high variation in both the load-bearing capacities while the variable cross-section of the left beam does not show any influence on the load-bearing capacity in TMA as the diagrams shows to reach rupture of the reinforcement at similar vertical displacement, but it affect the compressive membrane action which is transmitted to the adjacent element even though the effect is quite small.

In fact, the maximum value in CMA is variable between 37.5kN/m and 42.2kN/m, with a difference of 11.2% between the lower and highest capacities. The maximum value of compressive membrane actions transmitted to the adjacent beam is instead variable between -1000kN to -800kN with a percentage of variation of about 20%.

The effect that can be seen in the first analysis is instead much more marked, in fact the maximum load in bending resisting mechanism varies between 20kN/m and 50kN/m, while the maximum compressive membrane action changes from -1200kN to -600kN. The variation between the maxima load are respectively 40% and 50%. In this range of variation, the answer of the beam in the analyses with a variable Hb_1 changes from ductile to fragile with a decreasing base-height ratio, which is shown by the increase of the ultimate load in compressive membrane action condition and the decrease of ultimate vertical displacement.

Moreover, the development of the catenary mechanism become more difficult even though the ultimate reinforcement strain is kept equal for all the analyses. As a result, having a beam with a lower base–height ratio lead to a decrease of bending resistance, but it is more likely to develop catenary action and vice versa with a high base–height ratio, for example the analysis with $Hb_1 = 550\text{mm}$, the behaviour became fragile thus the bending resistance is quite high, but the development of TMA is almost null.

In addition, the ultimate displacement is not influenced by the variable Hb_2 and the top reinforcement in the beam–column connection shows to fail at the same values.

LENGTH

The analyses concerning the length of the adjacent beam does not show relevant effects on the load–bearing capacities of the RC beam as it can be seen in Figure 4.3.

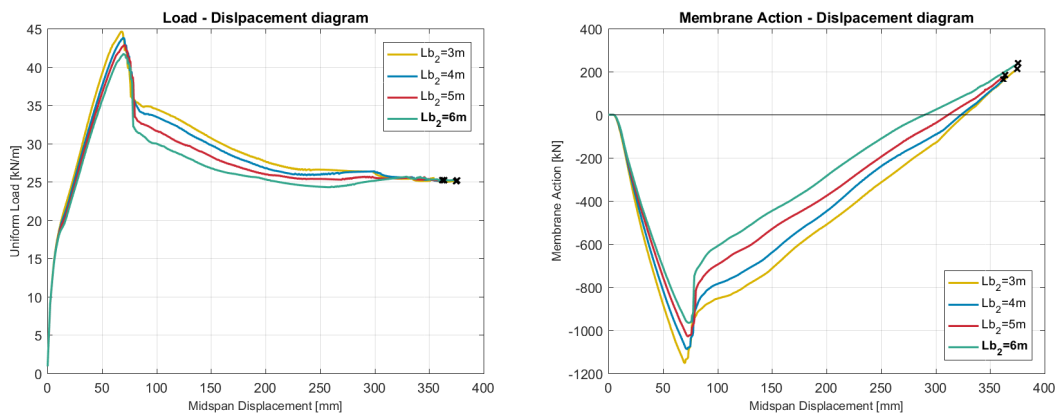
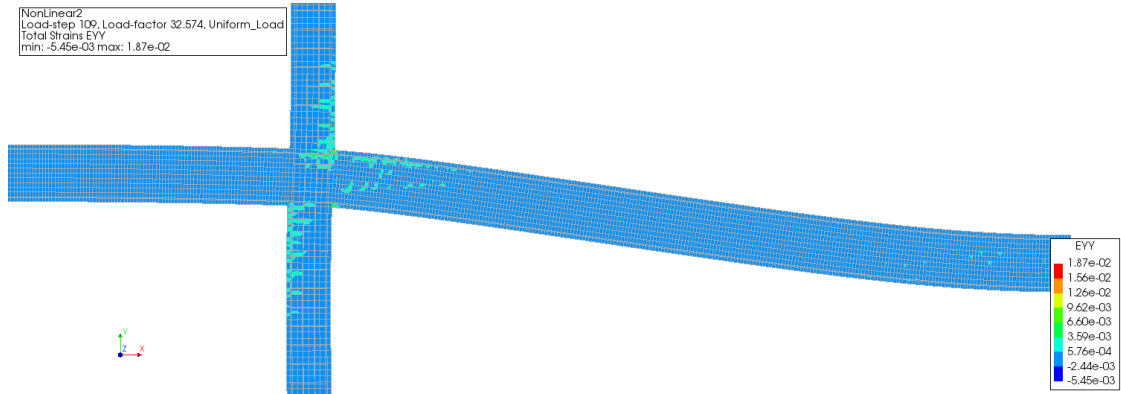


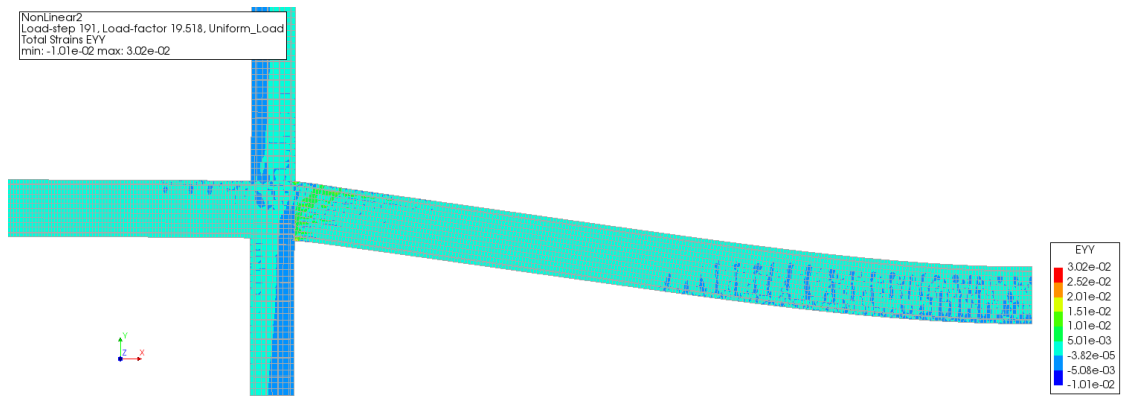
Figure 4.3: Load–bearing capacity curve for variable length of the adjacent beam

To complete the analysis of the results of this section, it is illustrated in Figure 4.4 the evolution of the concrete strain, thus the development of cracks in correspondence of the beam extremities and of the upper and lower column close to the joint, this evolution is in accordance to the experiment done by Lew et al. [9]. The following Figure 4.5 shows the reinforcement stresses at the peak load in bending resisting mechanism, at it define that the reinforcement has already reached yielding in correspondence of the top reinforcement at the beam–column joint and the bottom reinforcement at the other beam edge, where the

rupture occurs during the nonlinear analysis.



(a) Concrete strain at the bending peak



(b) Concrete strain after the bending peak

Figure 4.4: Evolution of the concrete strain in the members

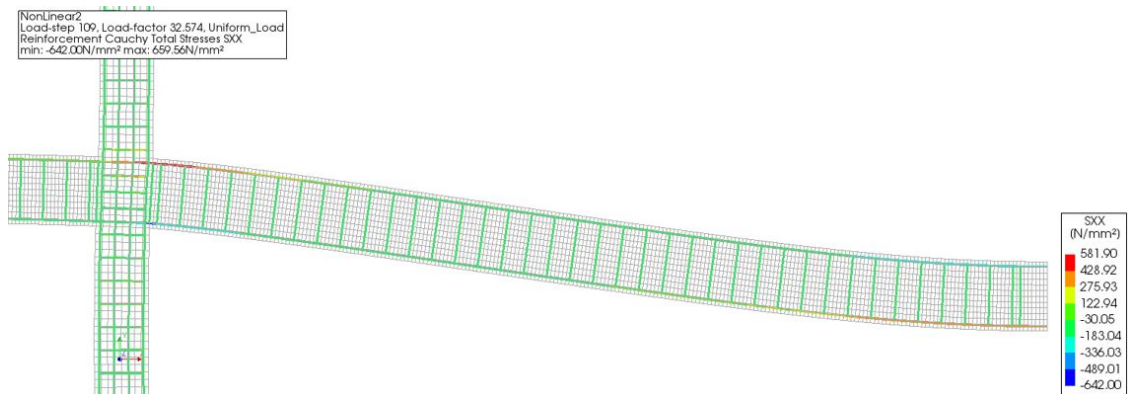


Figure 4.5: Reinforcement Stresses at the bending peak

4.2 Variable Columns Geometry

The range of variation used in the columns cross-section is the same as the one used in the analysis on the beam cross-section. The cross-section is changed for both the represented columns simultaneously.

It is clear that they influence the most the stiffness to the rotation in the joint, while their effect on the horizontal stiffness is very low comparing it to the horizontal stiffness of the beam. In fact, the contribute of the columns to the horizontal stiffness is more or less $0.02 \frac{E_c A_b}{L_b}$. In fact in Figure 4.7 and Figure 4.6, that show respectively the results obtained from the analyses with a variable column cross-section and a variable length, the parameter which is more influenced by the geometry of the columns is the ultimate displacement, while the maximum load in catenary mechanism is more or less the same in all the performed analyses. As a result, the load-bearing capacity during the development of tensile membrane action is not influenced, but it is affected the ability to change the resisting mechanism from bending resistance to the catenary action. There is a little influence on the bending resistance which decreases with a decreasing columns cross-section.

In particular, the two set of analyses show that with a decreasing area of the cross-section vertical displacement at failure of the top reinforcement in the joint increases, while with an increasing length the vertical displacement decreases, in fact they are directly and inversely proportional to the rotational stiffness respectively, as can be seen in the equation $\frac{E_c I_c}{L_c}$.

A comparison between the relevant parameters, such as the maxima resistances in compressive membrane actions and tensile membrane actions and the displacement at failure of the top reinforcement in the RC beam are shown in the following bar charts, considering all the analyses performed with variable beam and column cross-sections and lengths. It is easily notable that the influence given by the lengths is neglectable in all the analyses. On the contrary, the comparison regarding the analyses performed with variable cross-section show an high variability in all the results. Indeed, it is notable that, for all the analyses, with increasing cross-section the bending resistance and the TMA resistance increase, the failure vertical displacement decreases instead.

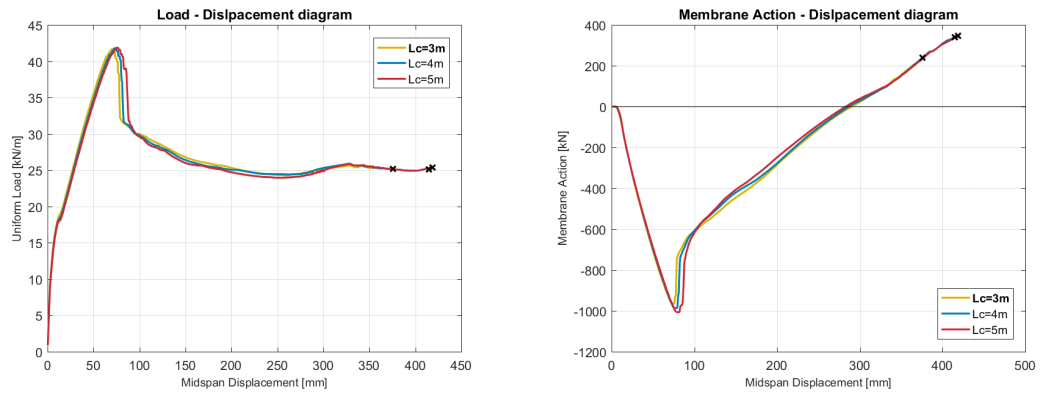


Figure 4.6: Load-bearing capacity diagrams for variable columns length

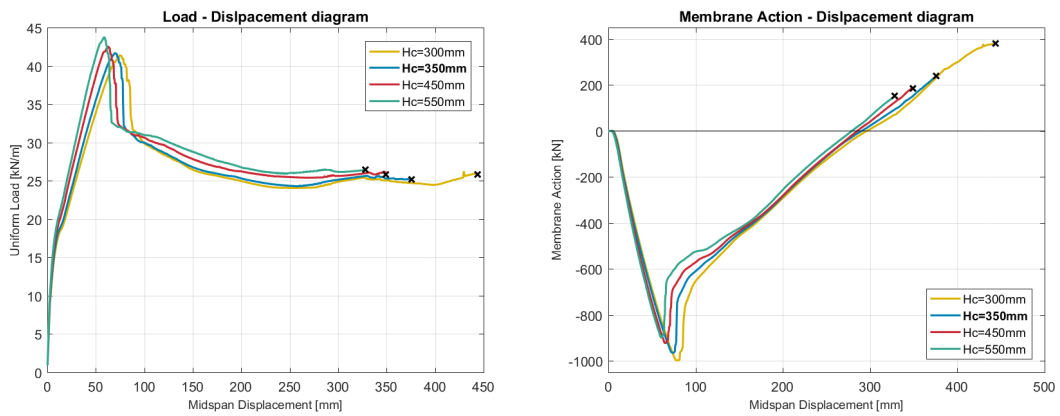


Figure 4.7: Load-bearing capacity diagrams for variable columns cross-section

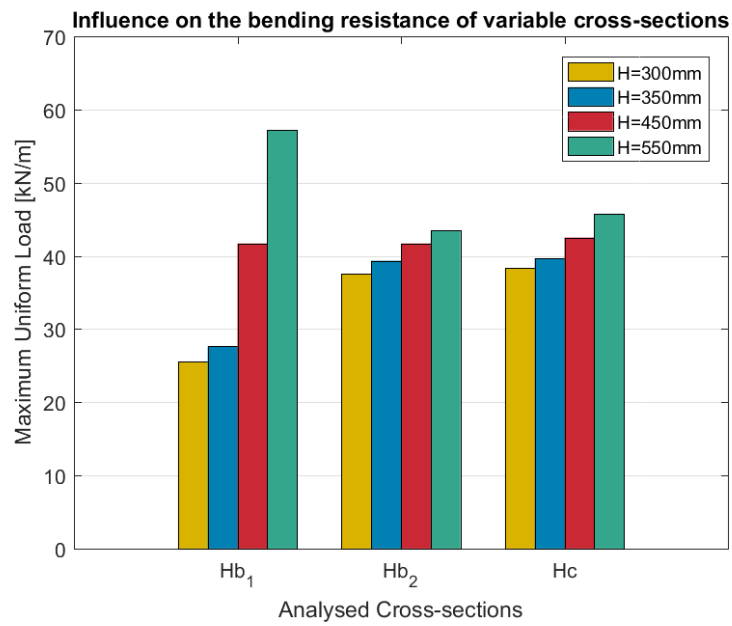


Figure 4.8: Comparison between the maximum load in CMA with variable cross-section

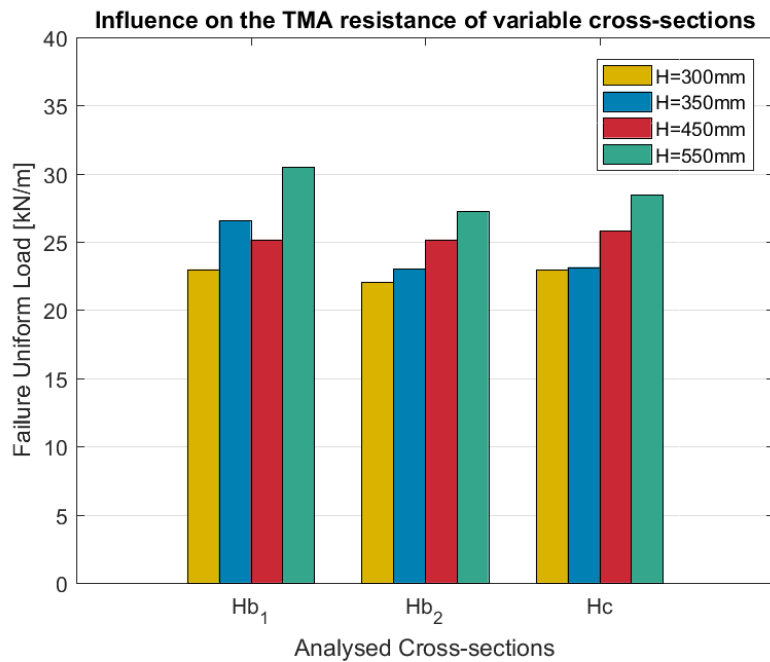


Figure 4.9: Comparison between the maximum load in TMA with variable cross-section

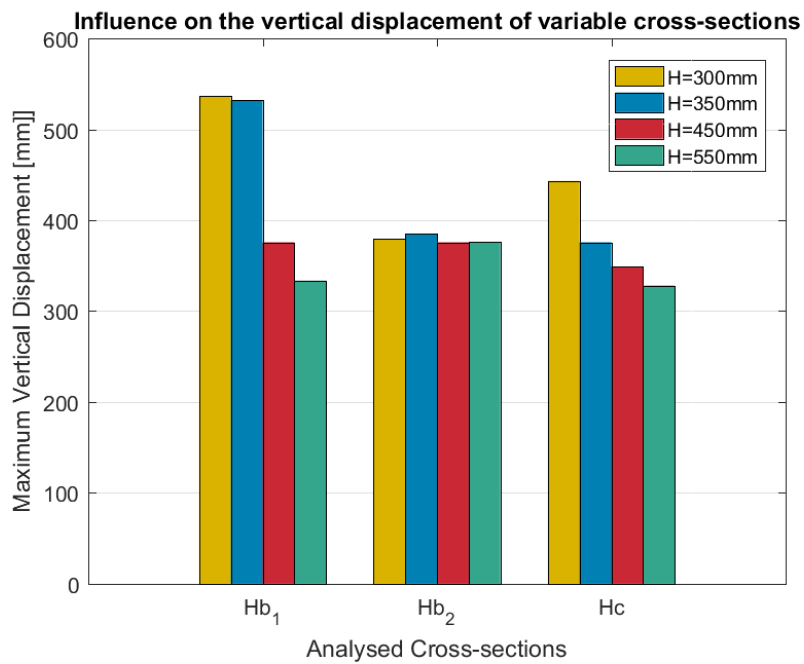


Figure 4.10: Comparison between the failure displacement with variable cross-section

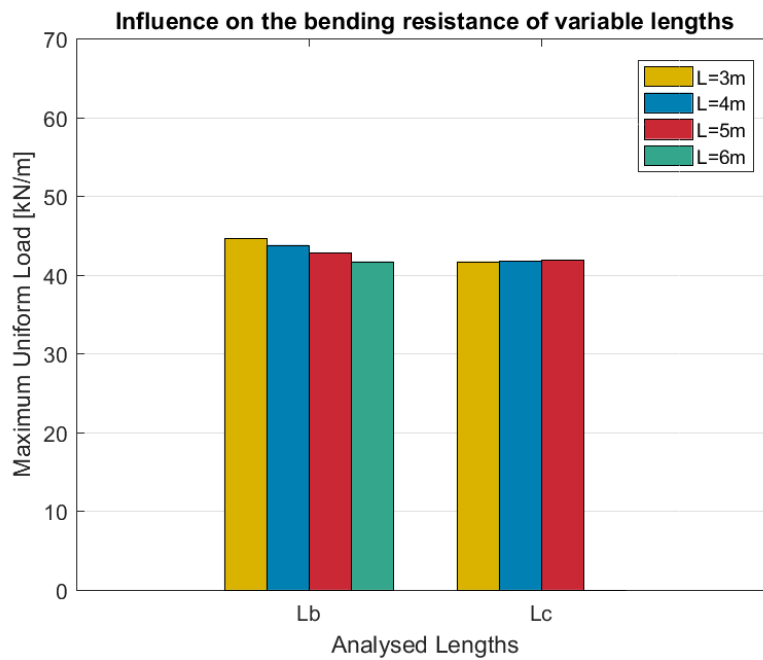


Figure 4.11: Comparison between the maximum load in CMA with variable length

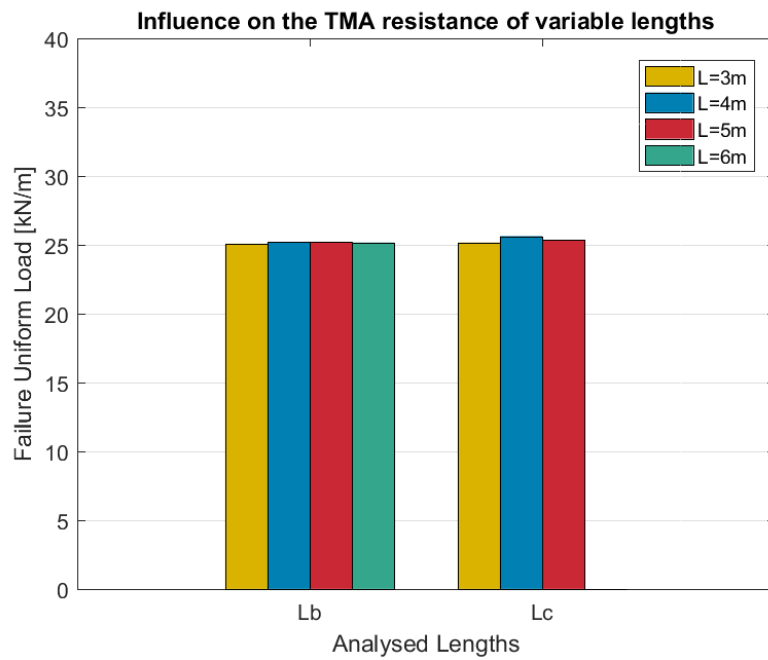


Figure 4.12: Comparison between the maximum load in TMA with variable length

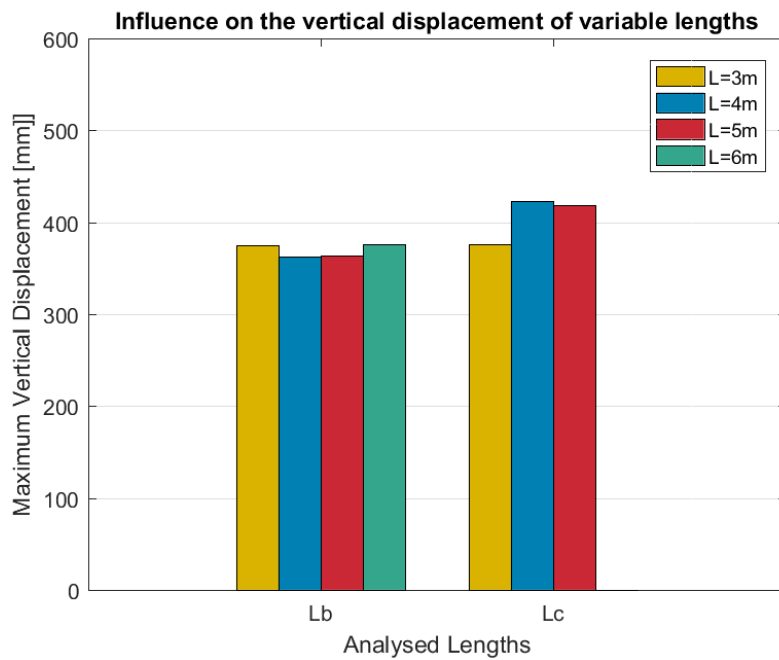


Figure 4.13: Comparison between the failure displacement with variable length

4.3 Influence of ϵ_{su}

The parametric analysis carried out on the geometry of the reinforced concrete frame is accompanied by an analysis of the mechanical properties, in this paragraph the results obtained by varying the ultimate deformation of the reinforcement for all the geometric analyses carried out are analysed.

This second parametric analysis showed to act similarly for all the different geometrical conditions, in fact this parameter affect only the reinforcement ductility, therefore it influenced only the ability of the RC element to develop tensile membrane actions thus the ability to change the resisting mechanism from the bending resistance to the catenary action.

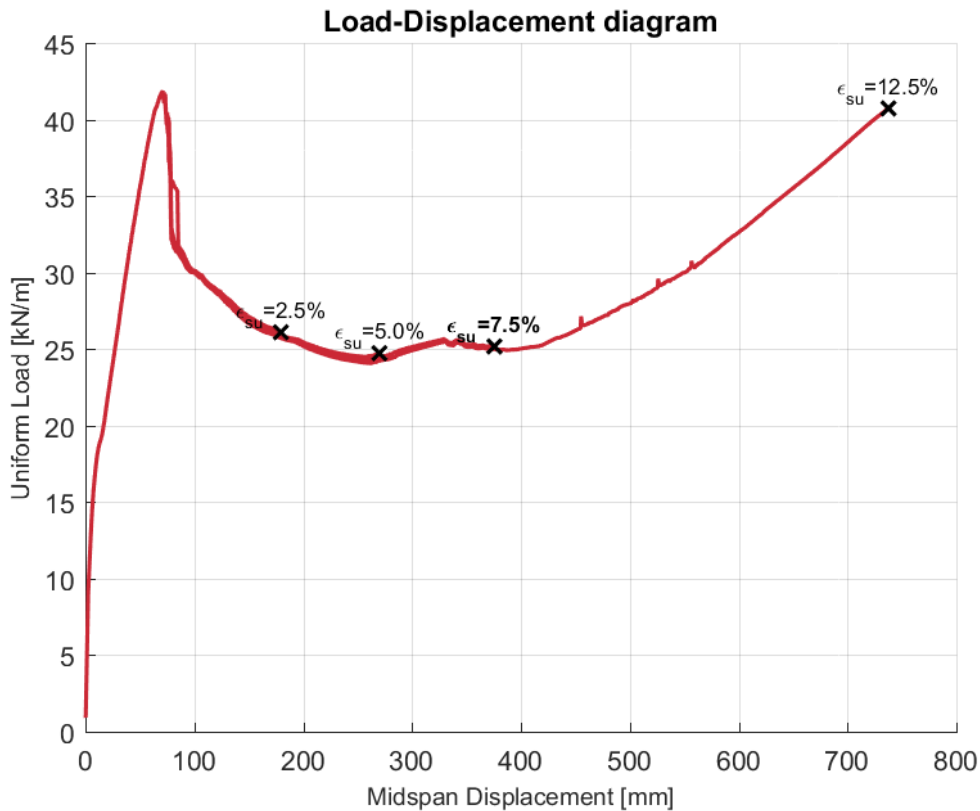


Figure 4.14: Load–displacement diagram with variable ϵ_{su}

In Figure 4.14 is illustrated the general effect on the load–displacement diagram derived from the starting geometry of the analysed RC frame, considering the range of the adopted

ϵ_{su} values. In particular it is possible to observe that this parameter affects only the ultimate vertical displacement which shows an high increase with an increasing ϵ_{su} . The results obtain from all the performed analysis with a variable reinforcement strain are depicted in the following Figure. It is clear that the bending resistance is not influenced and the ability to change the resisting mechanism increases with an increasing ultimate deformation.

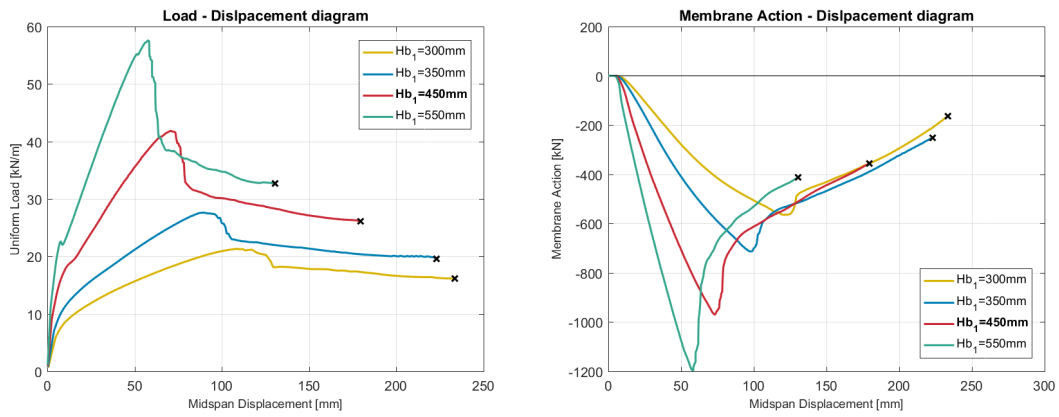


Figure 4.15: Load-bearing capacity diagrams for beam cross-section and $\epsilon_{su} = 0.025$

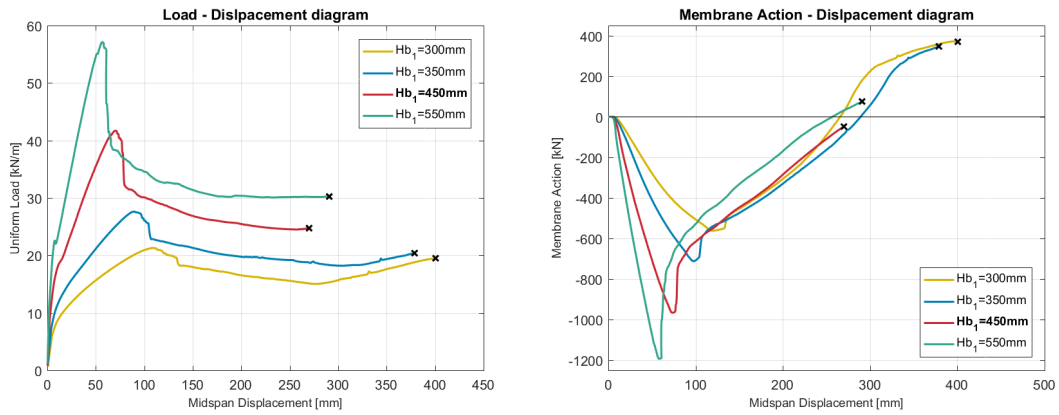


Figure 4.16: Load-bearing capacity diagrams for beam cross-section and $\epsilon_{su} = 0.05$

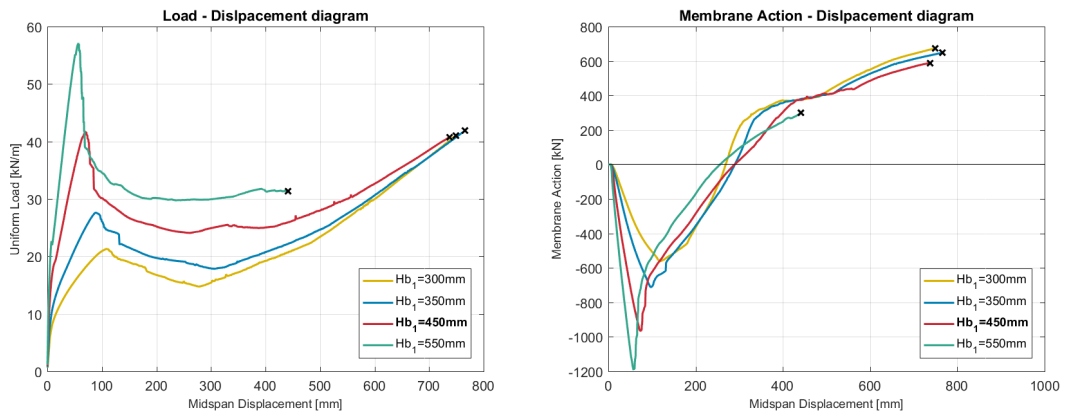


Figure 4.17: Load-bearing capacity diagrams for beam cross-section and $\epsilon_{su} = 0.125$

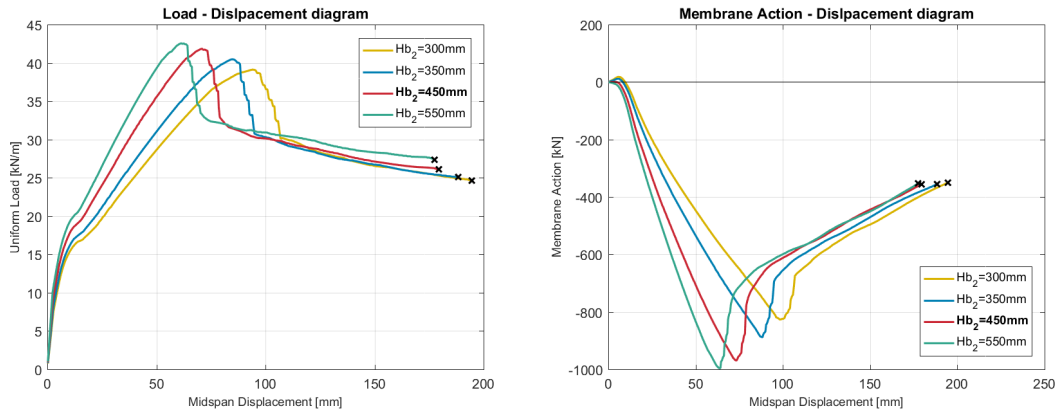


Figure 4.18: Load-bearing capacity diagrams for beam cross-section and $\epsilon_{su} = 0.025$

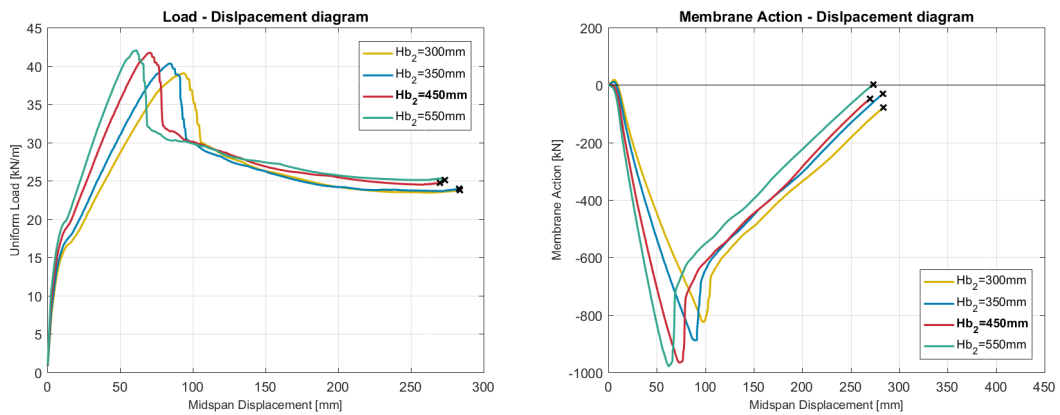


Figure 4.19: Load-bearing capacity diagrams for beam cross-section and $\epsilon_{su} = 0.05$

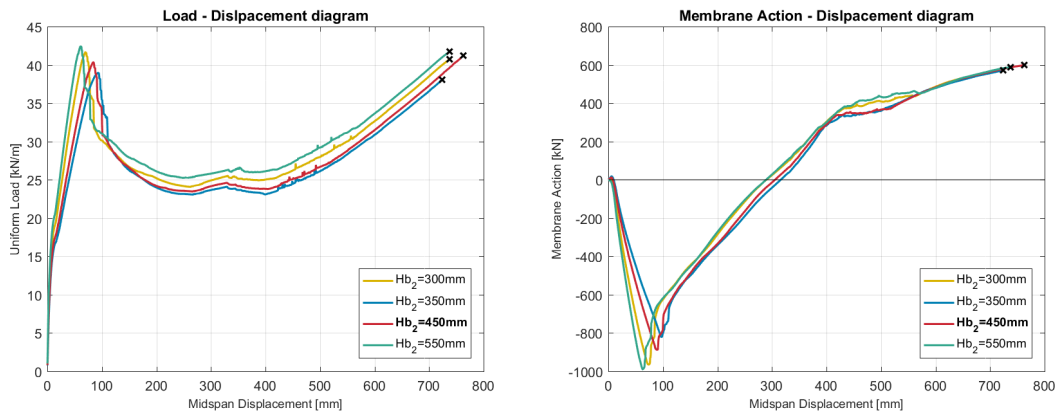


Figure 4.20: Load-bearing capacity diagrams for beam cross-section and $\epsilon_{su} = 0.125$

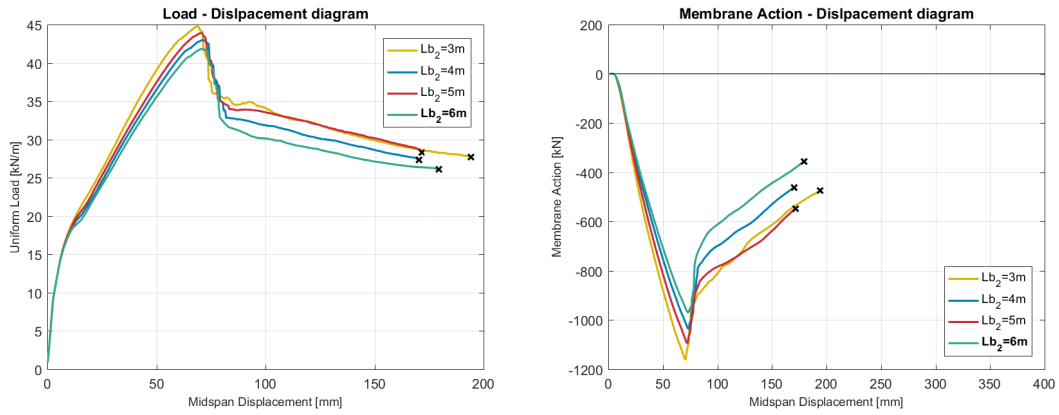


Figure 4.21: Load-bearing capacity diagrams for beam length and $\epsilon_{su} = 0.025$

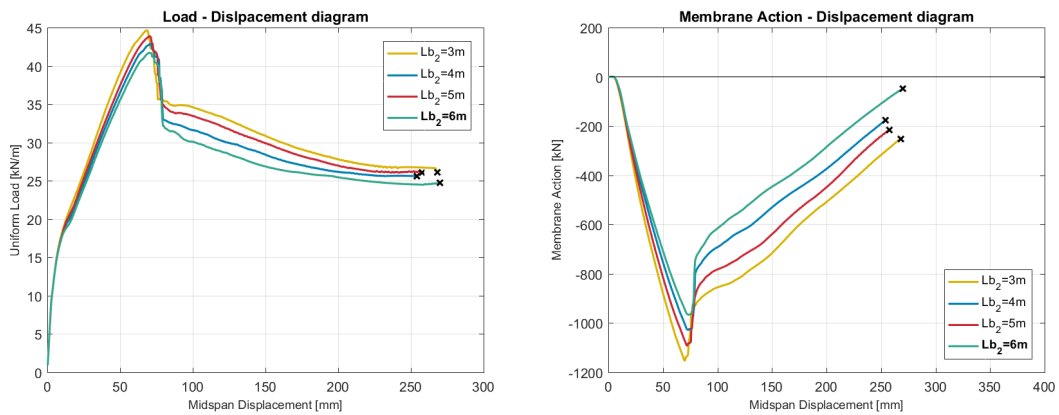


Figure 4.22: Load-bearing capacity diagrams for beam length and $\epsilon_{su} = 0.05$

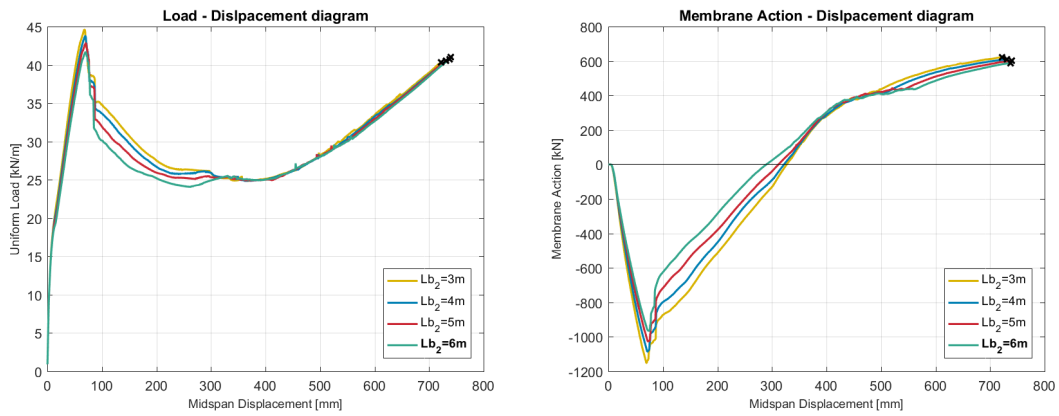


Figure 4.23: Load-bearing capacity diagrams for beam length and $\epsilon_{su} = 0.125$

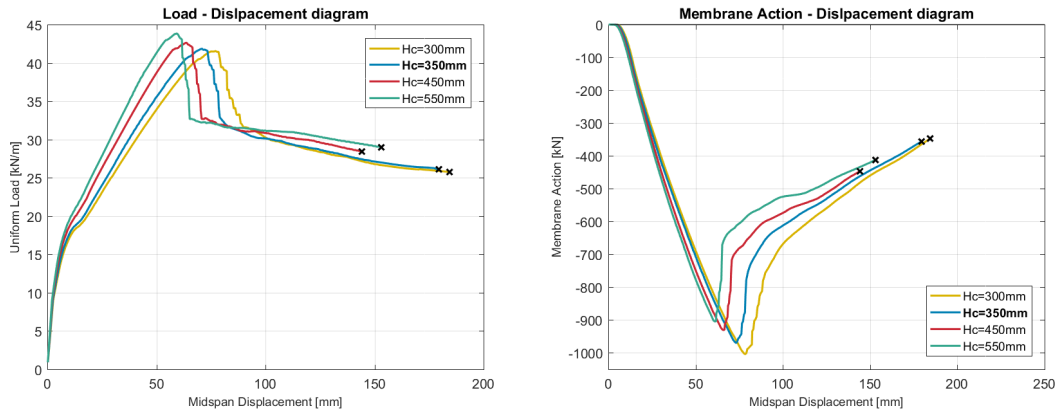


Figure 4.24: Load-bearing capacity diagrams for columns cross-section and $\epsilon_{su} = 0.025$

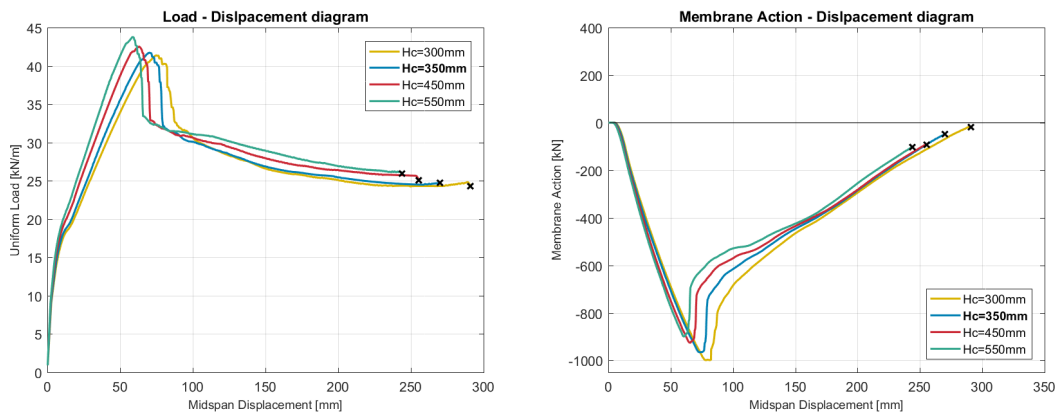


Figure 4.25: Load-bearing capacity diagrams for columns cross-section and $\epsilon_{su} = 0.05$

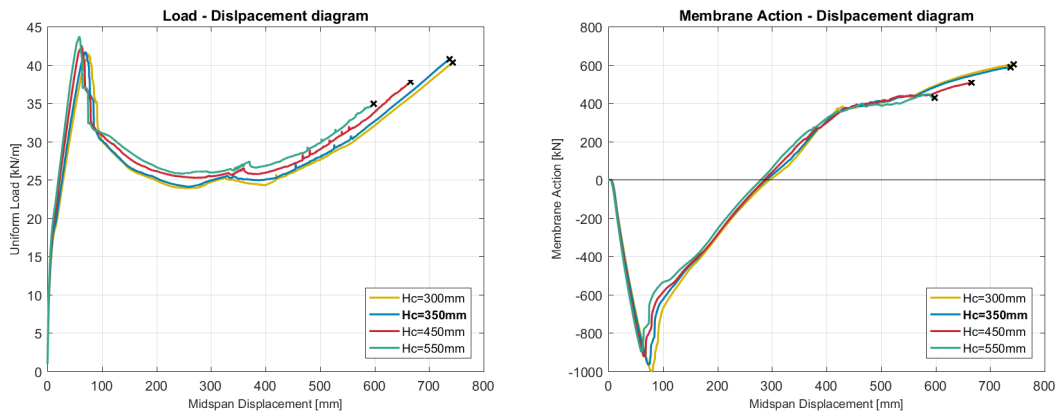


Figure 4.26: Load-bearing capacity diagrams for columns cross-section and $\epsilon_{su} = 0.125$

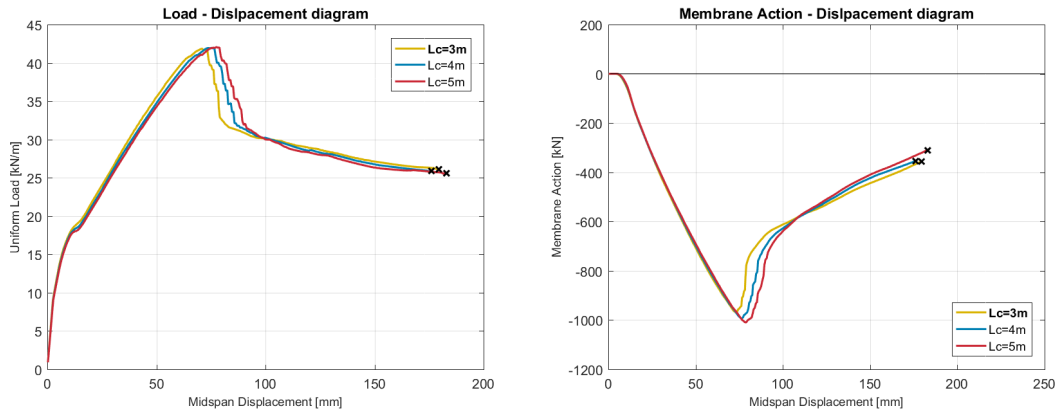


Figure 4.27: Load-bearing capacity diagrams for columns length and $\epsilon_{su} = 0.025$

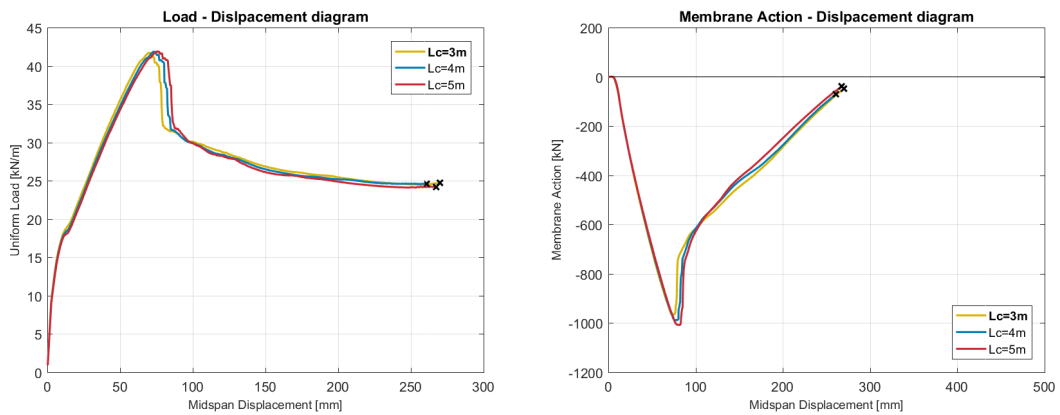


Figure 4.28: Load-bearing capacity diagrams for columns length and $\epsilon_{su} = 0.05$

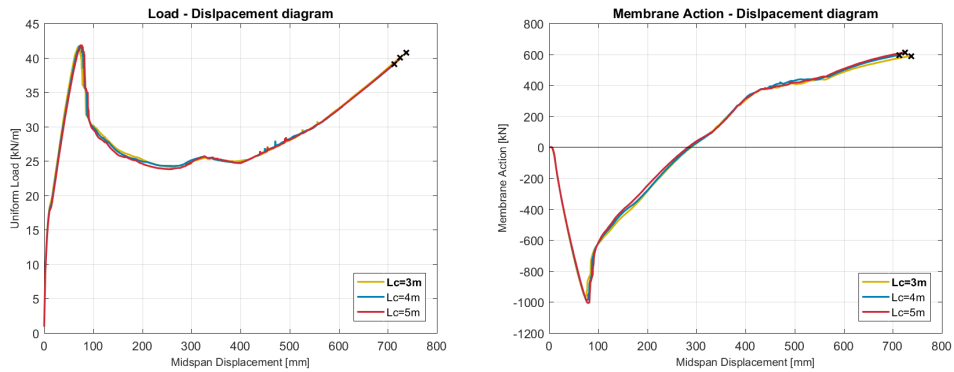


Figure 4.29: Load-bearing capacity diagrams for columns length and $\epsilon_{su} = 0.125$

All the results showed in the previous diagrams can be linked together in order to obtain a full view on the effects of the reinforcement strain on the load-bearing capacities. In Figure 4.30, 4.31, 4.32 and 4.33 it is illustrated this link between the analyses performed with a variable ultimate reinforcement strain with the parametric analysis carried out on the variable elements geometry. It is clear the influence of ϵ_{su} on the ability of the RC beam to develop the catenary action. For those geometries that are able to develop catenary actions themselves this effect is higher and vice versa.

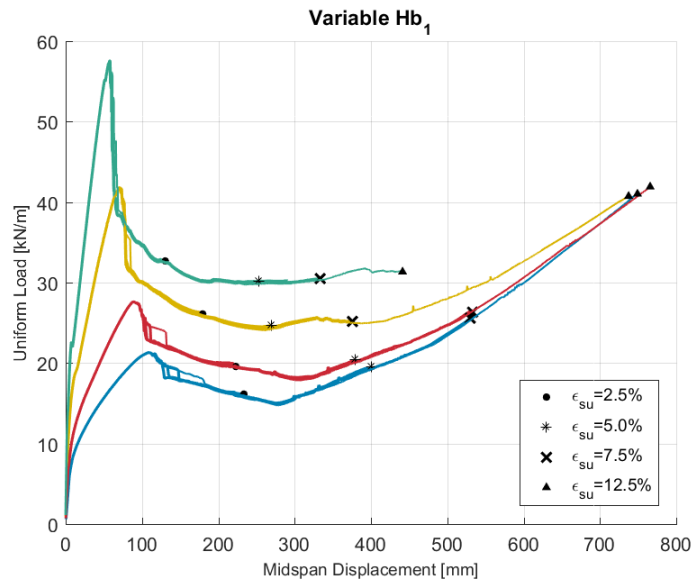


Figure 4.30: Superposition of load-displacement diagrams of with variable ϵ_{su} and variable Hb_1

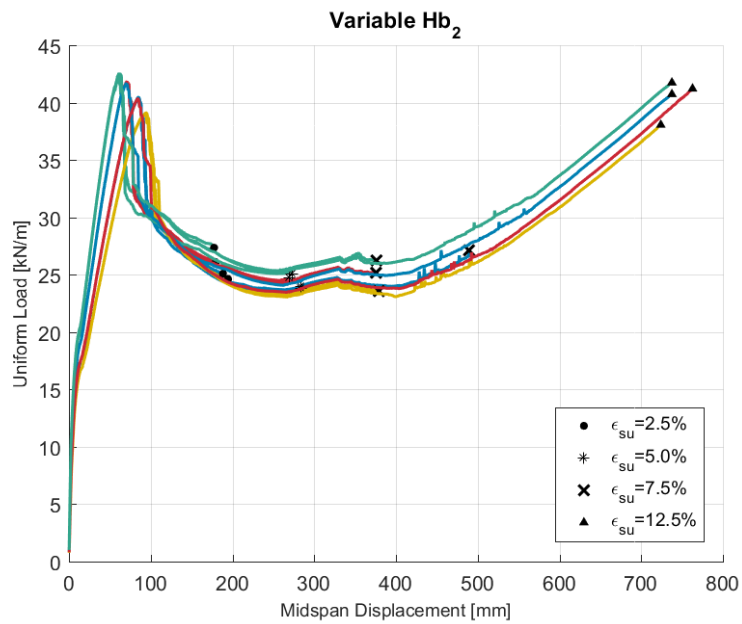


Figure 4.31: Superposition of load–displacement diagrams of with variable ϵ_{su} and variable Hb_2

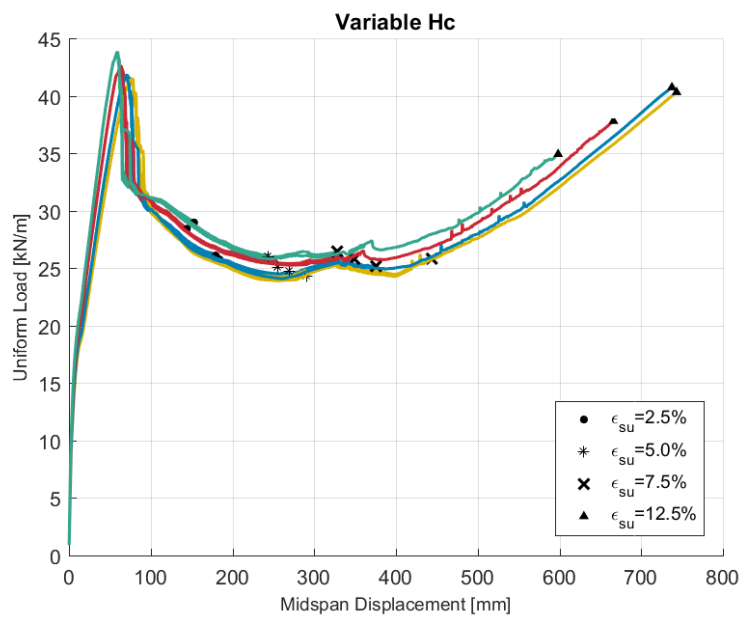


Figure 4.32: Superposition of load–displacement diagrams of with variable ϵ_{su} and variable Hc

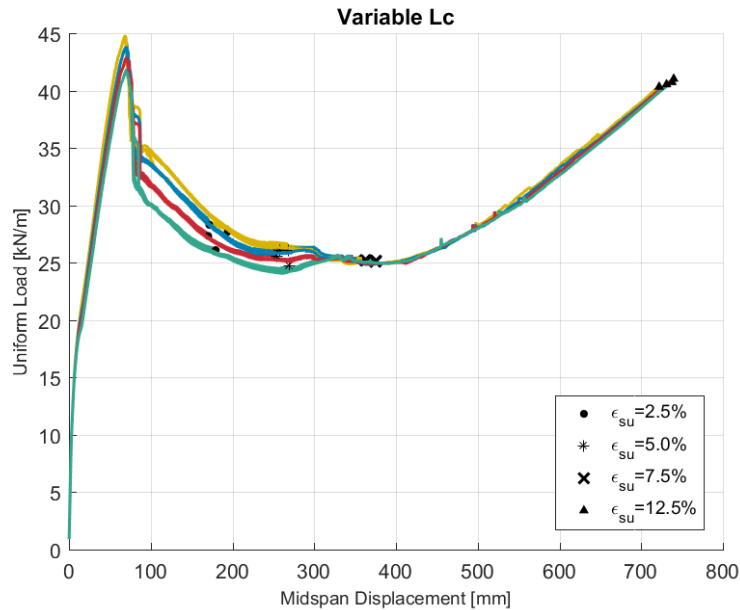


Figure 4.33: Superposition of load–displacement diagrams of with variable ϵ_{su} and variable Lb

4.4 Influence of constant M_{rd}

The results obtained from the performed analyses with a constant M_{rd} and a variable element geometry are illustrated in Figure 4.35 and Figure 4.37, that respectively shows the results obtained maintaining constant M_{rd} with a variable beam cross–section and a variable column cross–section. The results are coloured in red when considering the starting geometry condition and in blue the analyses performed with a constant resisting moment. In order to maintain constant the value of resisting moment computed in the analysed reinforced concrete frame while changing the cross–section of the load–bearing elements it is necessary to place a different quantity of reinforcement bars.

In cross–sections smaller than the starting geometry the reinforcement to insert in order to maintain the same value of M_{rd} is incremented, vice versa in bigger cross–sections. As a result the load–bearing capacities in the bending resisting mechanism and the catenary action are higher comparing them to the analyses where the reinforcement is kept constant for all the different cross–section. This led to an higher ability to develop the catenary action. The opposite happens for sections that are bigger than the one of the starting geometry, because the reinforcement to be placed to maintain constant the M_{rd} is lower

than the starting amount.

The TMA load-bearing capacity in the two cases with Hb_1 equal to 300mm and 350mm increases while in the case of $Hb_1 = 550$ mm is almost the same. In fact, the maximum load in catenary action are higher in the first two geometry, the corresponding vertical displacement has more or less the same value, while in the analysis with $Hb_1 = 550$ mm the load in catenary action is almost the same thus there no increment in the resistance, but the vertical displacement showed to increase.

The same analysis is performed for the variable geometry in the columns, the starting reinforcement is the one for the cross-section equal to $H_c = 350$ mm, thus equal to $8\Phi 14$ distributed symmetrically in the columns, this is the amount kept constant in the parametric analyses carried out with a variable geometry, from that it is then changed considering the M_{rd} equal to the cross-section of 350mm.

In Figure 4.37 it is possible to note that the influence on both the resistances, bending and

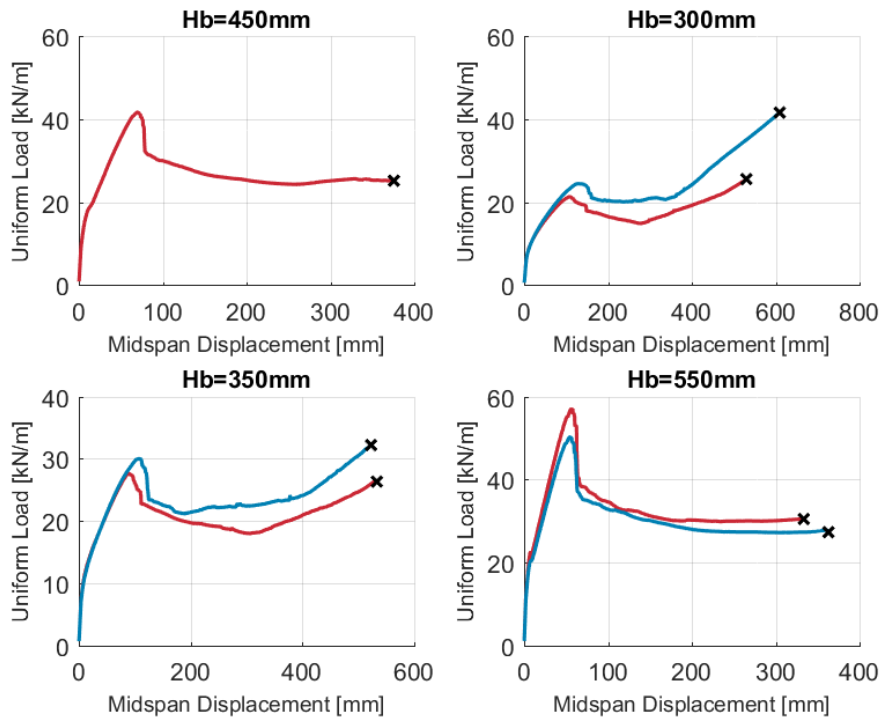


Figure 4.34: Load–displacement diagram with constant M_{rd} and variable H_b

catenary action, is very small. The only effect that can be evaluated from this analyses if

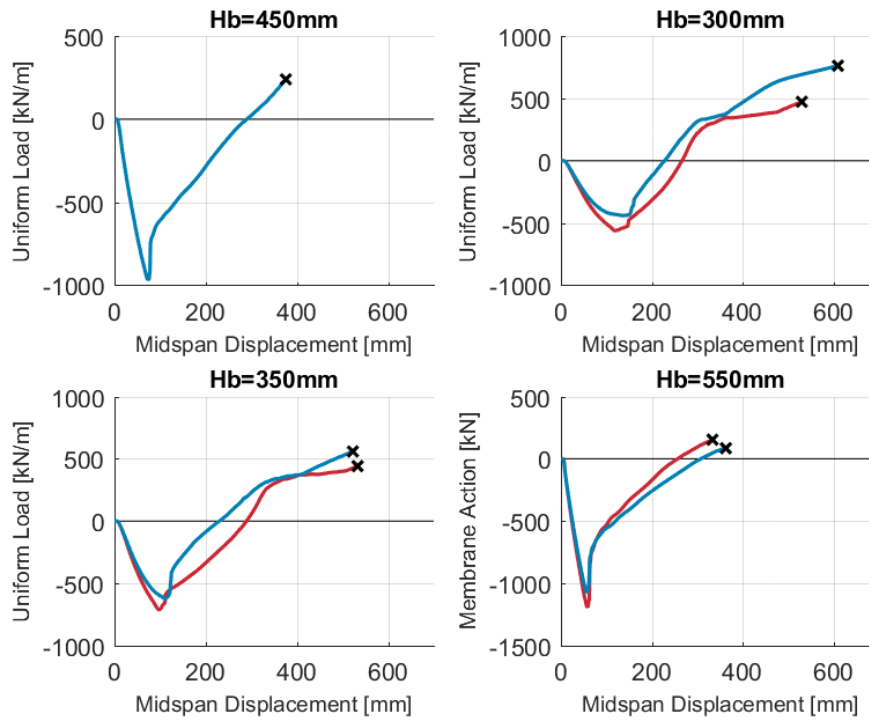


Figure 4.35: Membrane Action–displacement diagram with constant M_{rd} and variable H_b

that for smaller cross-sections the rotational capacity of the beam increases because the ductility of the columns is higher than the starting condition, due to the higher reinforcement area, thus the vertical displacement at rupture of the top reinforcement in the beam is higher, vice versa for bigger cross-section. All the comment about the analyses results on the relevant parameters in the capacity diagrams are highlighted in the bar charts that follows, which it easily shown the comparison between all the analyses maintaining constant the resisting moment, equal to the on computed in the design of the analysed RC frame.

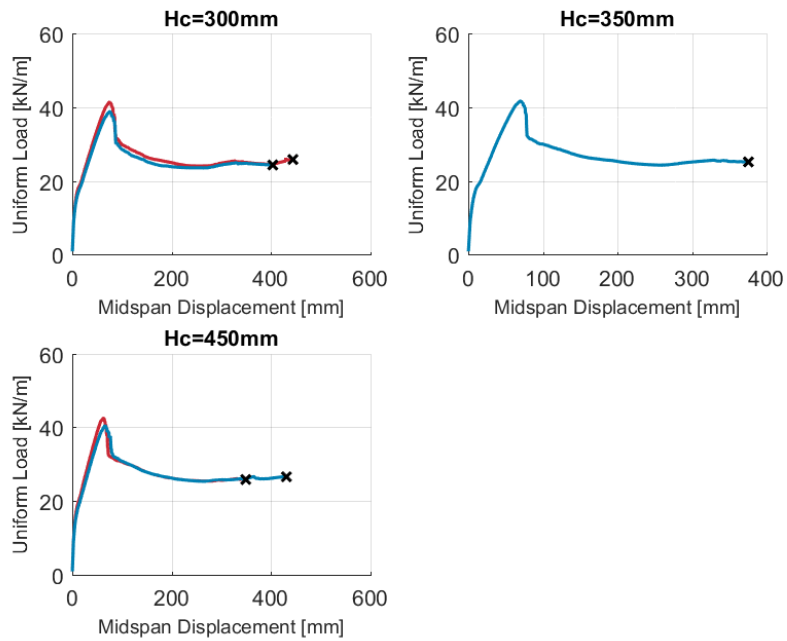


Figure 4.36: Load–displacement diagram with constant $M_{r,d}$ and variable H_c

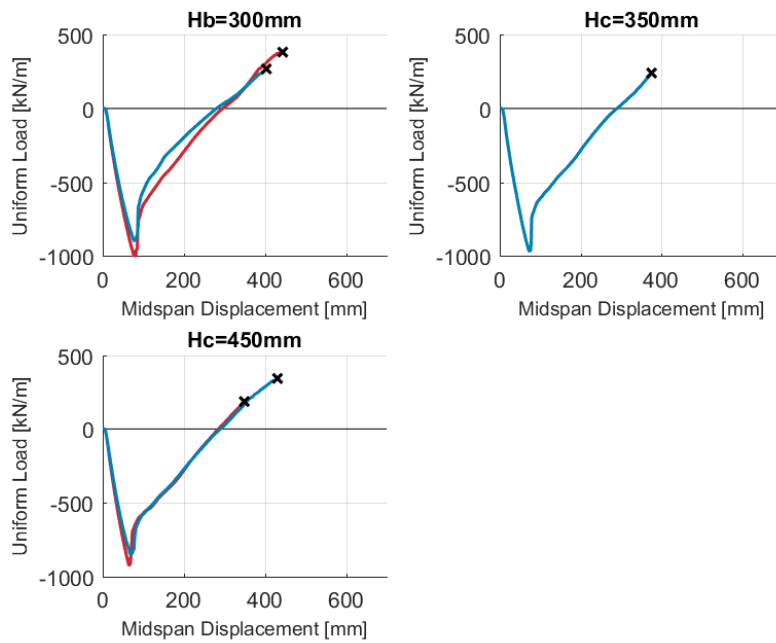


Figure 4.37: Membrane Action–displacement diagram with constant $M_{r,d}$ and variable H_c

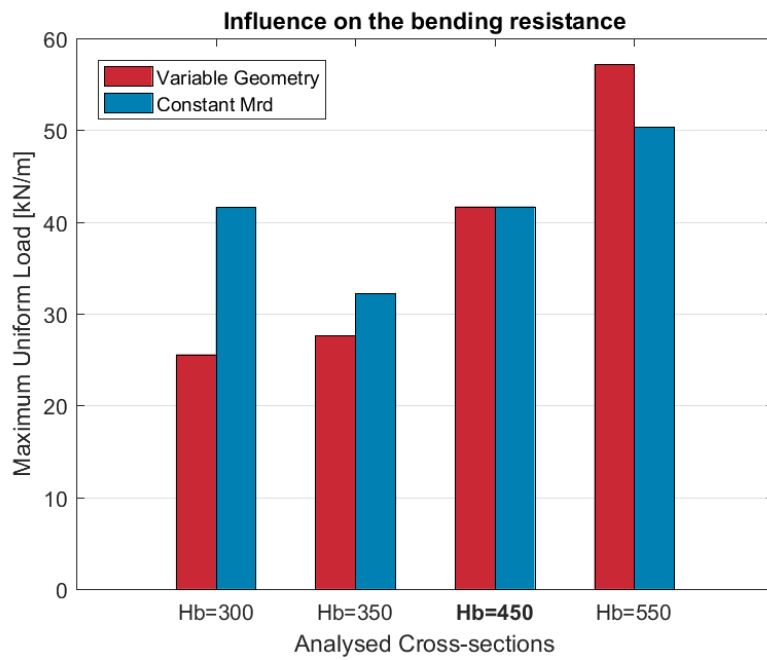


Figure 4.38: Comparison between the maximum load in CMA with constant M_{rd} and variable H_b

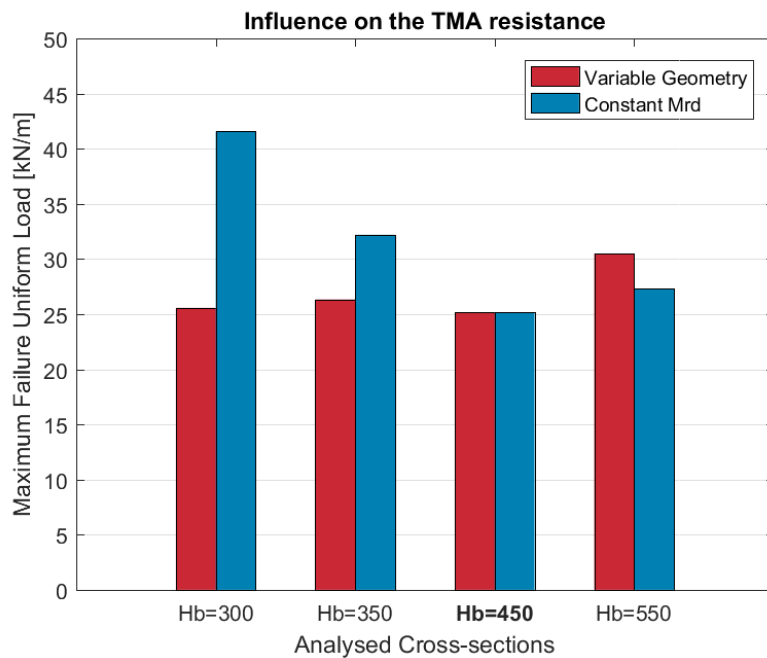


Figure 4.39: Comparison between the maximum load in TMA with constant M_{rd} and variable H_b

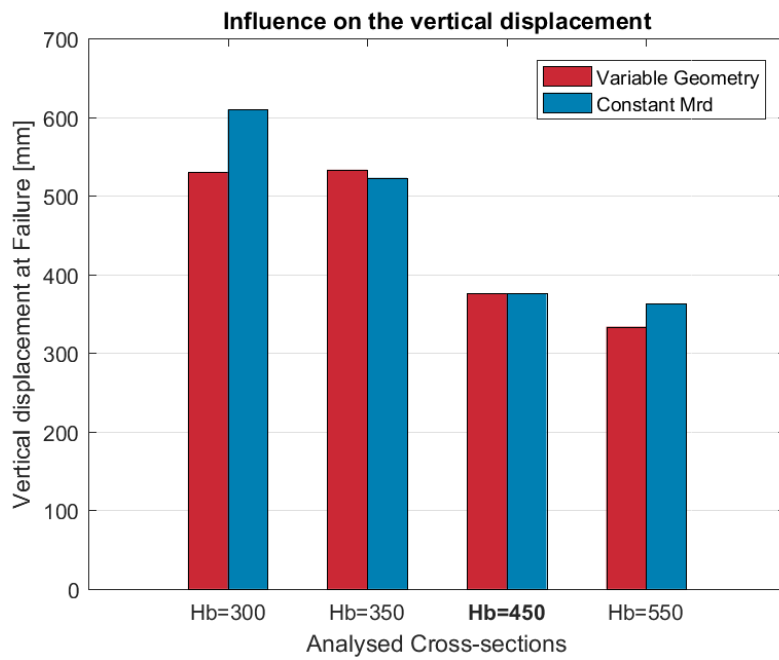


Figure 4.40: Comparison between the failure displacement with constant M_{rd} and variable H_b

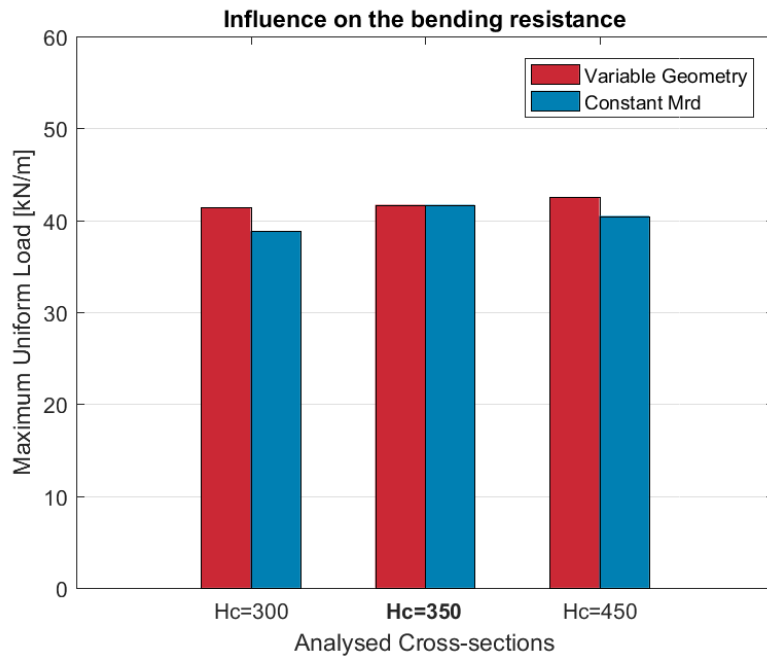


Figure 4.41: Comparison between the maximum load in CMA with constant M_{rd} and variable H_c

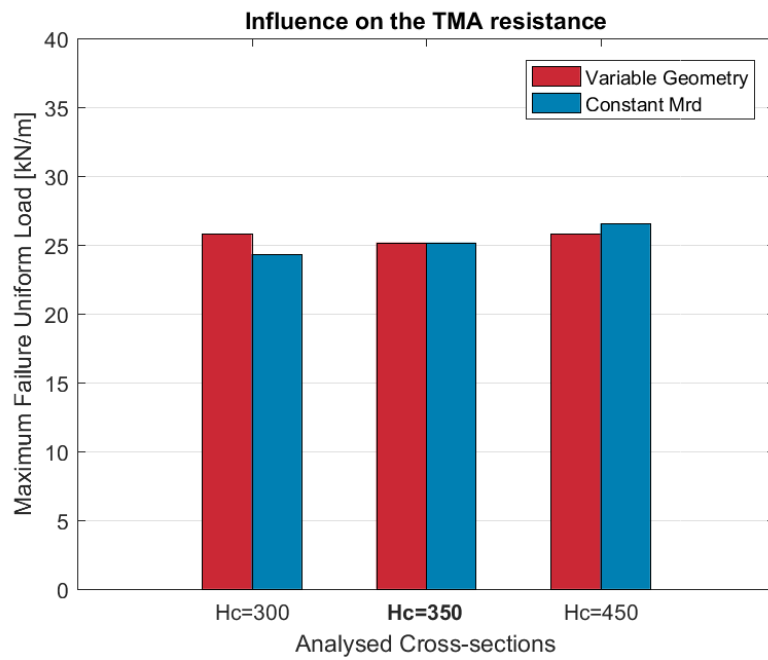


Figure 4.42: Comparison between the maximum load in TMA with constant M_{rd} and variable H_c

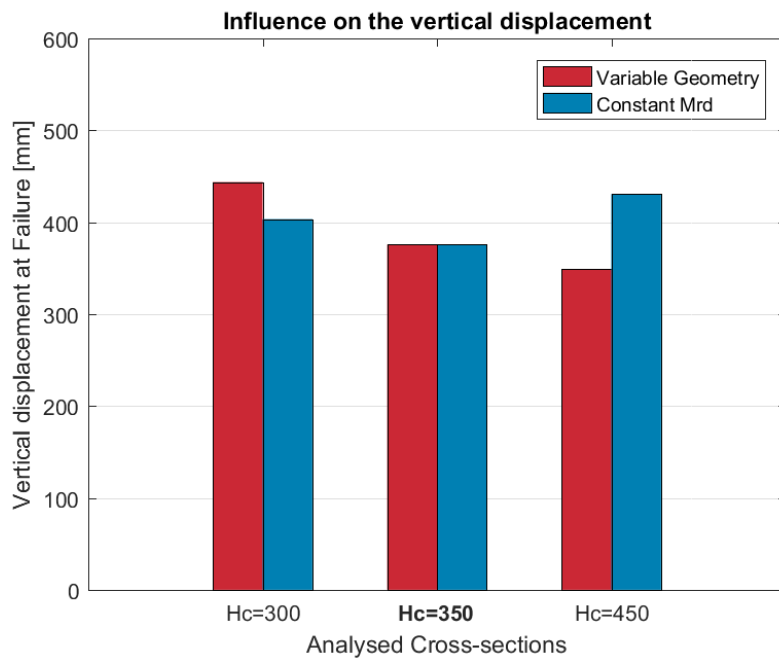


Figure 4.43: Comparison between the failure displacement with constant M_{rd} and variable H_c

4.5 Influence of the Stiffnesses

The previous Chapter illustrate the influence of the adjacent element stiffnesses to the horizontal displacement and rotation of the RC beam subjected to the column removal. The equations used to evaluate those two parameters are defined, accordingly to the CNR 2018 in the paragraph 1.2.2 of Chapter 1. The geometry parametric analysis and lots of researches showed that the horizontal restraining condition, which is derive from the stiffness to the horizontal translation of the adjacent element, $\frac{EA_b}{L_b}$ for the beam and $\frac{48EI_c}{L_c^3}$ for the columns, is the condition necessary to take into account when assessing robustness in order to define the increase in the resistance in the bending resisting mechanism, i.e. to develop compressive membrane actions, and also the ability of the frame to change the resisting mechanism from bending to catenary action. If it is not considered the development of membrane action in the structural members the load displacement diagram follows the curve depict in Figure 1.2, where after reaching the bending resistance a plateau at the same load take place until failure.

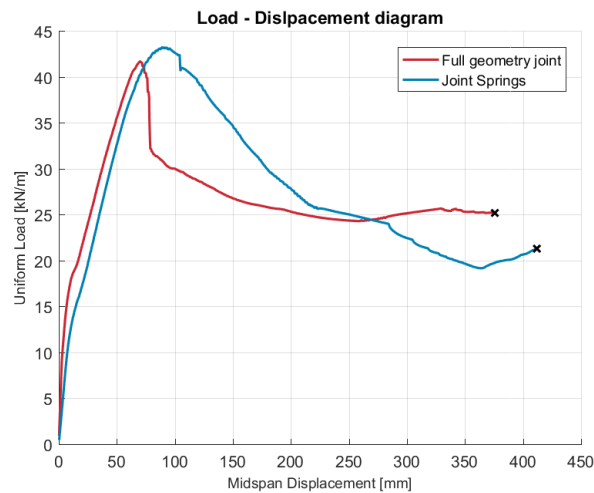


Figure 4.44: Load–displacement diagram for the two different FEM model

On the other hand, the ability of the structure to change the resisting mechanism from bending to the catenary action is more influenced by the cross–section of the direct affected beam. In fact tensile membrane actions are more likely to arise for high base/height ratios, and by the rotational stiffness given by the adjacent elements in correspondence of

the beam–column joint which depend also from the supports that are adopted to model the elements connection to the reinforced concrete frame.

Once the stiffnesses are computed from the solution defined in Science of Constructions by the linear elastic equation, it is possible to model their effect with spring elements, appropriately linked to the RC beam. In this simplified model two springs are modelled, one translational for the horizontal stiffness and one rotational which represent the rotational stiffness. The comparison between the load–displacement diagrams obtained from the two models is showed in Figure 4.44. In the diagrams it is depicted a more rigid behaviour in the FEM model in which is represented the full geometry accordingly with the complete representation of the stiffnesses in the FEM software, while considering linear spring element lead to a decrease in the stiffnesses in the model, thus the behaviour of the RC beam in the model with the two springs result more ductile than in the FEM model with the full geometrical representation of the structural members.

Chapter 5

Corrosion

Corrosion is the most common degradation process which affects the majority of the existing reinforced concrete structures. There are many methods to give a structure the necessary resistance measure to the attack of carbonation depending on the different exposure conditions, but most of the existing buildings at one point during their service life suffer of this degradation phenomenon.

This main deterioration mechanism leads to a loss of safety in the structures. Maintaining the safety and the serviceability of existing buildings is a significant challenge for the countries and to distribute the resources in a better way in order to guarantee the establishment of the correct safety level plays a crucial role. It is then very important in reinforced concrete structures to foresee proper maintenance over time, to prolong the service life of the building and to avoid degradation mechanisms, such as corrosion, causing excessive damage to the structure. In fact, during its service life, the structure is subjected to the designed serviceability loads and load paths develop in order to take the applied load to the last bearing members, the foundations.

The load paths develop following the adopted structural design. If the structure is damaged, the load paths need to change and thus the loads are taken to the foundations in a different way; an alternative load path arose within the structure.

The development of this alternative load path is possible only if the load bearing members are able to withstand the overload to which they are subjected. The condition of excessive damage or the removal of a load bearing element in a damaged condition can lead to the

structural disproportionate failure.



Figure 5.1: Cover detachment after corrosion of steel reinforcement

In the field of **Structural Robustness** is significant the ability to develop alternative load paths, but first the ability to withstand the applied load. Structures that are already damaged by some degradation processes cannot meet either the safety requirement in service conditions or in the occurrence of exceptional events such as vehicle impacts, human errors or terrorism attacks. It become then important the evaluation of ultimate bearing capacity of reinforced concrete frame in such conditions.

5.1 Degradation Mechanism of Corrosion

Corrosion is the degradation mechanism to which is subjected steel in wet environments. This process affects the steel surface, for this reason it can be avoided by adopting the various methods of protection available in the literature, such as using a corrosion resistant metal, protective coatings, environmental measures or sacrificial coatings.

Some metallic materials are able to cover their surface with a protective layer, this behaviour is known as passive behaviour. In the case of iron, it behaves like a passive metal if it found itself in a basic environment in the presence of oxygen and it is covered with a very thin oxide layer, the thickness of which is of a few molecular layers, under these conditions, which are called passive, its corrosion rate is practically zero. The reinforcement used in concrete structure is protected by the concrete layer called *cover* from the external environment and by the fact that concrete create a basic environment around the steel reinforcement, with a pH equal to more or less 13÷14.

However, it can happen in some very aggressive environment and with porous concrete, that water come inside the concrete covering layer starting the so-called process of *carbonation*. In fact, if the value of the pH goes down to 12 or less, the oxide film is damaged and corrosion can start. The process starts when its rate reaches a value where the corrosion is not neglectable. This rate depends on a variety of parameters, the most important are oxygen and moisture. The same happen when considering the concentration of chloride ions in the atmosphere, when this reaches the critical value, the localizide corrosion called pitting starts and the corrosion rate gives the evolution in time of the phenomenon.

Consequently, in literature the two main corrosion mechanisms are distinguished in:

- **CARBONATION:** This corrosion is due to the simultaneous presence of carbon dioxide, CO₂, and water, H₂O, in the atmosphere. The carbon dioxide neutralizes the alkaline property of concrete changing the pH value from 13 to 9. As it is shows in Figure 5.2, the CO₂ and H₂O start to enter in the concrete pores following the time-dependent law $s = K\sqrt{t}$. If the concrete pores are already full of water the carbonation speed decrease because carbon dioxide has to diffuse very slow into water, even though carbonation needs water to start. It is then defined a range of humidity within the carbonation is more likely to happen which is 50 to 80%. Carbonation is a uniform corrosion process.
- **PITTING:** This is the most dangerous corrosion process. It starts when chloride ions are present in the environment and their concentration reach the critical content equal to 0.4 ÷ 1.0% of the cement weigh. During the development of this phenomenon, corrosion is localized and pits occurs in the reinforcement, that correspond to a decrease of

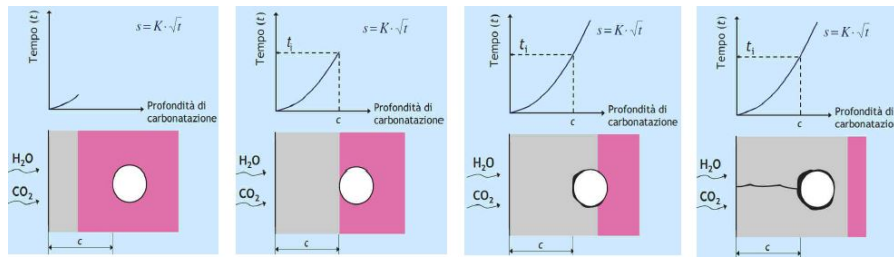


Figure 5.2: Carbonation evolution process

the reinforcement cross-sectional area in localized point. Chloride ions from de-icing salts or marine exposure are carried into the concrete in solution in water. At the steel surface, even in alkaline concrete, they attack and break down the passivating layer and then accelerate the steel corrosion process, following the development as shown in Figure 5.3

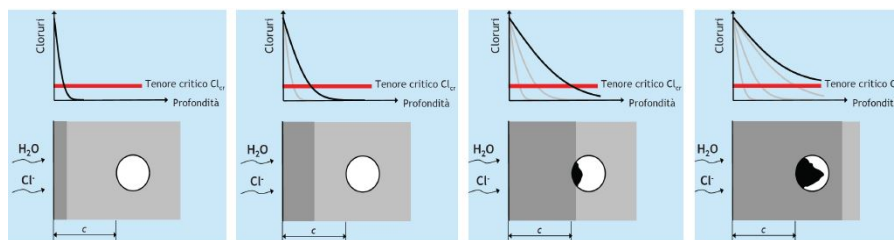


Figure 5.3: Pitting evolution process

The damage of the protective film is the necessary precondition for corrosion to occur. Once the film has been destroyed, corrosion occurs only if water and oxygen are present at the reinforcement surface. Depassivation occurs only on reinforcements reached by the carbonation front or the critical chloride content, therefore it is possible that corrosion affects only a part of the structure or a part of the structural element.

This circumstance can lead to the formation of a couple of forces between the corroded reinforcement bars and the remaining bars still in passive conditions but electrically connected to the previous ones by the stirrups. In particular conditions, the formation of this couple can increase the speed with which the attack is produced on the reinforcements that are already corroding.

As a result, it is possible to recognise two macro phases in the corrosion degradation process of reinforced concrete structures as it is illustrated in Figure 5.4:

- **Initiation period:** this phase occurs when the carbonation reaches the reinforcement or the chlorides concentration exceed the critical value, the reinforcement is depassivated, thus the protective film is uniformly or locally destroyed;
- **Propagation period:** during this second phase the reinforcement is directly affected and its cross-section is reduced. In addition, corrosion products are accumulated around the reinforcing bars and this may eventually lead to cracking and spalling of the concrete cover.

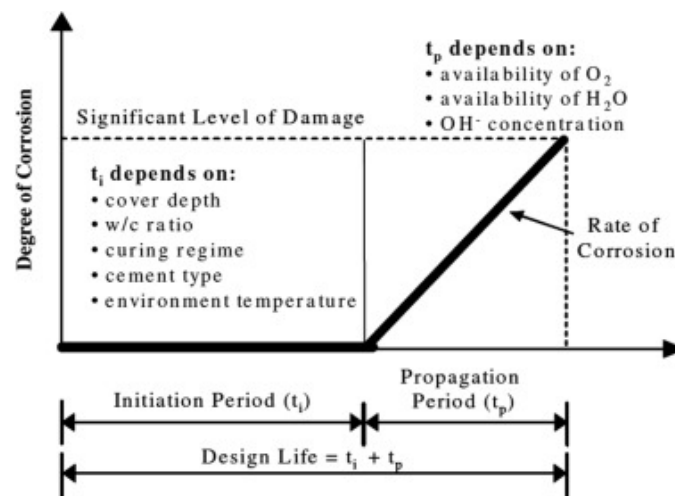


Figure 5.4: Initiation and Propagation periods in a structure subjected to Carbonation

The corrosion evolution process is governed by many parameters that can be associated with the design and execution phases (for example concrete cover, water/cement ratio...), in fact, the chlorides can derive from the concrete packaging phase, or it can be related to the environmental conditions. Furthermore, it is important to note that the corrosion mechanism affects only the reinforcing steel, but when the corrosion starts on the bar surface, rust and other corrosion products settle around it. As a result, the volume occupied by the bar and the corrosion products increases, creating a thrust on the surrounding concrete. This thrust can generate cracking and spalling of concrete and finally the failure of the whole structure if the corrosion process continues.

All the existing RC structures can be thus distinguished into two categories: RC structures which found themselves in the initiation period and RC structures that are in the propagation period, so it becomes important the evaluation of corrosion phenomenon in

time and its effects on the material and structural proprieties. In order to model the corrosion as a time-dependent mechanism, its evolution and its effects on the material properties are defined with time-dependent laws.

First of all, the corrosion initiation time, T_i , is computed with the Fick's diffusion equation and the available models are used to define the necessary inputs to the corrosion, such as the corrosion rate, i_{corr} [28], the loss of steel cross-sectional area, A_{pit} [25], the loss of steel ductility, $\epsilon_{su,rid}$ [14] [34], and in the end the loss of concrete cover, $f_{c,rid}$ [19]. All the parameters mathematical models and the necessary inputs are described in the following section. In the following analysis in order to analyse an aggressive environment, it is assumed an exposure environmental class XD1 or XS1 which is define in the Model Code 2010 as an aggressive environment in which the corrosion is induced by chlorides. A water/cement ratio of 0.5 is adopted. From these assumptions are derived the corrosion inputs as defined in DuraCrete.

5.2 Corrosion effects on material properties

The main effects of corrosion on concrete and steel are:

- Reduction of *Cross-section* of reinforcing bars;
- Reduction of reinforcement *ductility*;
- *Concrete strength* is affected by splitting cracks, delamination and spalling of the concrete cover;

Corrosion also affects the bond strength between steel and concrete, but this aspect is not modelled in this analysis.

As this mechanism affects all these material properties, it is clear that it causes a significant decrease in the structural safety. Consequently, it becomes important to evaluate the ability of a reinforced concrete structure to withstand different corrosion levels and to develop alternative load paths under different corrosion conditions. In this study the corrosion effects on the analysed reinforced concrete frame are investigated with an analysis in longitudinal direction of the reinforcement present in the structural members considering a simulated induced chloride corrosion for an attack length of 10mm in all the structural members at

the extremities near the beam–column joint.

The analyses are performed considering a simulated chloride corrosion in the RC frame modelled with the software DIANA FEA used in the geometrical and mechanical parametric analysis described in the previous chapters. To simulate the effects of corrosion by the reduction on the cross–section of the reinforcing bars and the materials proprieties, the sections where it is assumed the localized corrosion, are modelled considering the proprieties evolution in time during the building working life of 50years as defined for office building in the Eurocode 0, by implementing in the .py file which contains all the geometry, mesh and non linear analysis properties the mathematical models necessary to compute the evolution of corrosion in time. The models used to define the material proprieties reduction are described in the following sections, the results obtained for all the inputs in the different time instants are then illustrated in Table 6.1 in the following Chapter 6.

| Design working life category | Indicative design working life (years) | Examples |
|------------------------------|--|---|
| 1 | 10 | Temporary structures ⁽¹⁾ |
| 2 | 10 to 25 | Replaceable structural parts, e.g. gantry girders, bearings |
| 3 | 15 to 30 | Agricultural and similar structures |
| 4 | 50 | Building structures and other common structures |
| 5 | 100 | Monumental building structures, bridges, and other civil engineering structures |

(1) Structures or parts of structures that can be dismantled with a view to being re-used should not be considered as temporary.

Figure 5.5: Indicative design working life from EN 1990:2002

5.2.1 Corrosion rate and initiation time

The corrosion phenomenon starts when the chloride contents reaches the chloride critical concentration, C_{crit} , which is defined numerous researches to be around 0.1% and 1.96% measured as a percentage by weight of cement in the concrete mixture. Only a little percentage of chloride is sufficient to starts the pitting corrosion.

In this analysis is used a $C_{crit} = 0.4$ (wt%cement) as suggest in Gjorv [30] (see Figure 5.6).

When this value is reached at the rebar depth of the RC member the corrosion starts and the evolution in time of the chloride concentration can be evaluated from the Fick's

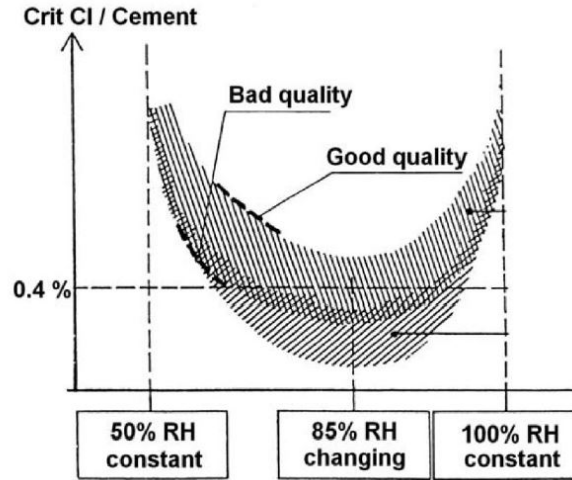


Figure 5.6: Qualitative connection between C_{crit} , environmental condition and concrete quality (Gjorv, 2009)

diffusion equation as described by DuraCrete [22] in the following equation 5.1:

$$C_{(x,t)} = C_s \left(1 - \operatorname{erf} \left(\frac{x}{2 \sqrt{k_t k_e D_{RCM} \left(\frac{t_0}{t} \right)^n t}} \right) \right) \quad (5.1)$$

with:

$$C(x=0, t) = C_s$$

$$C(x, t=0) = 0$$

where $C_{(x,t)}$ is the chloride concentration, C_s is the equilibrium chloride concentration at the concrete surface, both these values are expressed as a percentage by weight of cement (wt.% cement), x is the cover depth, k_t and k_e are coefficients that express respectively the transfer variable and the environmental transfer variable (k_t is taken equal to 1 according to FIB-CEB Task Group 5.6), D_{RCM} is the chloride migration coefficient measured in m^2/s , $t_0 = 0.0767 \text{ years}$ is the reference point of time corresponding to the concrete curing period of 28 days, t is the time in which corrosion is computed, n is an aging exponent and erf is the Gaussian error function. All the values of the variables necessary to compute $C_{(x,t)}$ are listed in table 5.1 or derived from the structure geometry.

From this equation it can be derived the corrosion initiation time by substituting the

critical chloride content to $C_{(x,t)}$ as it is employed in other studies [26][21][33]:

$$T_i = \left(\frac{x^2}{4k_t k_e D_{RCM} t_0^2} \left(\operatorname{erf}^{-1} \left(1 - \frac{C_{crit}}{C_s} \right) \right)^{-2} \right)^{\frac{1}{1-n}} \quad (5.2)$$

For the analysed RC structures the chloride content reaches the critical value around an initiation time of about $T_i = 5 \text{ years}$ which is in line with the concrete cover of 3cm and the assumed parameters of the corrosion process as it is assumed a highly aggressive environment.

Table 5.1: Mean values of the corrosion input parameter

| Parameter | Distribution | Mean(μ) | COV |
|-----------------------------|----------------------------------|---------------|------------------------|
| T °C | Normal | 17 | 0.20 |
| D_{RCM} m ² /s | Normal | 1.58E-11 | 0.20 |
| C_{crit} % | Beta truncated (limits: 0.2-2.2) | 0.4 | 0.25(a=9.2)(b=13.8) |
| C_s % | Normal | 1.2825 | 0.20 |
| n | Beta | 0.3 | 0.05(a=279.7)(b=652.6) |
| k_e | Normal | 0.67 | 0.10 |

Once it is defined the corrosion initiation time and time–dependent mathematical model of the chloride concentration at the rebar depth, it is possible to define the corrosion rate, i_{corr} . The corrosion rate is not constant in time, as a result its evolution in time need to be predicted. In various researches it was found that this variable depends on different parameters, some of them are:

- Chloride concentration C_t computed from equation 5.1 expressed in [kg/m³] of cement;
- Temperature at rebar depth T [K];
- Electrical resistance of concrete cover R_c [Ω];
- Time t [years].

From these parameters Liu and Weyers proposed a formulation for the corrosion rate as described in the following equation:

$$i_{corr} = 0.926 \exp \left(7.98 + 0.7771 \ln(1.69C_t) - \frac{3006}{T} - 0.000116R_c + 2.24t^{-0.215} \right) \quad (5.3)$$

where R_c is related to the chloride concentration, C_t , with the following equation:

$$R_c = \exp(8.03 - 0.549 \ln(1 + 1.69C_t)) \quad (5.4)$$

In the equation 5.3 the corrosion rate is computed in $\mu\text{A}/\text{cm}^2$ which is the measure of the current intensity of the metal. The corrosion rate is then defined in $\mu\text{mm}/\text{years}$ with the Faraday's law by multiplying i_{corr} with the conversion coefficient of 0.0116.

5.2.2 Loss of cross-section in the reinforcing bar

The first effect of corrosion is the damage and removal of the passive film in the reinforcement bars. As a result, the cross-section of the corroded bars is reduced with an increasing damage in time following the corrosion rate equation. Pits in corroded bars have an irregular shape as shown in Figure 5.7 which increases its depth and extension in bar surface during time. A more detailed effect on the bar cross-section is shown in Figure 5.8.

Various models have been developed in order to predict the evolution of the pitting corrosion in time. In this study it is followed the model depicted by Val et al. where it is assumed a pitting shape as illustrated in Figure 5.9 where it is assumed that the pit starts in the point A and follows an evolution in time within a circular shape with radius equal to the pitting depth $p(t)$, which is computed with the equation:

$$p(t) = R0.0116i_{corr}(t - t_i) \quad (5.5)$$

where R is the pitting corrosion factor assumed equal to 9 according to Biondini and Vergani [34], $0.0116i_{corr}$ is the corrosion rate in $\mu\text{mm}/\text{years}$ and $t - t_i$ is the time at which is evaluate the corrosion less the initiation time t_i .

The time-dependent evolution of the pit area, A_{pit} , is then described by the following equations:

$$\begin{cases} A_{pit}(t) = A_1 + A_2 & \text{if } p(t) \leq \frac{D_0}{\sqrt{2}} \\ A_{pit}(t) = A_0 - A_1 + A_2 & \text{if } \frac{D_0}{\sqrt{2}} \leq p(t) \leq D_0 \\ A_{pit}(t) = A_0 & \text{if } p(t) \geq D_0 \end{cases} \quad (5.6)$$

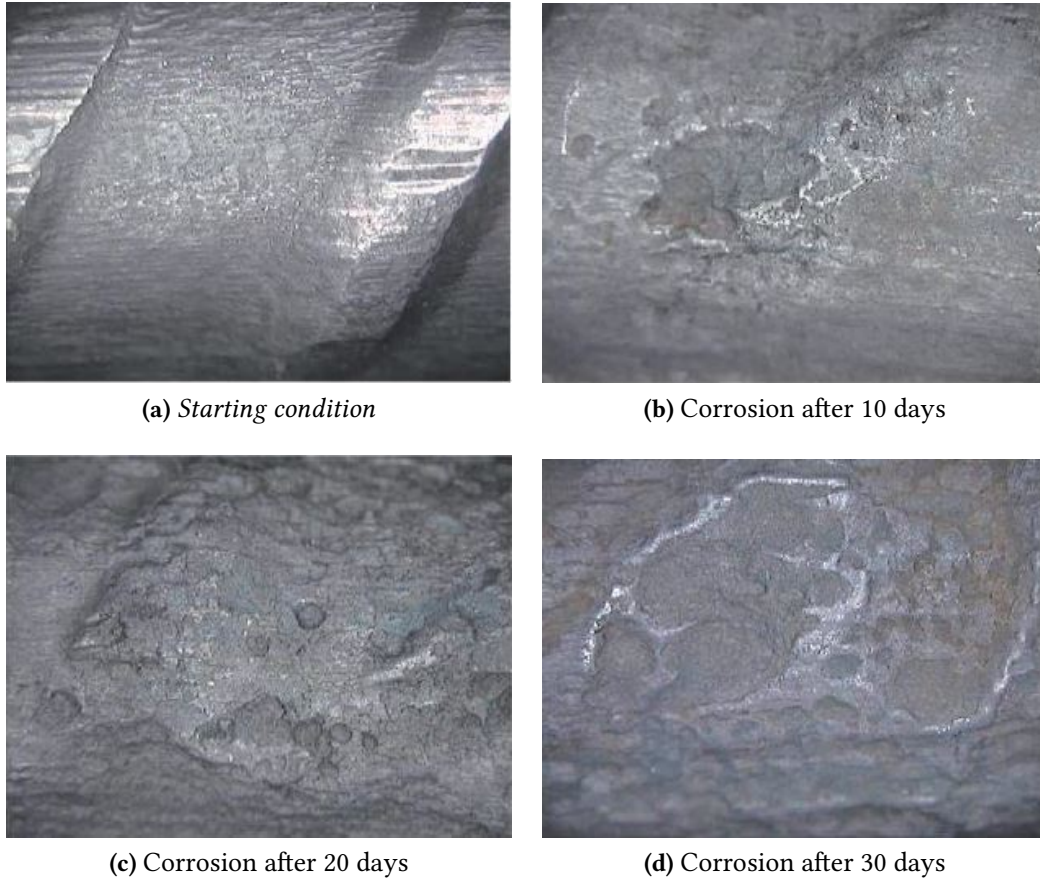


Figure 5.7: Different stages of pitting corrosion in a reinforcing bar (Apostolopoulos et al.,2008)



Figure 5.8: Loss of cross-sectional area due to pitting corrosion

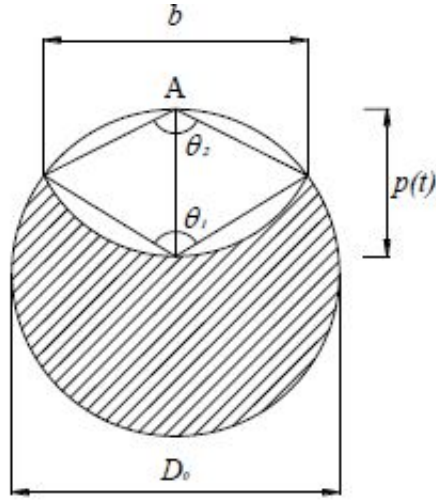


Figure 5.9: Pitting area shape model by Val-Melchers

where A_0 is the cross-sectional area of the reinforcing bar in the virgin state and the variables A_1 and A_2 are described as follow:

$$A_1 = 0.5 \left(\vartheta_1 \left(\frac{D_0}{2} \right)^2 - b \left| \frac{D_0}{2} - \frac{p(t)}{D_0} \right| \right) \quad (5.7)$$

$$A_2 = 0.5 \left(\vartheta_2 p(t)^2 - b \frac{p(t)}{D_0} \right) \quad (5.8)$$

$$A_0 = \frac{\pi D_0^2}{4} \quad (5.9)$$

$$b = 2p(t) \sqrt{1 - \left(\frac{p(t)}{D_0} \right)^2} \quad (5.10)$$

$$\vartheta_1 = 2 \arcsin \left(\frac{b}{D_0} \right) \quad \vartheta_2 = 2 \arcsin \left(\frac{b}{2p(t)} \right) \quad (5.11)$$

In conclusion, it is possible to define the net cross-sectional area of the corroded reinforcement as:

$$A_{net} = A_0 - A_{pit}(t) \quad (5.12)$$

and also the percentage of area reduction due to pitting corrosion as:

$$\alpha_{pit} = \frac{A_{pit}}{A_0} \quad (5.13)$$

parameter which is necessary in the evaluation of the loss of ductility in the reinforcement following the formulation defined by Coronelli et al. as explained in the next section 5.2.3

5.2.3 Loss of steel ductility

Another consequence of corrosion is the reduction of steel ductility which lead to a brittle behaviour in the reinforcement. This lack of ductility is taken into account modelling the reduction of the ultimate strain in the corroded bars, which is related also to the cross-sectional reduction of the steel bar.

In this study two different formulation are investigated to determine the reduction in the ultimate reinforcement strain, $\epsilon_{su,rid}$.

The first model to be analysed is the one proposed by Coronelli et al., which computes $\epsilon_{su,rid}$ considering the ratio between the percentage of area reduction consequently to the corrosion attack, α_{pit} , and the maximum percentage that this may reaches, $\alpha_{pit,max}$, thus the model works following the equation 5.14:

$$\epsilon_{su,rid} = \epsilon_{sy} + (\epsilon_{su} - \epsilon_{sy}) \left(1 - \frac{\alpha_{pit}}{\alpha_{pit,max}} \right) \quad \text{if } \alpha_{pit} \leq \alpha_{pit,max} \quad (5.14)$$

where the value of $\alpha_{pit,max}$ has been found to be variable between 0.1 and 0.5.

The second model which is analysed follows a different formulation to define the loss of steel ultimate strain and it is the one proposed by Biondini and Vergani [34]. In this model the reduction in the ultimate reinforcement strain is derived from experimental sample by computing a damage index $\delta_{\epsilon_{su}}$, which is applied as follow:

$$\epsilon_{su,rid} = \epsilon_{su0}(1 - \delta_{\epsilon_{su}}) \quad (5.15)$$

where the damage index is defined as:

$$\begin{cases} \delta_{\epsilon_{su}} = 0 & \text{if } \delta_{A_s} \leq 0.016 \\ \delta_{\epsilon_{su}} = 1 - 0.1521\delta_{A_s}^{-0.4583} & \text{if } \delta_{A_s} > 0.016 \end{cases} \quad (5.16)$$

where δ_{A_s} is the damaging index which refers to the reduction in the cross-sectional area of the reinforcing steel. In this formulation is considered the damage index related to the uniform loss in the cross section, as in the experimental samples is measured the mass loss and not the attack depth. Therefore, the equation 5.17 shows how to compute this damage index:

$$\begin{cases} \delta_{A_s}(\delta) = 4\delta(1 - \delta) & \text{if } 0 \leq \delta \leq 0.5 \\ \delta_{A_s}(\delta) = 1 & \text{if } \delta > 0.5 \end{cases} \quad (5.17)$$

where δ is the depth of the corrosion attack. A comparison between the two models results is given by Vergani in the diagram depicted in Figure 5.10. This diagram shows how the model proposed by Vergani et al. is able to accurately interpret the experimental results obtained from the tests.

In conclusion, by computing those two models, the first one was found to be highly dependent on the assumption of the $\alpha_{pit,max}$ value. According also to the researches by Botte et al. [14], *"using $\alpha_{pit,max} = 0.1$ provides very conservative estimates, while $\alpha_{pit,max} = 0.5$ provides unconservative estimates"*. On the other hand, the formulation by Biondini and Vergani gives values on the loss of steel ductility which are in between the values computed by the Coronelli et al. model and they are not influenced by external parameters, as it depends only on the loss of cross-sectional area of the steel bar, thus in these analyses it is chosen to follow the model proposed by Biondini and Vergani. The results are showed in Table 6.1.

5.2.4 Concrete cover reduction

During the corrosion process the reinforcement is the main material which is affected, but as this is embedded in concrete, the interaction between the two material generate a degradation also in the concrete proprieties.

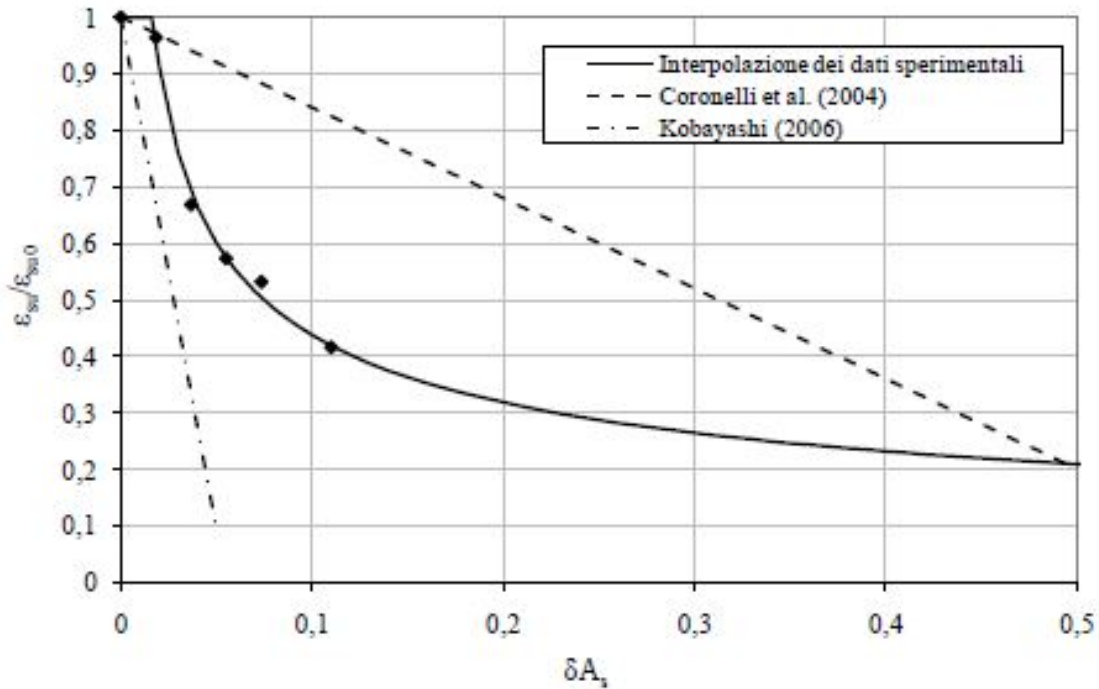


Figure 5.10: Ductility reduction as function of the cross-sectional bar loss

The most common degradation in concrete due to corrosion is the damage of the concrete cover and consequently there is a progressive damaging of its mechanical properties followed by its detachment from the reinforcing bar. In fact, corrosion products are formed around the steel bar and, as their volume is higher than the corroded steel, a radial pressure arise. This pressure can lead to cracking and spalling of the cover if it exceeds the tensile strength. In the end, cover detachment occurs when the crack opening due to corrosion become higher than 1mm.

This corrosion effect is taken into account by reducing the concrete cover strength according to the model proposed by Coronelli and Gambarova [19]:

$$f_{c,rid} = \frac{f_c}{1 + K \frac{\epsilon_t}{\epsilon_{c0}}} \quad (5.18)$$

where f_c is the concrete compressive strength, K is a coefficient related to the bar diameter and roughness which is taken equal to 0.1, $\epsilon_{c0} = 0.2\%$ is the concrete strain at the peak

compressive strength and ϵ_t is the average tensile strain in the cracked concrete due to the increasing of corrosion products. This last variable is computed as:

$$\epsilon_t = \frac{b_f - b_i}{b_i} = \frac{n_{bars} w_{cr}}{b_i} \quad (5.19)$$

where b_i is the section with in the integer state and b_f is the section with after expansion due to rust. $b_f - b_i$ is the increased section due to crack opening and it is approximated as defined in the equation 5.19 with $n_{bars} w_{cr}$, where n_{bars} is the number of bars in the layer under compression and w_{cr} is the total crack width for a given corrosion level, computed with equation 5.20

$$w_{cr} = \sum_i u_{i,orr} = 2\pi(v_{rs} - 1)x \quad (5.20)$$

where v_{rs} is the ratio of volumetric expansion of the corrosion products, it is assumed equal to 2 according to Simioni [20], x is the pitting depth and $u_{i,orr}$ is the opening of each single crack. When $u_{i,orr}$ reaches the limit value of 1mm, concrete cover detaches and its resistance is reduced.

Chapter 6

Analysis in simulated chloride corrosion

6.1 Modelling of Corrosion

The Static–Nonlinear analyses performed with variable geometrical and mechanical properties of the analysed RC structure is extended with a study concerning the evolution of the structure performance in time considering the effect of simulated chloride corrosion. The building working life is assumed of 50 years according to the Model Code 2010 for office buildings.

The reduction generated in the mechanical parameters affected by corrosion, such as A_s , f_c and ϵ_{su} , is implemented in the FEM model following the mathematical models as introduced in Chapter 5, defining the effect of corrosion at time instants of 10 years, 20 years, 30 years, 40 years, 50 years. In this way it is possible to represent the effect of corrosion on the load–bearing capacities of the structural members in time. The values obtained from the models for all the parameters necessary to evaluate the effect of corrosion in time are illustrated in Table 6.1. The starting values of the affected parameters are the one from the virgin state, such as:

- Virgin bar cross–section:
 - Beam reinforcement $\Phi 18$: $A_s = 254.47\text{mm}^2$;
 - Column reinforcement $\Phi 14$: $A_s = 153.94\text{mm}^2$;

- Virgin ultimate reinforcement strain $\epsilon_{su} = 12.5\%$;
- Virgin concrete compressive strength $f_c = 38.8\text{MPa}$;

The starting FEM geometry inputs are chosen to be compatible with the starting geometry used in the previous analyses.

Moreover, the parametric analysis performed with a variable ultimate reinforcement strain showed to increase the load-bearing capacity in the catenary mechanism in all the results with an increasing ϵ_{su} , as a consequence it is chosen to perform these analyses considering the value of ultimate reinforcement strain equal to 12.5% as it shows to increase consistently the load-bearing capacity in catenary action.

Table 6.1: Evolution of corrosion effect in time ($W_{life} = 50\text{years}$)

| Parameter | Corrosion time t [years] | | | | |
|---------------------------------------|----------------------------|--------|-------|-------|-------|
| | 10 | 20 | 30 | 40 | 50 |
| i_{corr} [A/cm ²] | 0.696 | 0.688 | 0.675 | 0.663 | 0.653 |
| C_t Kg/m ³ | 1.716 | 2.115 | 2.323 | 2.458 | 2.556 |
| α_{pit} % | 0.32 | 1.23 | 2.62 | 4.42 | 6.6 |
| $A_{s,rid_{\Phi 18}}$ mm ² | 253.65 | 251.34 | 247.8 | 243.2 | 237.7 |
| $\epsilon_{su,rid_{\Phi 18}}$ % | 12.5 | 10.05 | 8.43 | 7.46 | 6.79 |
| $A_{s,rid_{\Phi 14}}$ mm ² | 153.12 | 150.84 | 147.3 | 142.9 | 137.5 |
| $\epsilon_{su,rid_{\Phi 14}}$ % | 12.23 | 8.97 | 7.53 | 6.66 | 6.06 |
| $f_{c,rid}$ [MPa] | 37.97 | 37.20 | 36.49 | 35.83 | 35.20 |

Table 6.1 shows that the mean value of the corrosion rate evaluated in this study with equation 6.1 is around $0.675\mu\text{A}/\text{cm}^2$ which correspond to a category of medium corrosion phenomenon as defined qualitatively in Table 6.2.

Table 6.2: Corrosion rate qualitative classification (Brite–EuRam,1995)

| Corrosion rate [A/cm ²] | |
|-------------------------------------|-----------|
| Neglectable | < 0.1 |
| Low | 0.1 ÷ 0.5 |
| Medium | 0.5 ÷ 1 |
| High | > 1 |

Consequently, having a medium corrosion level lead to a reduction in the reinforcement cross-section of about 7% and 11% for bar diameters of 18mm and 14mm respectively. The decrease of the area among the assumed working life period is showed in Figure 6.1 in comparison with the cross-sectional area in the virgin state. The reduction in the concrete strength is 10%.

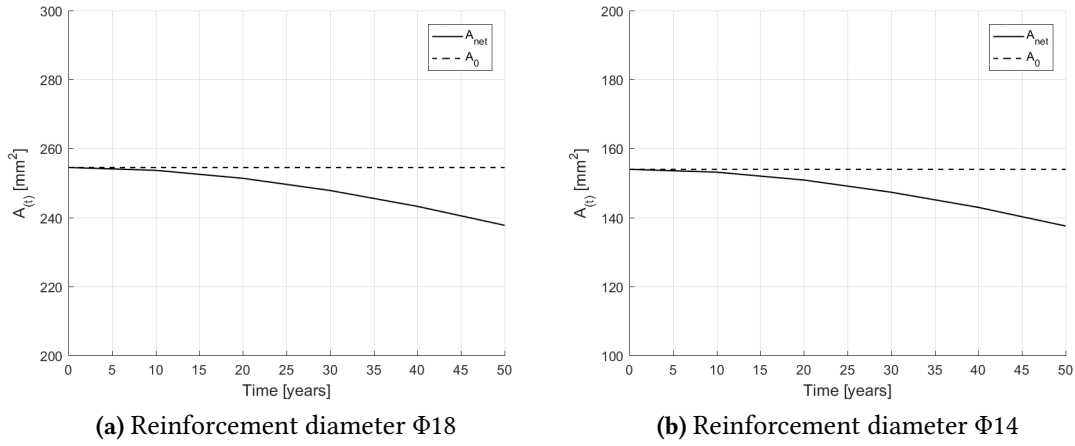


Figure 6.1: Reinforcement cross-sectional area reduction during 50 years

Furthermore, it is notable that the evolution of pits area percentage, α_{pit} , is the same for both the bar diameters, while the reduction in steel ductility is a bit higher in the bar with a diameter of 14mm. This is in accordance with the evolution depicted in the model by Biondini and Vergani of the damage index δ_{A_s} , which assumes the values defined in Table 6.3, where are also listed the values of the damage index $\delta_{\epsilon_{su}}$.

Table 6.3: Evolution of damage indexes in time ($W_{life} = 50\text{years}$)

| Damage index | Corrosion time t [years] | | | | |
|--|----------------------------|--------|--------|--------|--------|
| | 10 | 20 | 30 | 40 | 50 |
| δ_{A_s} ($\Phi 18$) | 0.0134 | 0.0264 | 0.0387 | 0.0506 | 0.0622 |
| $\delta_{\epsilon_{su}}$ ($\Phi 18$) | 0.0 | 0.1957 | 0.3252 | 0.4031 | 0.4567 |
| δ_{A_s} ($\Phi 14$) | 0.0172 | 0.0339 | 0.0497 | 0.0648 | 0.0795 |
| $\delta_{\epsilon_{su}}$ ($\Phi 14$) | 0.0217 | 0.2825 | 0.3978 | 0.4671 | 0.5148 |

The diagrams defining the evolution of the ratio ϵ_{su} and ϵ_{su0} , which define the complementary value of the damaging index equal to $(1 - \delta_{\epsilon_{su}})$ are illustrated in Figure 6.2. They

show, together with Table 6.3 that for a maximum δ_{As} of about 8% the reduction on the steel ductility, after 50 years, is 50%.

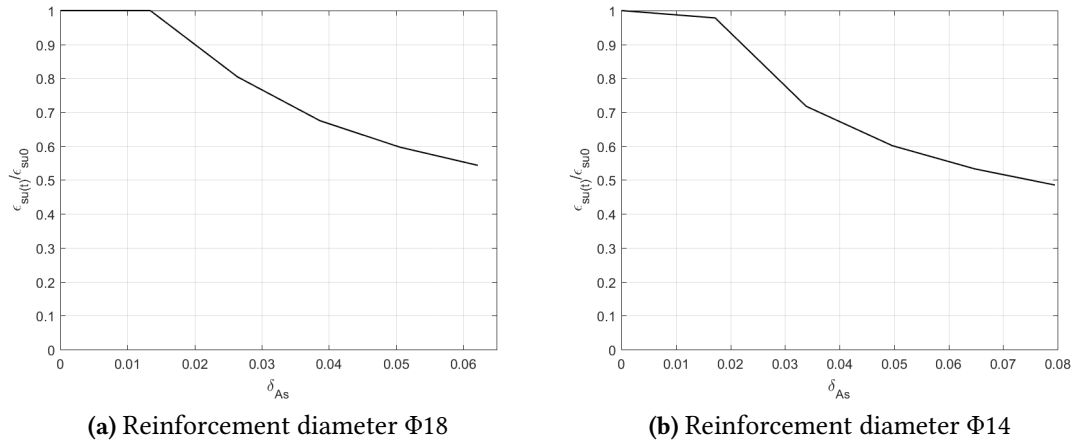


Figure 6.2: Loss of steel ductility during 50 years

After computing all the input parameters necessary to evaluate the corrosion effects during the building working life, to perform the analyses on simulated chloride corrosion, it is necessary to define some sections where to apply the reduction in the material properties, as this phenomenon consists in a localized pitting corrosion.

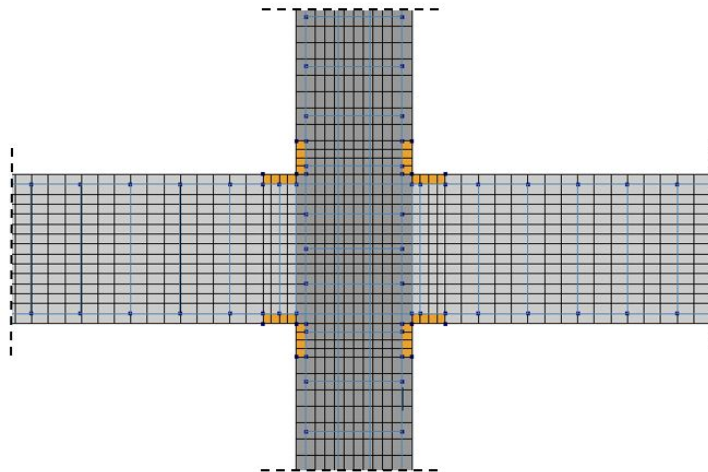


Figure 6.3: FEM model to assess robustness under the corrosion effects

In order to investigate the effects provides on the load-bearing capacities of the analysed RC frame, the corroded elements are applied in the FEM model considering a length of $10 \div 20\text{cm}$ in correspondence of all the structural members extremities close to the joint, where the failure of the RC beam subjected to the column removal happens for crushing of concrete and rupture of the top reinforcement, as it is shown in Figure 6.3.

6.2 Analysis of the Results

This section thoroughly presents the analysis of the results on the corrosion effects over time. As it is explained in the previous section, a nonlinear analysis considering a load controlled procedure is performed using the arc-length algorithm method by applying the corrosion localized effect in longitudinal direction affecting the elements close to the frame integer joint, that are the most stressed after the removal of the load-bearing column.

In these analyses are investigated all the effects of corrosion on the material properties as explained in Chapter 5. One may notice, from the values obtained by computing the mathematical models, that the higher effect from localized pits is on the loss of bars cross-section and consequently on the steel ductility which is highly reduced during the period of 50 years. In fact, starting from a ultimate reinforcement strain of $\epsilon_{su} = 12.5\%$, for both the diameters that are used in the RC frame of 14mm and 18mm, after a period of 50 years the reduction is around 45% and 50% respectively.

The load-displacemet diagram and the membrane action-displacement diagram obtained from the Static-nonlinear analyses are shown in Figure 6.4 for the different time instants defined in the previous section.

First of all, it should be noted that the load-bearing capacity in compressive membrane action is not influenced, for all situations. This is in accordance with the diagram shown in Figure 4.14, which illustrates the results obtained varying the ultimate reinforcement strain in all the member reinforcement thus with the highest influence on ϵ_{su} by pitting.

Moreover, it is clear that, as the main effect due to localized corrosion is the reduction of the reinforcement strain, during the period of 50 years the load-bearing capacity is highly decreased. In fact, the percentage of decrease is about 50% and it lead to a complete loss

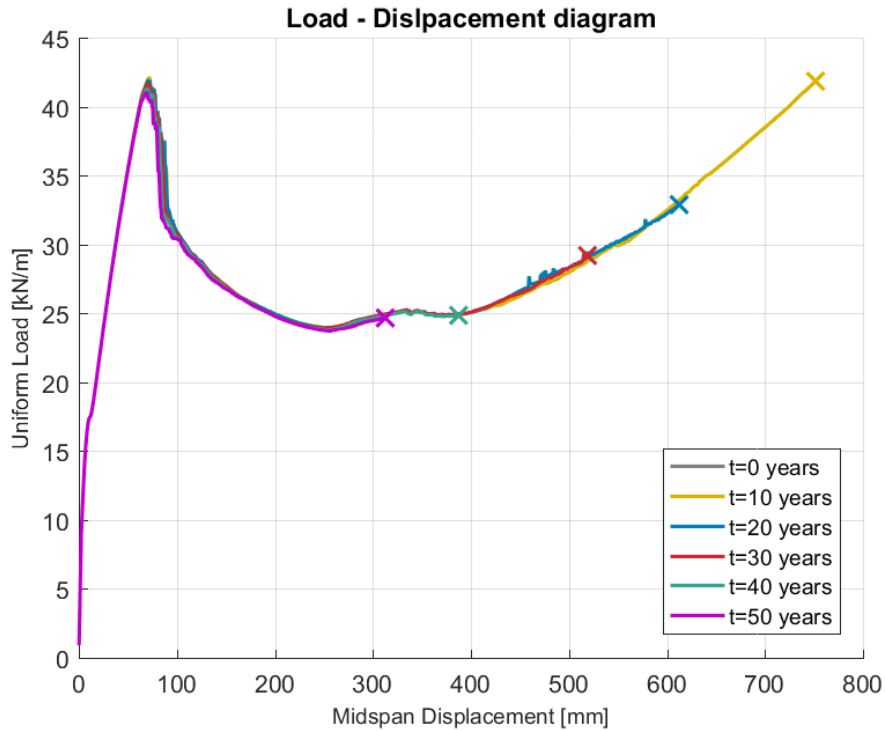


Figure 6.4: Load-bearing capacity diagram in simulated chloride corrosion

in the structure ability to develop catenary action, following also what is depicted in Figure 4.14.

In conclusion, although localised pitting corrosion has many effects on material properties, the major effect affecting the load-bearing capacity of the structure, considering a longitudinal analysis to assess the robustness under the degradation phenomenon, is the reduction in the steel ductility. Consequently, as the analysis performed increasing the ultimate reinforcement strain leads to an increase in load-bearing capacity in the catenary mechanism thus to the vertical displacement in correspondence of it, corrosion has the exact opposite effect. Indeed, it leads to the reduction of the TMA resistance and to the failure vertical displacement, until the last analysis with $t_{corr} = 50\text{years}$ where the RC frame is not capable to change the resisting mechanism and TMA do not occurs.

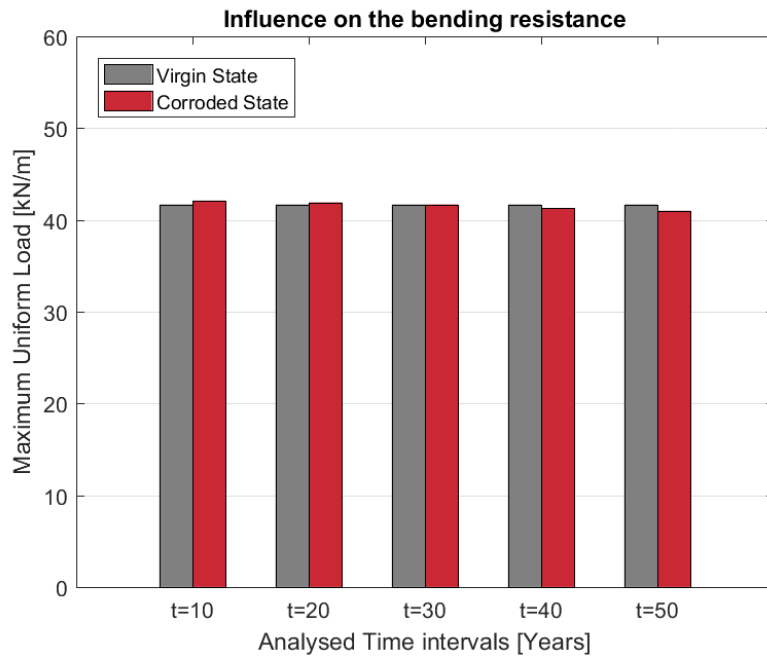


Figure 6.5: Comparison between the maximum load in CMA under corrosion evolution in time

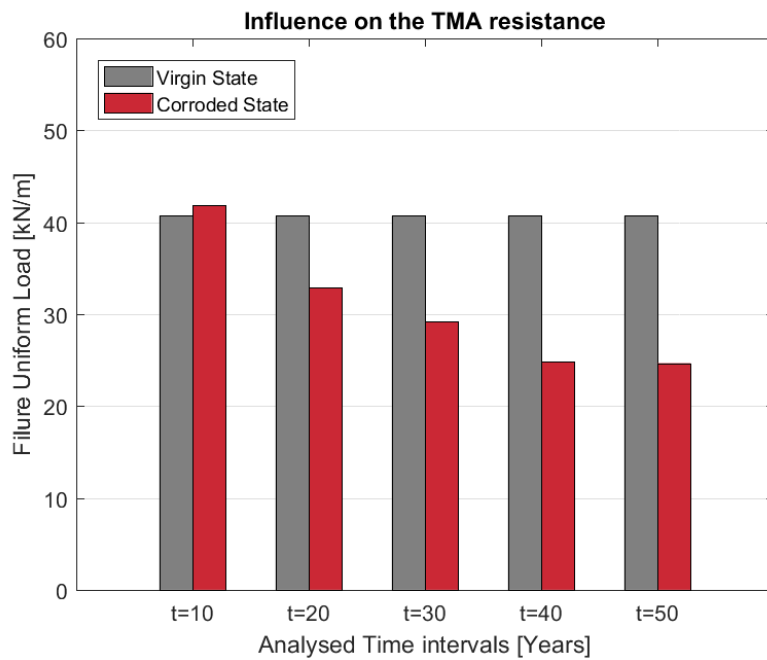


Figure 6.6: Comparison between the maximum load in TMA under corrosion evolution in time

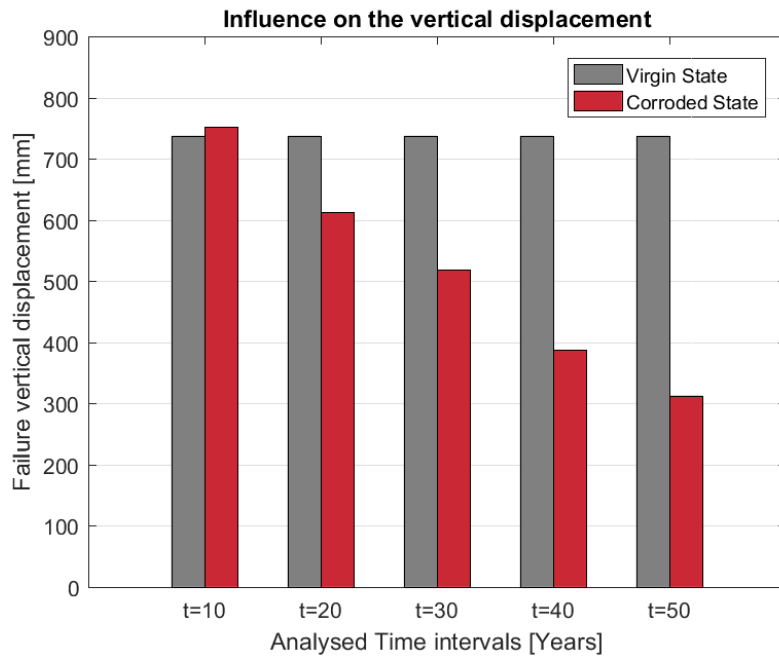


Figure 6.7: Comparison between the failure displacement under corrosion evolution in time

Chapter 7

Conclusions

In this thesis, the concepts of **Structural Robustness** and **Corrosion** of reinforced concrete structures have been addressed.

These two phenomena are, to date, of relevant importance with regard to existing structures, in terms of both corrosion and robustness, and for newly designed structures in assessing structural robustness.

The latter is related to the ability of a structure to develop alternative load paths following the occurrence of exceptional events, whose mode of computational representation consists in the removal of a load-bearing column. Therefore, a FEM model is developed using the DIANA FEA software, taking as reference the building designed by Drogneè et al. [5], from which a part of the outer frame subject to the removal of an intermediate column is extrapolated. The FEM model and nonlinear analysis properties are also defined following the validated FEM model by Botte et al. [11] and, also, according to *Guidelines for non linear finite element analysis of concrete structures* [7] .

In the first part of this thesis, a parametric analysis is performed varying the geometrical and mechanical characteristics of the investigated RC frame.

From the parametric analysis of the geometry, it can be seen, as in other studies, that the cross-section of the beam, which is connected to the point where the column is removed, is the one that most affects the resistant mechanisms of the frame. In particular, as the height of the section increases, the peak of bending resistance increases, while the capacity of the structure to change the resistant mechanism to the catenary mechanism decreases and

therefore, it is not able to develop alternative load paths.

Since the geometric analysis on the variability of the geometry of the adjacent elements and on the rotational capacity of the beam–column joint was then performed, it was possible to observe that the greatest influence comes from the cross–section of the columns. In fact, by increasing the section of the columns, the rotational capacity decreases and, consequently, a decrease in the ultimate vertical displacement is observed. With regard to bending resistance and resistance during the development of tensile membrane actions, the influence of the geometrical properties of adjacent members is very low and in some cases null.

The analysis carried out with the variation of the ultimate reinforcement strain has led to a considerable variation in the failure load at which the rupture of the top reinforcement of the beam occurs. This is due to the fact that the ductility of the reinforced concrete section is consistently modified. The analyses cover a range of variation starting from ductility values too low to be able to develop the catenary mechanism to sufficiently high values to ensure an increase in resistance following the bending peak. In particular, the analyses carried out with a ultimate strain of 12.5 percent guarantee in almost all the analyses the development of tensile membrane actions in the frame during the static non–linear analysis.

The last parametric analysis is carried out keeping the resistant moment constant in the structural elements. In this case there was an increase in both resistances for beam cross–sections smaller than that corresponding to the starting geometry and vice versa for bigger ones. The analysis keeping constant the resistant moment in the columns did not produce significant results in terms of resistances, but only a small variation in the rotational capacity of the joint, accordingly to the analyses carried out with variable column cross–section, a decrease in the overall column cross–section lead to an increase in the vertical displacement.

Finally, after defining which geometrical and mechanic characteristics have the greatest influence on the capacity diagram of the reinforced concrete frame, an analysis is carried out considering the evolution in time of the effects due to simulated chloride corrosion on the robustness, whereas the structure has deteriorated over a working life of 50 years.

For this purpose, the outer frame has been extrapolated and a parametric analysis has been carried out under simulated chloride corrosion conditions considering different time

instants. The corrosion effects are localized in correspondence of the beam column joint where failure occurs. The analyses carried out showed that, the reduction of the reinforcement area and the consequent reduction of the steel ductility, are the parameters that most influence the ultimate behaviour of the reinforced concrete frame, considering the performed analyses in longitudinal direction. As a result, with the evolution in time of the corrosion effect the reduction in the steel ductility lead to a decrease in the maximum load under catenary actions, until the capacity of the reinforced concrete structure to develop alternative load paths is completely nullified, due to the assumed highly aggressive environment.

Bibliography

- [1] CEN, 1-7 (2006) *Eurocode 1: Actions on structures - Part 1-7: General actions – Accidental actions*, In: *European committee for Standardization*, Brussels, 1991.
- [2] CEN, 0-2 (2002) *Eurocode 0: Basis of the design*, In: *European committee for Standardization*, Brussels, 1990.
- [3] CNR-DT 214/2018, *Istruzioni per la valutazione della robustezza delle costruzioni*, Roma, 2018.
- [4] COST Action TU0601, *Structural robustness design for practising engineers – Canisuis*, T.D.G. (Editor), 2011.
- [5] Didier Droogné et al., *A multilevel calculation scheme for risk-based robustness quantification of reinforced concrete frames*. In: *Engineering Structures* 160 (2018), pp. 56-70.
- [6] Rajesh Prasad Dhakal e Koichi Maekawa, *Modelling of postyielding buckling of reinforcement*. In: *Journal of Structural Engineering* 128.9 (2002), pp. 1139-1147.
- [7] Rijkswaterstraat Ministry of Infrastructure and the Environment, *Guidelines for non linear finite element analysis of concrete structures*; 2012.
- [8] The Guardian, 1968.
- [9] H.S. Lew et al., *An experimental and computational study of reinforced concrete assemblies under a column removal scenario*, NIST Technical Note 1720, 2011.
- [10] D. Gouverneur et al., *Experimental investigation of the load-displacement behaviour under catenary action in a restrained reinforced concrete slab strip*. In: *Engineering Structures* 49 (2013), pp. 1007-1016.
- [11] Wouter Botte et al., *Influence of design parameters on tensile membrane action in reinforced concrete slabs*. In: *Structural Engineering International* (2015), 25;50-60.
- [12] DIANA FEA 10.2 User's Manual.

- [13] P. Castaldo, B. Palazzo, A. Mariniello, *Effects of the axial force eccentricity on the time-variant structural reliability of aging r.c. cross-sections subjected to chloride-induced corrosion*. In: *Engineering Structures* 130 (2017), pp. 261-274.
- [14] Wouter Botte, Robby Caspeele, Luc Taerwe, *Membrane behaviour in RC slabs subjected to simulated reinforcement corrosion*. In: *Engineering Structures* 123 (2016), pp.45-58.
- [15] Fabio Biondini & Matteo Vergani (2015), *Deterioratin beam finite element for nonlinear analysis of concrete structures under corrosion*, *Structures and Infrastructures Engineering*, 11:4, 519-532, DOI: 10.1080/15732479.2014.951863
- [16] Kesio Palacio (2013), *Practical Recommendations for Nonlinear Structural Analysis in DIANA*, TNO DIANA.
- [17] Luca Bertolini, *Materiali da costruzione, Volume Primo, Struttura, Proprietà e Tecnologie di Produzione*, CittàStudi Edizioni.
- [18] Tuuti, K. (1982). *Corrosion of steel in concrete*. Swedish Cement and Concrete Research Institute, Stockholm.
- [19] Coronelli D., Gambarova P., *Structural assessment of corroded reinforced concrete beams: modeling guidelines*. In: *Journal of Structural Engineering* 2004;130(8):1214–24.
- [20] Simioni P., *Seismic response of reinforced concrete structures affected by reinforcement corrosion PhD thesis*. Faculty of Architecture, Civil Engineering and Environmental Sciences, University of Braunschweig – Institute of Technology and the Faculty of Engineering University of Florence; 2009.
- [21] Choe DE, Gardoni P, Rosowsky D, Haukaas T, *Seismic fragility estimates for reinforced concrete bridges subject to corrosion**Structural Safety* 31 (2009), pp. 275–83.
- [22] DuraCrete, *Modelling of degradation*, EU-project (Brite EuRam III) no. BE95-1347. Probabilistic performance based durability design of concrete structures. Report 4–5; 1998.
- [23] Apostolopoulos CA, Papadakis VG, *Consequences of steel corrosion on the ductility properties of reinforcement bar*. In *Construction and Building Materials* 22 (2008), pp. 2316–2324.
- [24] Charis A. Apostolopoulos, Sotiris Demis, Vagelis G. Papadakis, *Chloride-induced corrosion of steel reinforcement – Mechanical performance and pit depth analysis*. In *Construction and Building Materials* 38 (2013), pp. 139–146.
- [25] Dimitri V. Val, Mark G. Stewart and Robert E. Melchers, *Effect of reinforcement corrosion on reliability of highway bridges*. In *Engineering Structures*, Vol. 20, No. 11, pp.

1010–1019, 1998.

- [26] K. D. Pitilakis, S. T. Karapetrou, S. D. Fotopoulou, *Consideration of aging and SSI effects on seismic vulnerability assessment of RC buildings*. Bull Earthquake Engineering (2014) 12:1755–1776.
- [27] Ueli Angst, Bernhard Elsener, Claus K. Larsen, Øystein Vennesland, *Critical chloride content in reinforced concrete – A review*. In *Cement and Concrete Research 39* (2009), pp. 1122–1138.
- [28] T. Liu, R.W. Weyers, *Modelling the dynamic corrosion process in chloride contaminated concrete structures*. In *Cement and Concrete Research*, Vol. 28, No. 3, pp. 365-379, 1998.
- [29] P. Spiesz, H.J.H. Brouwers, *The apparent and effective chloride migration coefficients obtained in migration tests*. In *Cement and Concrete Research 48* (2013), pp. 116–127.
- [30] Gjorv, O.E., *Durability design of concrete structures in severe environments*. Taylor and Francis, 2009.
- [31] CEB-FIB Task Group 5.6, *Model code for service life design*. Fédération Internationale du Béton FIB 2006. Bulletin 34.
- [32] fib, *Model code for concrete structures*. Fédération Internationale du Béton FIB 2013.
- [33] Jayadipta Ghosh, S.M.ASCE; and Jamie E. Padgett, A.M.ASCE, *Aging Considerations in the Development of Time-Dependent Seismic Fragility Curves*. In *Journal of Structural Engineering 136(12)* (2010), pp. 1497-1511.
- [34] Fabio Biondini & Matteo Vergani , *Damage modeling and nonlinear analysis of concrete bridges under corrosion*. In Biondini F, Frangopol DM, editors. Proceedings of the sixth international conference on bridge maintenance, safety and management (IABMAS 2012), Stresa, Italy, 2012. Bridge maintenance, safety, management, resilience and sustainability. CRC Press, Taylor and Francis Group, 2012.

Ringraziamenti

La tesi magistrale è un traguardo che ho atteso con ansia, la conclusione di un percorso spesso difficile, che porta a crescere personalmente e professionalmente. Lungo questo percorso ho avuto la possibilità di confrontarmi e conoscere molte persone, senza il cui ausilio sarebbe stato molto più difficile arrivare a questa conclusione e che, quindi, desidero ringraziare.

Innanzitutto, ringrazio il mio relatore Paolo Castaldo, che mi ha permesso di svolgere questo lavoro e che mi ha guidata in questi mesi, insieme a Diego Gino. Un doveroso ringraziamento va al Prof. Dr. Ir. Robby Caspeepe che mi ha accolta nel suo gruppo di ricerca all'Università di Ghent, dove ho potuto sviluppare la conoscenza sui concetti legati alla robustezza, grazie anche alla supervisione da parte di Wouter Botte.

Ringrazio soprattutto i miei genitori *Giancarlo* e *Anna Maria* che mi hanno sempre sostenuto durante il mio percorso di studi e che hanno reso possibile la mia crescita personale e professionale a Torino e all'estero. Insieme a loro, voglio ringraziare *Cristina* e *Stefano*, i quali fanno ormai parte della famiglia e i cui preziosi consigli mi hanno accompagnata lungo tutto il mio percorso universitario.

A *Mary*, amica di una vita. Dal momento in cui ci siamo squadrate il primo giorno di Geometra fino ad adesso siamo rimaste unite, anche se i nostri percorsi ci hanno divise. La tua amicizia mi ha permesso di crescere e sei stata la prima a dover sopportare le mie ansie, ma non sarebbe stato lo stesso senza *Rosa*, *Anna* ed *Elisa*. Insieme abbiamo condiviso tra i momenti più belli e, se anche saremo da un capo all'altro del mondo, ci ritroveremo sempre a Viadana tutte insieme per confidarci e consigliarci.

A *Luciano*, mio mentore e fonte di grande saggezza. Il tuo supporto morale per tutto questo periodo è stato fondamentale, nonostante gli infiniti audio e chiamate, hai sempre saputo darmi il giusto input per andare avanti e rimbocarmi le maniche e *'la vita non è uno sprint, è una maratona. Una competizione, ma non si può competere con tutti'* è uno di questi.

Ai miei coinquilini *Vittoria e Antonio*, con cui ho condiviso tra le esperienze più varie. *Vittoria*, miglior cuoca coinquilina, con cui ho passato tutte le sofferenze degli esami del Politecnico e la prima esperienza lontana da casa. Le gioie che ci ha portato la casa in Corso Rosselli sono state poche ma buone, prima fra tutte *Nanu*. *Antonio*, la nostra convivenza è iniziata nel peggiore dei momenti per entrambi, ma hai saputo spronarmi nello scrivere questa tesi e fare tutte le analisi, che alla fine le scommesse le hai vinte tutte tu e, nonostante i miei Up&Down, la fine è arrivata.

Ringrazio gli amici della *Movida Torinese* con cui ho condiviso i momenti di festa e spensieratezza in questi tre anni al Poli. Ognuno di voi ha contribuito a suo modo nel rendere questa città meno grigia. In particolare ci tengo a ringraziare *Ludovico*, in cui ho scoperto una grande amicizia e affinità come poche.

Ringrazio anche tutti coloro che non ho nominato, ma che hanno avuto un ruolo importante in questi tre anni e in questo periodo di tesi, sia qua a Torino che a Ghent dove ho potuto conoscere persone nuove e che hanno lasciato un segno, anche se per un breve periodo.